NITROGEN DIFFUSION

IN

ZIRCONIUM NITRIDE

NITROGEN DIFFUSION
IN
ZIRCONIUM NITRIDE

By

JEAN DESMAISON, Docteur en Chimie

A Thesis

Submitted to the Faculty of Graduate Studies

in Partial Fulfilment of the Requirements

for the Degree

Master of Science

McMaster University

August 1973

MASTER OF SCIENCE (1973)
(Materials Science)

McMaster University
Hamilton, Ontario

TITLE: Nitrogen Diffusion in Zirconium Nitride

AUTHOR: Jean DESMAISON, Doctorat en Chimie, University of Bordeaux

SUPERVISOR: Professor W. W. Smeltzer

NUMBER OF PAGES: xi, 109

SCOPE AND CONTENTS:

Diffusion of nitrogen in zirconium nitride was studied using the ^{15}N gas-solid exchange technique.

Two kinds of samples were used: $ZrN_{0.71-0.79}$ spheres, 60μ and 90μ diameter and $ZrN_{0.93}$ slabs 254μ thick. The spheres were prepared by dropping 99% powdered zirconium nitride through an electric arc while the slabs were obtained by direct nitridation of 99.995% zirconium sheets at 1150°C in very pure nitrogen at 1 atm. These samples were carefully characterized by chemical analysis, density and lattice parameter measurements, electron probe microanalysis, X-ray diffraction and scanning electron microscopy techniques.

The diffusion annealings were performed at a pressure of 200 Torr and in the temperature range 1000-1200°C. The rate of depletion of ^{15}N in the isotopically enriched gas phase was measured by a mass spectrometer and used to calculate the self-diffusion coefficient.

The diffusion coefficients for spheres and slabs could be respectively represented by

$$D_{spheres}(cm^2/sec) = (2.97^{+18.76}_{-2.56}) \times 10^{-10} \exp(-(23,000 \pm 5,400)/RT)$$

and

$$D_{slabs}(cm^2/sec) = (4.08^{+88.23}_{-3.90}) \times 10^{-6} \exp(-(36{,}000 \pm 4{,}500)/RT)$$

These results are in good agreement with the chemical diffusion coefficients available in the literature. It is shown that the rather low activation energies, in particular in the case of spheres, do not preclude a vacancy mechanism for nitrogen diffusion.

ACKNOWLEDGMENTS

Grateful acknowledgment is made to Dr. W. W. Smeltzer for his continuing guidance, help and advice throughout all stages of this project. The author is indebted to Dr. D. J. Young, many of the faculty, graduate students and technical staff in the Department of Metallurgy and Materials Science for their helpful discussion and aid.

We gratefully acknowledge the following groups for their financial support: The Department of Metallurgy and Materials Science of McMaster University for the graduate fellowship and the National Research Council for the research grant to Dr. Smeltzer.

TABLE OF CONTENTS

LIST OF TABLES

LIST OF FIGURES

CHAPTER I

INTRODUCTION

Up till now nitrides of the transition metals have attained only cursory interest as compared with the carbides. Despite their excellent high temperature properties, good corrosion resistance, and hardness the practical application of nitrides has been limited to the formation of hard and wear resistant surface layers in the nitriding of steels or other iron alloys. The relatively stable nitrides of the group IV of the periodic table (TiN, ZrN, HfN) have been used as refractory materials for the fabrication of crucibles with fair thermal shock resistance but poor oxidation resistance. Several other refractory applications of TiN and ZrN have been reported.[1] Attempts to cement nitrides with binder metals to form hard alloys have been up to now only partly successful.[2] The major future use of the nitrides may depend upon their electrical properties which are attractive for potential applications such as integrated circuitry and in superconducting devices.[3]

While the compounds formed by the transition metals, in particular with carbon and nitrogen, have been known since the turn of the century, only very recently has an appreciation of their difficult properties been combined with sophisticated techniques for their examination. Now it is becoming increasingly clear that these compounds occupy a class which is indeed unusual and that their studies are capable of yielding information of considerable value to solid state theory. "Where once metallurgists and ceramicists roamed free, chemists and solid state physicists are now

beginning to build fences and farm the land more deeply" (Storms).[14]

The different names given to these compounds is a good indication of the multiplicity of the questions that they are posing. They are sometimes called "refractory hard metals" because of their metallic properties, "interstitial compounds" because the small non-metal atom appears to fill the octahedral void between the metal atoms, and "defect compounds" because both the metal and non-metal lattices can tolerate atom vacancies in rather large concentration. The main task of today's investigators is to correlate the bonding, crystal chemistry and defect structure of these compounds with their physical and chemical properties. Three main difficulties are plaguing investigations: the effects of dissolved oxygen, variable stoichiometry which requires that the material be well characterized and the fact that many compounds can change structure upon cooling due to the ordering of vacancies in the non-metal sublattice.

In the postscript of his recent book on carbides and nitrides, Toth[3] summarized several problems for future research. Diffusion studies are first in the list. The topic was not included in the main body of the text because the knowledge of this area was found too limited and contradictory. However, the same year (1971) De Poorter and Wallace[5] reviewed the experimental and theoretical work pertinent to diffusion in refractory metal carbides and uranium carbides, and Williams[6] devoted one section of his review on transition-metal carbides to diffusion. Up to now no similar information is available in the case of nitrides.

The main purpose of this work was to examine the available knowledge on diffusion in transition nitrides and to measure the self-diffusion coefficient of nitrogen in zirconium mononitride using the solid-gas isotopic

exchange method. We chose this nitride and this technique because a method for preparation of zirconium nitride spheres, suitable for diffusion studies, has been recently presented by Streiff and Smeltzer.[7] In addition, all the values determined to the present for this compound are chemical diffusion coefficients calculated from data of kinetic studies of diffusion-controlled reactions.

The following sections present a literature survey on the subject of defect structure and diffusion in zirconium nitride with some reference to other refractory nitrides, description of the experimental techniques, experimental results and discussion. Further, the experimental results are used to understand the diffusion mechanism.

CHAPTER II

REVIEW OF THE LITERATURE

The purpose of the present review is to give a selective and critical discussion of the research on zirconium nitride published since approximately 1960 with particular reference to defect properties and diffusion studies. A compilation of diffusion coefficients for nitride compounds in general will also be given but only the results concerning the nitrides with properties close to those of zirconium nitride will be discussed in some detail. The compounds in question are the mononitrides of the other metals from column IVa along with those of metals from column Va. Several reviews or texts on nitrides were consulted[2,3,8-20] but many new pieces of literature were analyzed, in particular for diffusion studies.

2.1 Preparation

To prepare pure zirconium nitride, direct reaction of metal or hydride powders in NH_3 or N_2 or deposition on a substrate from the gas phase by reacting $ZrCl_4$ in a N_2-H_2-Ar atmosphere are preferred to the nitridation of metal oxide powders in the presence of carbon.[3] Contrary to titanium nitride, the zirconium nitride obtained by this last method is significantly contaminated by carbon and contains considerable amounts of unreacted oxide.[8] Even when using the two first methods it is necessary to employ high-purity gases in order to prevent the formation of ternary solid solutions upon addition of small amounts of oxygen. Once the nitride has been contaminated by oxygen, it is almost impossible to purify. To make

matters worse, the amount of oxygen is difficult to determine analytically but it is considered that samples seldom contain less than a few hundred p.p.m.[20] Therefore the best technique for sample preparation is to avoid all possible contamination.

2.2 Zirconium-Nitrogen Phase Diagram

The phase diagram for the Zr-N system is not well established.[21-23] Storms[10,20] has reviewed the earlier literature and summarized the information into a probable phase diagram shown in fig. 1.

The addition of N to Zr stabilizes both the α- and β-Zr metal. The β-Zr melts in a peritectic at 1880°C, only 15°C above the melting point of pure β-Zr. The α-Zr undergoes peritectic melting at 1985°C. The only intermediate compound formed appears to be the f.c.c. ZrN phase which has a fairly wide range of homogeneity. Its stability limits are not too certain but seem to be $ZrN_{0.55}$ and $ZrN_{1.0}$.[20,24-27] However, $ZrN_{0.68}$[28], $ZrN_{0.74}$[29] and $ZrN_{0.89}$[30] alloys were found to have respectively at 600, 750 and 1600°C, a two-phase (α + ZrN) structure. Samsonov et al. placed successively the lower limit at $ZrN_{0.67}$[31] and $ZrN_{0.85}$[32] while Gal'braikh et al.[28] are placing it at $ZrN_{0.78}$ at 600°C.

Other nitride forms have been prepared by ammonolysis of Zr halides. Reacting ZrI_4 at 750°C, $ZrBr_4$ and $ZrCl_4$ at slightly higher temperatures, Juza et al.[33] obtained a zirconium nitride Zr_xN ($0.812 < x < 0.91$) dark blue with f.c.c. structure. Under a modified method of ammonolysis they obtained a brown Zr_3N_4.[34] Heating $ZrCl_4 \cdot 4NH_3$ at 900°C in an NH_3 stream Orlovskii et al.[35] prepared a compound with this same formula. At temperatures higher than 1000°C, Zr_3N_4 turns into zirconium mononitride according

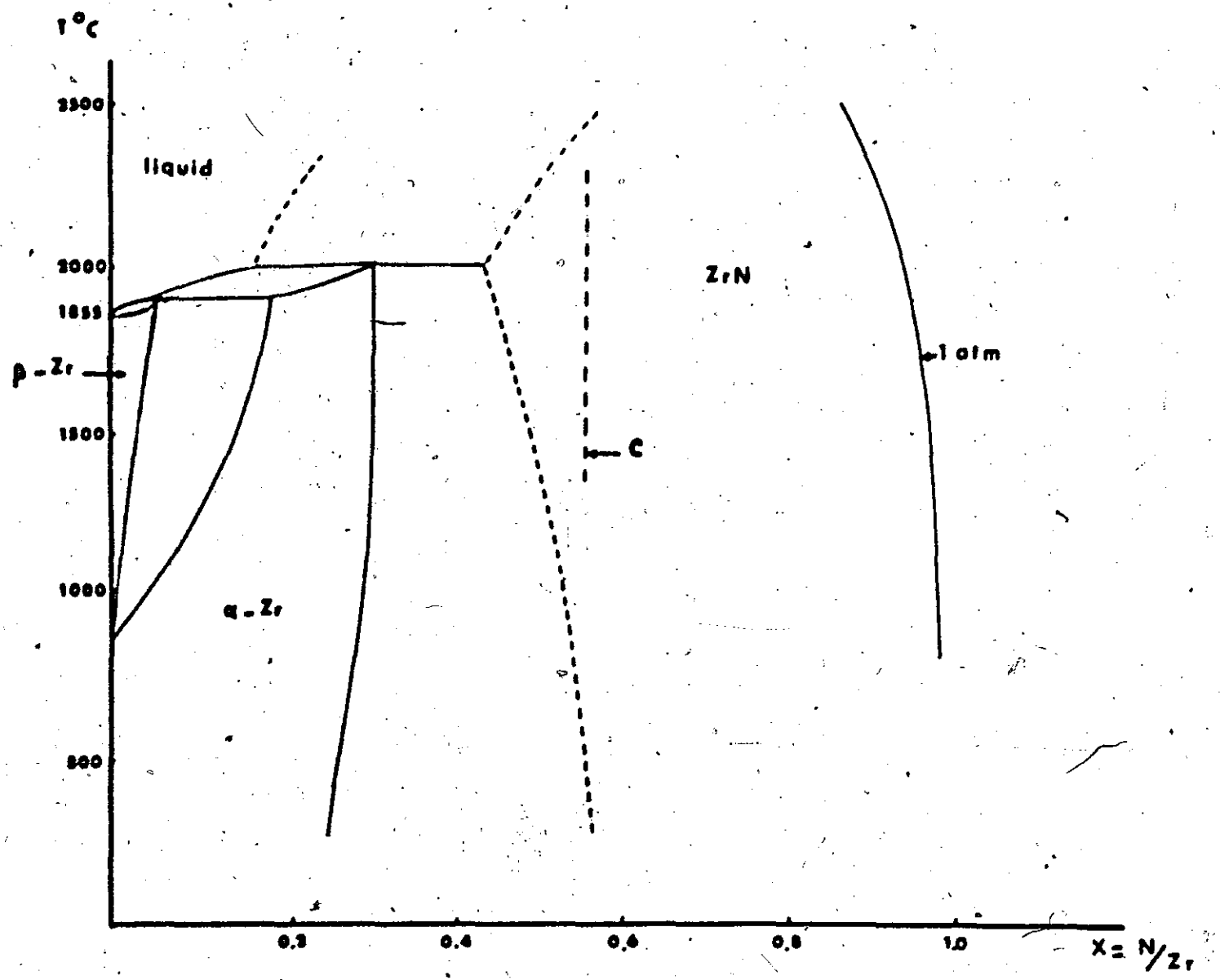

Figure 1 Phase Diagram of the Zr-N System (after Storms[20])

to the following irreversible reaction:

$$Zr_3N_4 \rightarrow 3ZrN + 1/2\ N_2 \qquad (2.1)$$

Neither the relationship between the blue and brown nitrides of Juza nor the influence of oxygen on their stability are well known. They are considered to be unstable with respect to ZrN and N_2 (at 1 atm) but from the work of Collongues et al.[36] and Gilles[37] on the system Zr-O-N it is possible to suggest that these nitrides could be stabilized by the oxide impurities often found in the preparations because of the ease of hydrolysis of the starting or intermediate compounds. Two years before the publication of Juza's papers these authors were led by their results to suppose that the oxynitrides ($ZrO_{2-2x}N_{4x/3}$) obtained from the reaction of zirconium dioxide with ammonia or by solid state reaction between ZrO_2 and ZrN are intermediate phases between zirconia and a hypothetical nitride Zr_3N_4 and not between zirconia and ZrN. Therefore, Zr can apparently exist with nitrogen in an oxidation state between +4 and metallic.

The melting points observed near 3000°C[38-40] apply probably to a congruently vaporizing composition, indicated by C on fig. 1, located somewhere in the low nitrogen region ZrN_{1-x} and not to $ZrN_{1.0}$. Indeed Storms[4,20] showed that pressures in excess of 50 atm must be applied to retain $ZrN_{1.0}$ at this temperature. This makes it very difficult to obtain a true melting point because very few laboratories are equipped to melt this compound under such a pressure. However, recently Eron'yan et al.[41] determined the melting point at nitrogen pressures higher than 60 atm and found a temperature as high as 3700±70°C.

2.3 Bonding

From a chemist's viewpoint ZrN, like most of the mononitrides or monocarbides of transition elements, offers a unique collection of properties to be reconciled, namely

(a) metallic bonding, indicated by electrical conductivity, Hall effect measurements, magnetic properties, appearance (luster), and presence of homogeneity regions,

(b) covalent or ionic bonding suggested by high melting points, hardness and brittleness, and

(c) ionic bonding inferred from chemical behaviour, X-ray emission bands and Mossbauer spectroscopy.

There are numerous contradictory theories of bonding for these phases.[3,8,15,17,18,31,32,42] Several theories have emphasized the metal-nonmetal bonds, others the metal-metal bonding, the interstitial nature of nitrogen, and the role of the nonmetal as a donator of electrons to the metal atoms. In the most recent theories both strong metal-metal and metal-nonmetal bonds are stressed. Even these theories, however, disagree with each other in considerable detail and available experimental evidence is insufficient to distinguish unambiguously between these theories. Nevertheless, certain features of bonding that have been clarified are useful in interpreting physical properties.

In the particular case of ZrN there is good agreement among investigators to say that the bonding is of a mixed type, with both metallic and covalent components, the latter being partially polarized but they do not agree about the degree of bond ionization. Straumanis et al.[43,44] found that the chemical behaviour supports a dominantly ionic model but they

were unable to say to what extent. The nitride Zr_3N_4 which shows non-metallic conductivity is of iono-covalent type with a considerable degree of bond ionization.[34,45,46]

2.4 Defect Structure

Perhaps the most important property of transition-metal nitrides or carbides is their defect structure. Zirconium mononitride is not an exception to the rule.

By comparing X-ray density d_x with experimentally determined density d_p several authors[26,27,43,44] determined the vacancy concentration in both metal and nonmetal lattice sites. Their results, corrected from some conceptual or arithmetical errors found by Storms[20] for Straumanis's papers[43,44] and by Shevchenko[27] for Smagina's work[26] are shown in fig. 2 and 3. The X-ray density was computed assuming a structure with vacant nitrogen sites for $x < 1$ and vacant zirconium sites for $x > 1$. In all the cases data show that $d_x > d_p$. This could be ascribed to the presence of micropores and cracks but this explanation was found not very plausible mainly because all the authors outgassed carefully their powders during the pycnometric determination of the density. The difference was attributed to defectiveness of the metallic sublattice. It can be seen that raising the nitrogen content of zirconium nitride increases the defectiveness of its metallic sublattice, the most complete filling and highest d_p occurring about $x \sim 0.9$. Even at stoichiometry vacancy concentrations as high as 6-7% coexist on both sublattices. However, Yanchur et al.[40] were unable to detect any appreciable difference between d_x and d_p for nitrided platelets of iodide grade zirconium with an oxygen

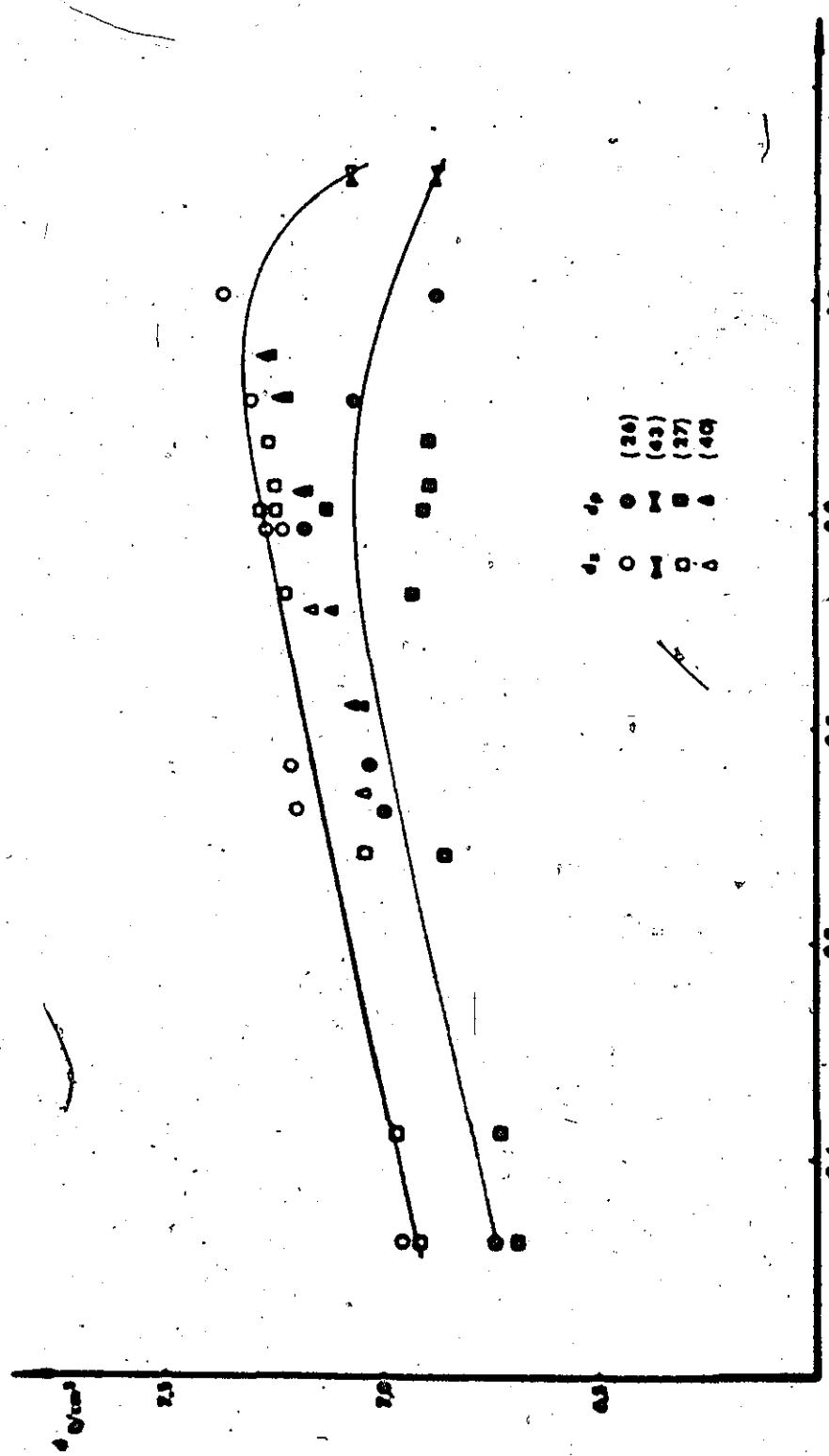

Figure 2 Variation with Composition of the Pycnometric and X-ray Densities

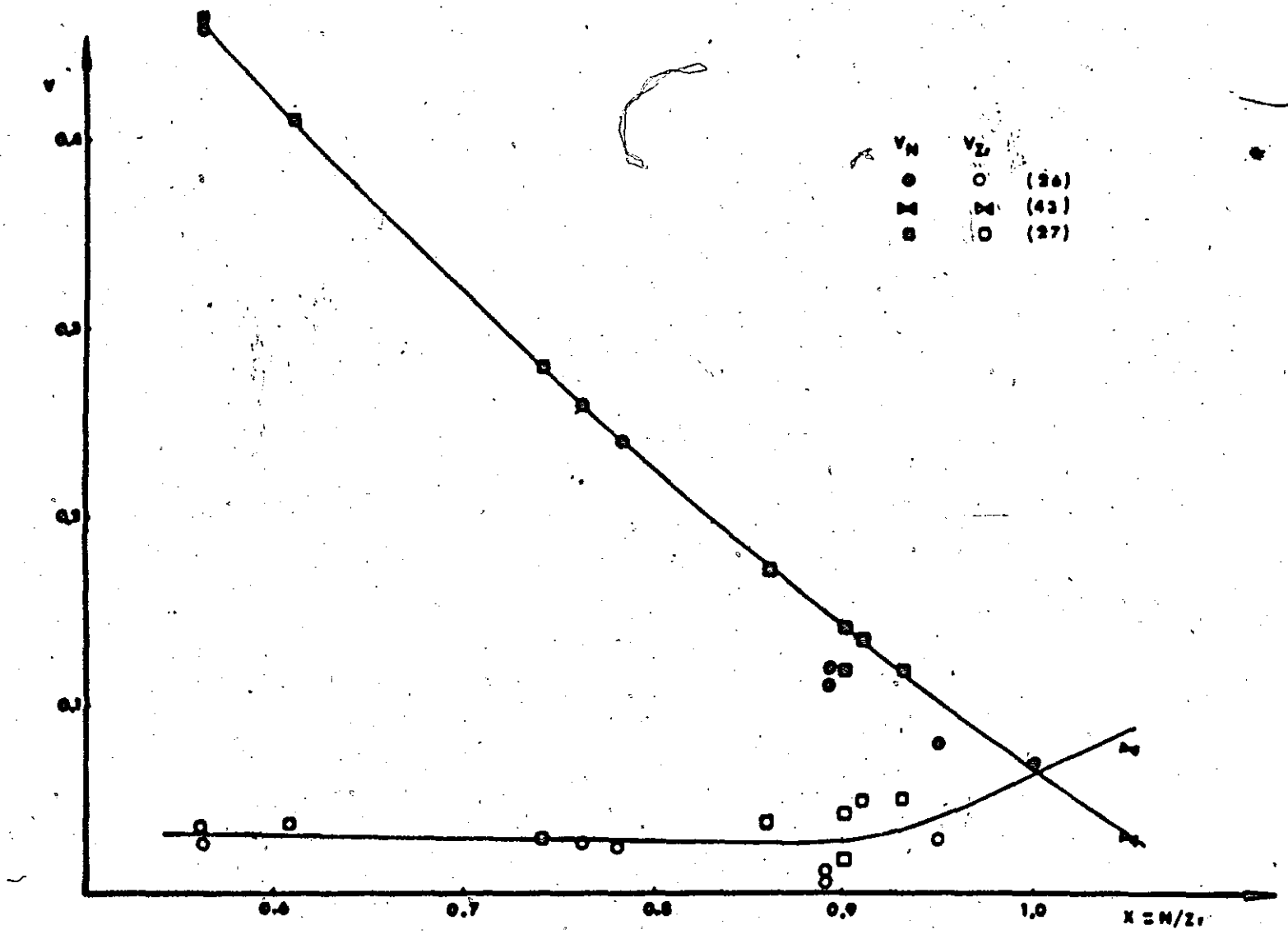

Figure 3 Variation with Composition of the Proportion of Vacant Sites in the Zr and N Sublattices

content less than 0.015%. Together with Shevchenko,[27] by measuring the densities of zirconium nitride powders containing up to 0.2 wt.% O, they have shown that a difference between d_x and d_p is characteristic for samples contaminated by oxygen impurities. These authors are of the opinion that the defectiveness of the metallic sublattice of zirconium nitride is linked with dissolution of oxygen in this compound. Therefore differences between d_x and d_p should vanish as the purity of the material is increased. We will note that the vacancy concentration is difficult to determine because of inaccuracies in measuring the exact overall chemical composition. This being particularly true in the case of mononitrides where nitrogen content can be analyzed only to within 1% (3).

From a bonding point of view Samsonov et al.[32] gave an explanation of the defectiveness of the metallic sublattice in nitrides at stoichiometric composition and of the existence of nitride phases with nitrogen contents in excess of 50 at.%. Some kind of nitrogen-nitrogen interaction resulting in the formation of stable $s^x p^y$ configurations of nitrogen atoms would be responsible for these phenomena.

2.5 Lattice Parameter

As Storms[20] has suggested that the lattice parameter should be used as a criterion of purity in the absence of an oxygen analysis we have plotted as a function of composition some of the values reported in the literature. The line drawn in fig. 4, considered to be characteristic of the variation of the lattice constant of the ZrN phase,[10] was reported by Rudy and Benesovsky.[24] It indicates that the lattice parameter remains constant at about 4.577 Å above $ZrN_{0.78}$ and rises slightly at lower

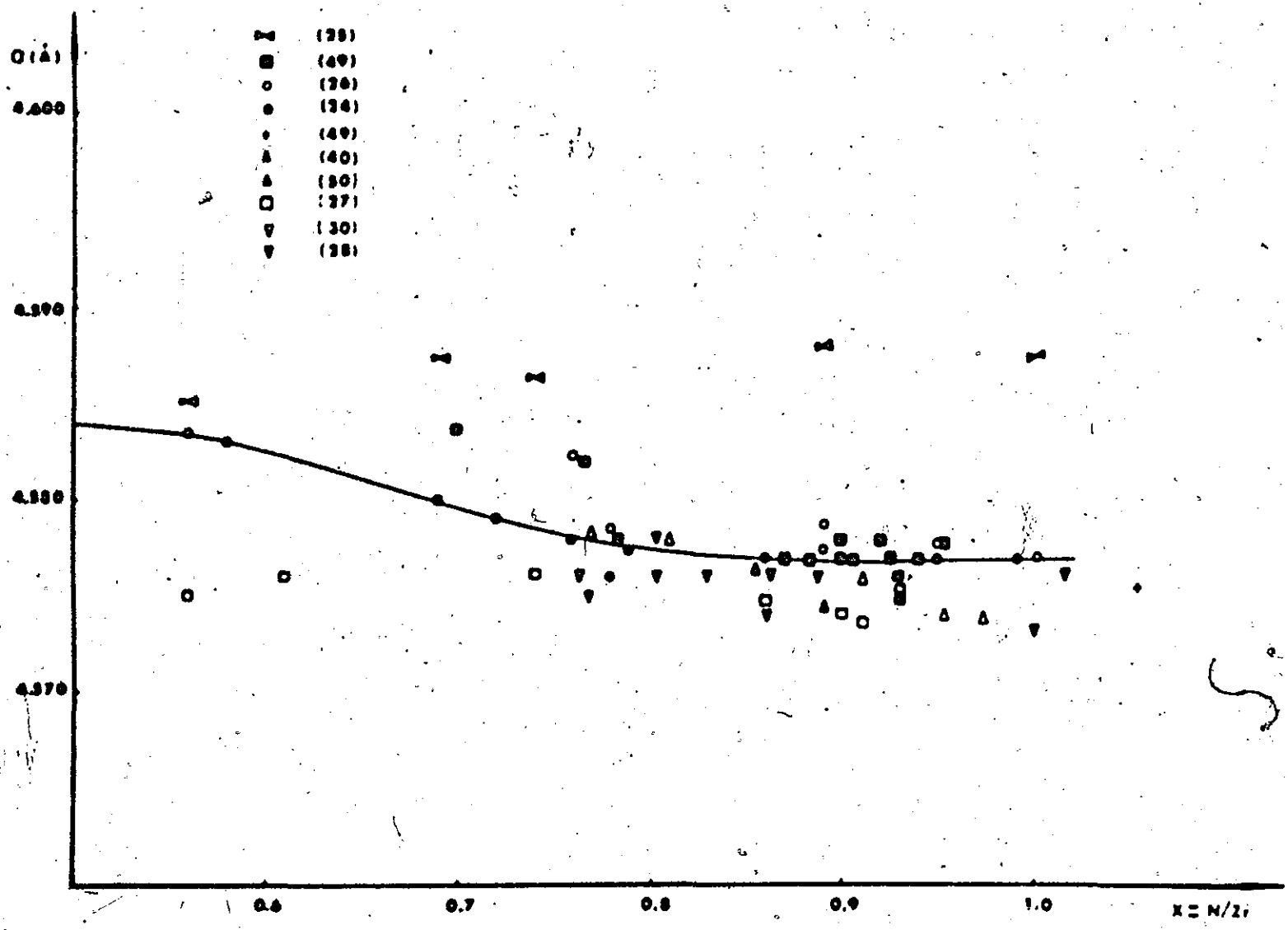

Figure 4 Lattice Parameter of the ZrN Phase as a Function of Composition

compositions to reach the value 4.584 Å at the lower phase boundary $ZrN_{0.55}$. Schönberg[47] found smaller values in the range 4.537 to 4.562 Å and suggested that the values as high as 4.63 Å given by some earlier authors are most likely due to the presence of oxygen in the lattice. Indeed Gilles[45] prepared a solid solution of oxygen in zirconium nitride having 4.65 Å for parameter. However, recently Zainulin et al.[48] showed that despite considerable variations in composition the lattice parameter of the single-phase specimens ZrN_xO_y studied vary only within very small limits from 4.574 (for $ZrN_{0.57}O_{0.29}$) to 4.578 Å (for $ZrN_{0.84}O_{0.09}$). Therefore the lattice parameter seems not to be sufficiently sensitive to the presence of dissolved oxygen to be used as a criterion of purity.

2.6 Physical and Chemical Properties in the Homogeneity Region

One of the significant developments in the understanding of nitrides is an increased awareness of the importance of defect structure on the properties. The presence of a large concentration of vacancies, ordered or disordered, significantly affects properties and therefore nearly all of them depend upon nonmetal-to-metal ratio. Failure to realize these dependencies has resulted in many erroneous literature reports and much confusion about certain properties. We will examine here the main dependencies reported in the case of zirconium nitride.

2.6.1 Appearance

$ZrN_{1.0}$ has a golden yellow color when pure. A lower stoichiometry or impurities lead to a darkening until a dark gray-brown or black color results.

2.6.2 Electrical and Magnetic Properties

The electric resistivity, Hall constant and magnetic susceptibility were found to increase monotonically by decreasing the nonmetal-to-metal ratio (i.e. increasing the total number of vacancies) from 0.972 to 0.770. This points to the absence of any transformation whatsoever within this concentration range.[40] The negative sign of the Hall coefficients means that the current carriers are electrons. Their effective concentration for $ZrN_{0.95}$ is about 5.10^{22} cm^{-3}, i.e. a value characteristic of good conducting metals.[51] According to Yanchur et al.[40] there is also a marked contribution by hole conduction. The resistivity has a positive temperature coefficient[51,57] and the values of the magnetic susceptibility are characteristic of paramagnetic materials.[40,51,53] Even for a given composition large differences appear in reported values. They are probably associated with differing amounts of impurities, particularly other interstitial elements such as oxygen, differing residual porosities and empirical formulas used for correcting this porosity. For example, in the case of the electrical resistivity different values are reported for zirconium nitride obtained by vapor deposition,[51,54,55] powder metallurgical methods[11,12,52,56] or nitridation of zirconium platelets.[40]

For the same reasons different superconducting critical temperatures, T_c, have been observed between 8.9 and 10.7°K.[57,58] They should be considered as lower limits and not characteristic of those fundamental properties which produce superconductivity. T_c decreases with decreasing nonmetal - to - metal ratio, the highest value being associated with the stoichiometric composition.

2.6.3 Thermodynamic Properties

Measurements of the enthalpy of formation, by combustion calorimetry, have shown that this property varies with composition from -56.1 Kcal/mole at $ZrN_{0.56}$ to-87.9 Kcal/mole at $ZrN_{1.0}$ with a slightly positive deviation from a straight line between these limits.[25] Gal'braikh et al.[28] did measurements in a wider concentration range including the nitrogen solid solution in α-Zr. They found a linear relationship with a change in the slope of the straight line at the composition $ZrN_{0.78}$. This change was attributed to the passage from a two-phase (α + ZrN) structure to a single phase (ZrN) structure and explained by a difference in the character of chemical bonding.

Vaporization experiments have been performed by Smagina et al.[49] and Kibler et al.[59] Their work shows that the N_2 pressure varies greatly with composition of the ZrN_x phase. However, considerable disagreement exists between the two workers. Thus, Kibler et al. performed effusion measurements, and Smagina et al. used tensimetric measurements in the higher pressure range of 0.1 to 100 mm Hg. The pressure data obtained by the latter for a range of compositions $ZrN_{0.7}$ to $ZrN_{0.96}$ are considerably higher than the comparable data of the former. Krieger[60] studied the thermodynamics of the zirconium nitride/zirconium-nitrogen vapor system performing calculations on the ablative material ZrN, at 2000-6000°K and 1.5×10^{-7}- 66 atm.

2.6.4 Mechanical Properties

As stoichiometric composition is approached micro-hardness decreases while the modulus of normal elasticity and the flexure strength increases.[40]

According to the authors this effect could be associated with the development of microplasticity which facilitates a certain redistribution and decrease in the stress concentrations.

2.6.5 Chemical Properties

Zirconium nitride is very weakly attacked by HCl, HNO_3 and H_2SO_4 concentrated acids from room temperature to 50°C. When the temperature is raised to 95°C the rate of decomposition increases sharply. The rate also increases with increasing nitrogen content, the lowest rate being observed in the case of nitric acid. ZrN is decomposed congruently by hydrochloric acid and incongruently by sulfuric and nitric acids and solutions of oxidizing agents, liberating elementary nitrogen.[61] Stoichiometric ZrN is stable in both cold and boiling water and weakly dissolved in boiling concentrated alkalies with the formation of NH_3.[10,62] The hydrolysis of zirconium nitride in superheated steam was studied by Kyo et al.[63] They found that the reaction products were H_2, N_2, and NH_3 at 700°C in isothermal reactions and at higher temperatures NH_3 was gradually replaced by N_2.

2.7 Oxidation Resistance

The oxidation resistance of ZrN is generally considered to be poor.[10,11,13,15] It is the main reason why this material has received so little application as a refractory compound despite its relatively high thermal stability. Heated in air at atmospheric pressure powdered zirconium nitride begins to oxidize between 400 and 600°C.[64,65] The change in phase composition in this temperature range is rather controversial. Glasson and Jayaweera[64] reported the formation of metastable cubic ZrO_2 (a = 5.09Å), somewhat stabilized by the remaining cubic ZrN, while Lyutaya et al.[65]

found, at 580°C, an heterogeneous mixture consisting of zirconium dioxide and cubic oxynitride of general formula ZrN_xO_y (a = 4.45Å). At higher temperatures there is only formation of monoclinic zirconia which subsequently sinters above 1000°C. Over 1200°C the oxidation is complicated by the formation of tetragonal ZrO_2. Zirconium nitride has the poorest oxidation resistance of the mononitrides of the fourth group, hafnium nitride having the best.[65] However, the difference is not great. By means of differential thermal analysis it was found that the initial decomposition temperatures are respectively 600, 580 and 650 for TiN, ZrN and HfN. There is no information available for the oxydation of ZrN at reduced pressure but Billy and Teyssedre[66] found an appreciable oxidation of HfN at 10^{-3} torr with the intermediate formation of the body-centered cubic oxynitride Hf_2N_2O. Toth[3] considers that fourth-group nitrides should not be heat treated in vacuums of less than 10^{-6} torr, these phases being best treated in high-purity inert gases.

2.8 Diffusion

In table I are compiled the diffusion coefficients for zirconium nitride that have been reported in the literature. Except for the tracer coefficient of carbon all the available results are for nitrogen diffusion and were evaluated in terms of data from kinetic studies of diffusion controlled reactions. Before discussing these coefficients we will examine the experimental methods used to measure them.

2.8.1 Nitriding kinetics

All the studies have demonstrated that the reaction of zirconium with nitrogen obeys parabolic kinetics.[19,67-74] However, a recent study[75]

of the initial stages of the nitridation, at 1440°C and pressures between 2 and 10 millitorr , has shown that there is an initial linear reaction whose duration is inversely proportional to the square of the pressure and which is followed by a transition to the typical parabolic kinetics. This linear portion corresponds to the reaction of nitrogen with a β-Zr surface and continues while the α-Zr phase is formed, ending when the α-Zr surface saturates and a thin ZrN layer forms. Further reaction proceeds by diffusion of nitrogen through this nitride film probably via the vacancies present in the nitrogen sublattice, reaction of one part of this nitrogen at the nitride-metal interface and dissolution of the other part in the metal substrate. It has been determined that both the nitride growth and nitrogen dissolution in the α-Zr metal at temperatures below 862°, i.e. the α-β transformation temperature, or both the growth of the ZrN and α layers and nitrogen dissolution in β-Zr at higher temperatures obey parabolic relationships. Furthermore Paidassi and Le Delliou[74] found that a very thin oxide film formed on the outer surface of a nitrided sample was a positive replica of the initial surface of the metal. All this indicates that the growth of the ZrN and α layers occurs by the inward diffusion of nitrogen and that this diffusion is the controlling factor in the nitriding mechanism of zirconium.

To analyze the kinetics of diffusion controlled nitridation of zirconium slabs several unidirectional, two-phase ($T < 862°C$) or three-phase ($T > 862°C$), volume diffusion models were proposed.[19,72,74,76] In fact all the models are very similar and based on the same assumptions:

(a) The metal phase is regarded as an infinite plate

(b) The intrinsic diffusivities in the ZrN and α phases are independent of concentration.

(c) The volume changes associated with the formation of ZrN from α and α from β are negligible.

(d) Interfacial equilibrium exists, the concentration at the interfaces can thus be obtained from the equilibrium diagram.

(e) The diffusion of zirconium is negligible in comparison with nitrogen.

Combining weight change and thickness measurements with equations established from the above models Rosa and Hagel,[77] Eremeyev et al.,[78] Levinskii et al.,[79] Paidássi and Le Delliou,[74] and Iyer[19] calculated D_N the intrinsic diffusion coefficient of nitrogen in zirconium nitride. As an example we will examine briefly the analysis of the last author. He simplified the problem by using thin samples. In these thin samples the nitrogen saturation of the β-core is rapid, and the kinetics of the reaction with nitrogen may be viewed essentially as the growth of the α and ZrN layers on a nitrogen-saturated β-core. A further simplification was obtained by studying the nitridation of nitrogen presaturated αZr which results in the growth of a single layer ZrN. The corresponding schematic diagrams of the concentration profile of nitrogen are illustrated in fig. 5a and 5b. In case a, assuming that the nitrogen drop across the ZrN and α-layers follows an error function relation, D_N may be obtained from the equation

$$\gamma \operatorname{erf} \gamma = \frac{(C_{\delta N} - C_{\delta \alpha})\, K_p(\delta)}{\sqrt{\pi}\, K_N} \qquad (2.2)$$

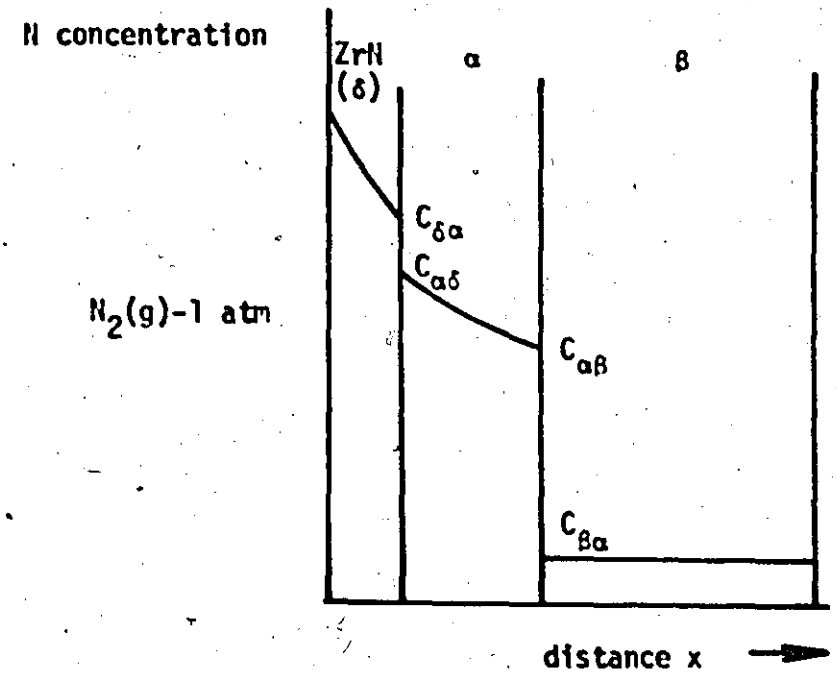

(a) Nitridation of Nitrogen Saturated β-Zr

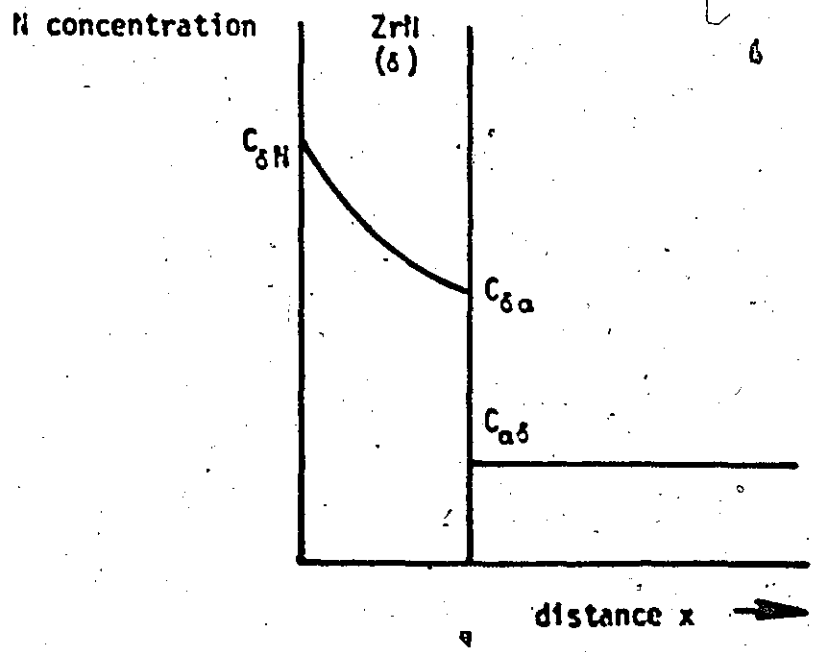

(b) Nitridation of Nitrogen Saturated α-Zr

Figure 5 Scheratic Diagrams of the N Concentration Profile During Nitridation of Nitrogen Saturated β- and α-Zr (after Iyer[19])

where $\gamma = \frac{K_p(\delta)}{2\sqrt{D_N}}$

and $K_p(\delta)$ and K_W are the experimentally determined layer growth and weight gain parabolic rate constants while $C_{\delta N}$ and $C_{\delta\alpha}$ are equilibrium phase boundary concentrations. The corresponding equation for case b is

$$\frac{C_{\delta N}-C_{\delta\alpha}}{C_{\delta\alpha}-C_{\alpha\delta}} = \pi^{\frac{1}{2}}\,\gamma\; e^{\gamma^2}\,\mathrm{erf}\,\gamma \qquad (2.3)$$

or

$$K_W = \frac{2(C_{\delta N}-C_{\delta\alpha})}{\sqrt{\pi}\,\mathrm{erf}\,\gamma} \qquad (2.4)$$

2.8.2 Diffusion saturation

Spivak[80] prepared cylindrical single-phase $ZrN_{0.76}$ specimens, 0.66 mm in diameter, by direct nitridation of zirconium wires at 1700°C for 4 h followed by 8 h homogenizing anneal carried out in argon at 1800°C. Then they studied the nitriding of these specimens over the temperature range 1600-2200°C. From a knowledge of the initial uniform nitrogen concentration, C_0, and the surface concentration C_S supposed constant and presumably equal to the nitrogen - with phase boundary, they estimated the diffusion coefficient D by determining the mean nitrogen concentration, $\bar{C}$, at time t and using the following expression for the specific saturation F:

$$F = \frac{\bar{C}-C_0}{C_S-C_0} = -1 - \sum_{n=1}^{n=\infty} \frac{4}{\xi_n^2}\left(\frac{\xi_n^2\,Dt}{R^2}\right) \qquad (2.5)$$

where ξ_n is the root of the zero Bessel function, and R is the radius of the cylinder.

2.8.3 Sintering Kinetics

Andrievskii et al.[81] studied the sintering of cylindrical wires (d = 0.66 mm) of zirconium nitride of various compositions: $ZrN_{0.96}$, $ZrN_{0.863}$ and $ZrN_{0.683}$. They followed the radius change of the surface of contact (neck) between the wires as a function of time and assuming that sintering aas occurring by volume diffusion they calculated the diffusion coefficient with the following formula.

$$\frac{x^5}{R^2} = \frac{20\sigma a^3}{kT} Dt \qquad (2.6)$$

In this expression x and R are the radii of the neck and of the wire, σ is the surface tension, a the lattice constant and t the time.

2.8.4 Tracer Diffusion

Using serial sectioning and residual activity methods Khromov et al.[82] studied the diffusion of C^{14} in large-grained (grain size ~ 1 mm) $ZrN_{0.95}$. No similar studies have been carried out for zirconium or nitrogen diffusion.

2.8.5 Discussion

In order to facilitate the comparison of the results compiled in table 1 we have plotted, in fig. 6, $\log_{10}D$ versus the inverse of the absolute temperature. The agreement between the data obtained from the two first methods is rather good, mainly above 1100°C, while those calculated from sintering kinetics show higher values of D_0 and Q. The diffusion of carbon in zirconium nitride seems to be slower than that of nitrogen. As we are chiefly interested in nitrogen diffusion we will examine in more detail the results relevant to this type of diffusion.

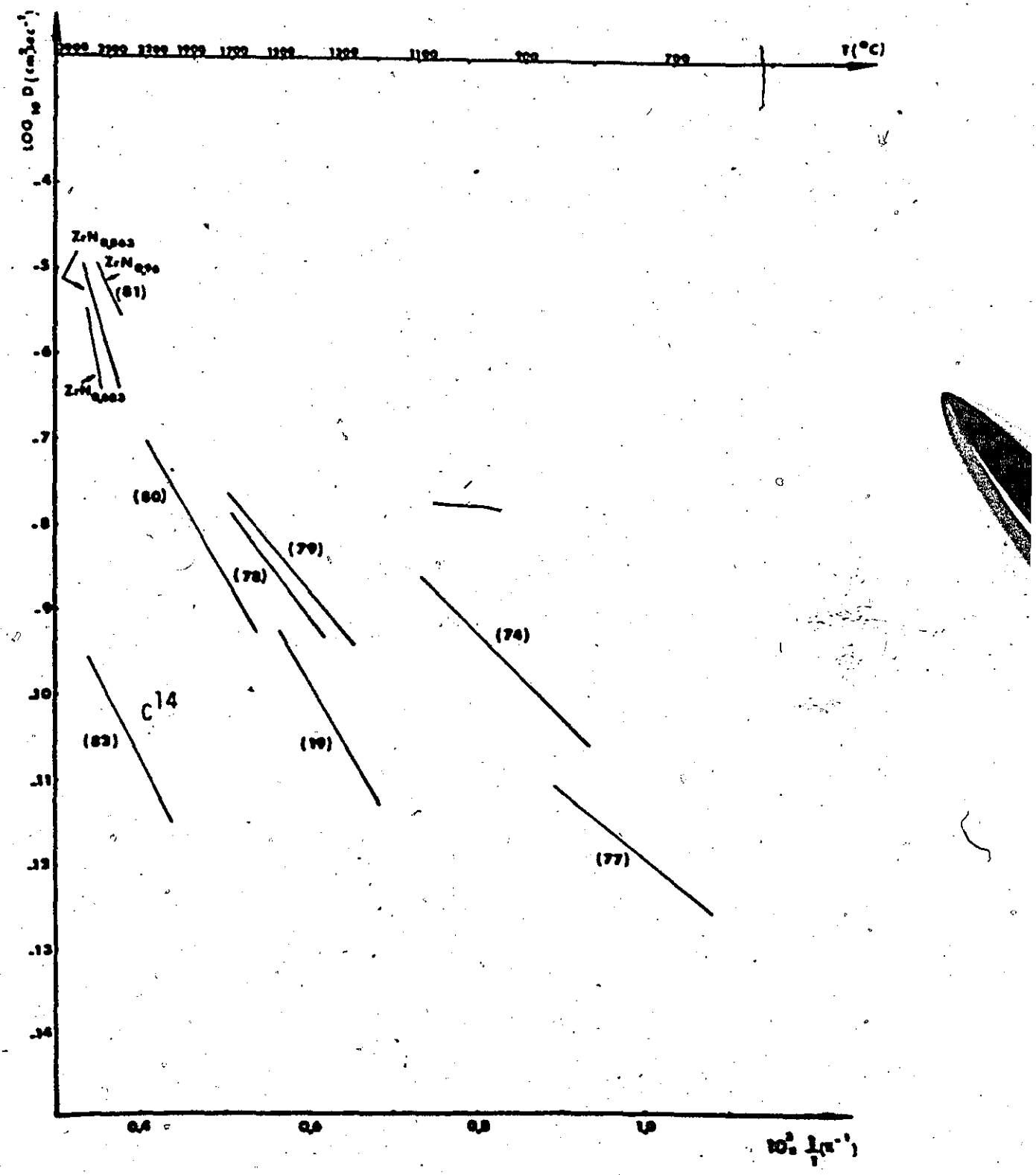

Figure 6 Nitrogen and Carbon Diffusion in Zirconium Nitride as a Function of Temperature

In comparing these coefficients several important points should be emphasized:

(a) All the available data are chemical diffusion coefficients which were measured on polycrystalline samples. In all the methods described above the various mathematical solutions are based on the assumption that isotropic lattice diffusion is the only process that is occurring. In reality diffusion samples contain grain boundaries. Thus it is possible to expect an increasing contribution of short circuit diffusion leading to an apparent decrease of the activation energy at lower temperatures. This effect perhaps explains the relatively low values of Q obtained in the 650-1100°C temperature range.[77,74]

(b) In the computations outlined in section 2.8.1 the intrinsic diffusion coefficient D_N is assumed to be independent of composition. In phases that have a wide range of homogeneity this assumption may not be valid and one might question the usefulness of a concentration-independent value of D_N. However, Iyer[19] showed that a vacancy mechanism predicts that D_N should be essentially independent of composition, while the interstitialcy mechanism predicts a sharp decrease in the pre-exponential factor with increasing vacancy concentration. Diffusion studies in two other transition mononitrides (see following section) TiN and VN support a vacancy mechanism for diffusion of nitrogen. Thus the assumption D_N independent of composition, appears reasonable. This fact has an interesting thermodynamic implication. D_N can be related to the tracer diffusion coefficient D^*_N and the chemical diffusion coefficient $\tilde{D}$ for diffusion of nitrogen atoms and nitrogen vacancies in the nitrogen sublattice.[5,19] Indeed considering that diffusion occurs only on the nitrogen sublattice and taking nitrogen

TABLE I

Diffusion Coefficients for Zirconium Nitride

The diffusivities are expressed in Arrhenius form: $D = D_o \exp(-\frac{Q}{RT})$

Material	Diffusing Element	Temperature Range	D_o (cm^2/sec)	Q (Kcal/mole)	Method	Ref.
ZrN	N	650-850	7.87×10^{-5}	35.9	Nitriding kinetics	77
ZrN	N	1250-1700	6.0×10^{-2}	60.0	-	78
ZrN	N	1260-1720	1.69×10^{-2}	53.66	-	79
ZrN	N	800-1100	2.5×10^{-2}	44.2	-	74
ZrN	N	1200-1500	3.12	79.4±6.0	-	19
$ZrN_{0.76}$	N	1600-2200	7.5×10^{-1}	78.3	Diffusion saturation	80
$ZrN_{0.683}$		2550-2700	3.5×10^{12}	245.0	Sintering kinetics	81
$ZrN_{0.863}$		2400-2750	7.9×10^{5}	150.0	-	81
$ZrN_{0.96}$		2400-2600	2.6×10^{2}	97.0	-	81
$ZrN_{0.95}$	C^{14}	2030-2690	$(1.59^{+0.27}_{-0.22}) \times 10^{-3}$	92.1±0.9	Radiotracer	82

as one component and nitrogen vacancies as the second component in Darken's equation leads to

$$\tilde{D} = [(1-x)\, D_N + x\, D_V] \qquad (2.7a)$$

$$= [(1-x)\, D^*_N + xD^*_V] \left(\frac{\partial \ell n a_N}{\partial \ell n x}\right) \qquad (2.7b)$$

where D_V and D^*_V are the intrinsic and self-diffusion coefficients for vacancies, and x is the nitrogen to metal ratio. If D^*_N is assumed equal to D^*_V, then the preceding equations reduce to

$$\tilde{D} = D_N = D^*_N \left(\frac{\partial \ell n a_N}{\partial \ell n x}\right) \qquad (2.8)$$

This means that the chemical diffusivity is directly proportional to the tracer self-diffusivity and the thermodynamic gradient. Therefore a concentration independent value for D_N implies that an increase of D^*_N with increasing nitrogen-vacancy concentration is cancelled by a corresponding decrease in the thermodynamic gradient. This should be applicable to the chemical coefficient obtained from the diffusion saturation experiments.

(c) In section 2.8.1 it was also shown that the values of D_N depend on precise phase diagram information. Unfortunately the position of the α + ZrN/ZrN phase boundary is not well known. Furthermore, nearly all the authors used the data proposed by Domalga et al.[30] which are considered in error.

(d) The results obtained from sintering kinetics seem to be different in nature than the others due to their high values of D_0 and Q and their concentration dependence. Such high values of activation energy and

pre-exponential terms along with a reduction of the sintering rate with deviation from stoichiometry were also reported in the case of oxides.[83,84] Many explanations were given for these phenomena but none was found completely satisfactory. Using the concepts of the thermodynamics of irreversible processes, Andrievskii[81] obtained an equation for the effective (or mean) self-diffusion coefficient which enters into the sintering equations for volume diffusion transport:

$$D_{eff} \approx \frac{C_1^2 D_1 + C_2^2 D_2}{C_4^2} \qquad (2.9)$$

In this expression C_i are atomic fractions, D_i partial self-diffusion coefficients, and indices 1, 2, 4 refer respectively to metal atoms, metalloid atoms and metalloid vacancies. Due to the lack of information on the partial diffusion coefficients in zirconium nitride it is impossible to obtain a quantitative confirmation of this relationship. However, the fact that an increase of stoichiometry induces an increase of the effective self-diffusion coefficient implies that the above equation is at least qualitatively confirmed.

(e) In conclusion to this discussion we will note that an estimation of the activation energy for self-diffusion of N in ZrN based on volume fluctuation theory gave a value of 81.7 kcal/mole.[19] This result is in good agreement with the majority of the energies measured in the 1200-1700°C temperature range and confirms the exceptional nature of Andrievskii's results as well as the possible influence of high-diffusivity paths at low temperatures.

2.9 Diffusion in Other Binary Nitrides

Diffusion coefficients have been reported in the literature for TiN,[19,78,85-87] VN,[19,88] NbN,[89] Cr_2N,[90] Fe_4N,[91] ε iron nitride phase,[92], ThN[93] and UN.[94-99] All the corresponding values are compiled in Table II except some for UN.[97,99] We will only disucss here the data pertinent to nitrogen diffusion in TiN, VN and NbN because these nitrides have very similar general properties to ZrN. Nevertheless we will note that in the case of UN tracer diffusion coefficients are available for both nitrogen and uranium diffusion. This is an exception in diffusion studies in nitrides.

The only distinctive feature in the nitridation of Ti, V, and Nb compared to that of Zr is the possible formation of an intermediate M_2N nitride layer between the mononitride and the α phase. Nevertheless D_N can be computed in very similar ways to those outlined in section 2.8.1. In addition to nitriding kinetics and diffusion saturation methods a rather new technique was used in the case of TiN[19] and VN.[19,88] Presaturated α-Ti samples or V_2N samples were nitrided between 1200 and 1500°C in the first case and only at 1500°C in the second one. The reaction results in the formation and growth of a single layer of mononitride. The nitrogen gradients across the product layer were determined using an electron-microprobe analyzer. The variation of the chemical diffusivity of nitrogen with the composition of the MN phase was determined from the concentration profile using the following expression:

$$D_N)_{C^*} = -\frac{1}{2} t \left(\frac{\partial C}{\partial x}\right)_{C^*} \int_{C_0}^{C^*} x\,dc \qquad (2.10)$$

TABLE II

Diffusion Coefficients for Other Binary Nitrides

Nitride	Diffusing Element	Temperature Range	D_o (cm^2/sec)	Q (Kcal/mole)	Method	Ref.
TiN	N	900-1520	5.4×10^{-3}	52.0±3.5	Nitriding kinetics	85
TiN	N	1300-1600	4.42	72.8	-	86
TiN	N	1350-1700	2.0x10	90.0	-	78
TiN	N	1200-1450	5.8×10^{-1}	66.7±7.0	-	19
TiN	N		2.29×10^{-3}	50.2	Diff. saturation	87
VN	N	1500	$D_N = 2.5(\pm 0.3) \times 10^{-8}$		Nitriding kinetics	19,88
NbN	N	1405-2035	2.1×10^{4}	112.0	-	89
Cr_2N	N	1200	$D_N = 4.2 \times 10^{-8}$		-	90
Fe_4N	N	504	$D_N^* = 3.2 \times 10^{-12}$		-	91
-	-	554	$D_N^* = 7.9 \times 10^{-12}$		-	
ϵ Fe nitride	N	580-730	4.43×10^{-3}	27.05	Boltzman Matano method	92
ThN		1900-2400	2.54×10^{2}	99.4±30	layer growth	93
UN	N^{15}	1500-1900	2.6×10^{-4}	55.0	N^{15} mass spec.	94
UN	N^{15}	1792	$D_N^* = 8.1 \times 10^{-11}$		N^{15} nucl. activ.	95
UN	N^{15}	1700-2000		~56.0	-	97
UN_{1-x}	U^{233}	1100-1600	3.24×10^{-7}	60.0	α degrad. tech.	96
UN_{1+x}	U^{233}	1420-1830	7.54×10^{-2}	105.0	-	
UN_{1+x}	U^{233}				-	99
UN	N	1800-2400	1.2x10	170±25	layer growth	98

where $D_N)_{C^*}$ is the chemical diffusivity of nitrogen at a concentration C*, and C* is any particular concentration between C_α and C_N , C_o is the concentration of nitrogen in the sample at t = 0, and t is the time. In establishing this formula the outward diffusion of metal was considered negligible in comparison with the inward diffusion of nitrogen. The calculated values of D_N indicated no significant trend in the variation of the intrinsic diffusivities of nitrogen with composition, this result being consistent with a vacancy mechanism of diffusion.[19] Furthermore, the value for the activation energy, in the case of TiN, was found in surprisingly good agreement with the value predicted (65.3 Kcal/mole) using the volume fluctuation model. This value is considerably smaller than the one for ZrN, the diffusivity of nitrogen in ZrN seems to be smaller than in TiN.

In CONCLUSION, in this review of the literature we emphasize the importance of the defect structure of zirconium nitride. This defect structure combined with a wide range of homogeneity and particular bonding is the main feature of this compound. Diffusion seems to occur by a vacancy mechanism in the nitrogen sublattice, i.e. diffusion of nitrogen atoms via octahedral-vacant octahedral site jumps or from an octahedral site to a vacant octahedral site via vacant tetrahedral sites. Due to the high concentration of nitrogen vacancies the rather low diffusivities are surprising. The type of chemical bonding existing in nitrides and a possible effect of oxygen impurities are perhaps responsible for this phenomenon.

CHAPTER III

EXPERIMENTAL TECHNIQUES

This chapter will deal with the preparation and characterization of samples and with the diffusion experiments.

3.1 Sample preparation

Two kinds of zirconium nitride samples were used in this work: spheres, 45-105μ diameter, and platelets 254μ thick.

3.1.1 Preparation of spheres

The spheres were prepared by dropping particles in the 45 to 75μ size range through an electric arc where they melted and spheroidized due to surface tension.

3.1.1.1 Arc assembly description

The arc assembly shown in fig. 7 was used before by Madeyski and Smeltzer[100] for the preparation of zirconia spheres and by Streiff and Smeltzer[7] for the preparation of zirconium nitride spheres. It was equipped with tungsten electrodes and a graphite body in the hot zone, connected to a Vycor glass tube in the lower, cooler part of the furnace. The tungsten electrodes were held by two graphite rods. One of the rods was stationary while the other could be moved manually by means of a fiber glass handle to adjust the length of the arc. Ceramic "Pyro-phyllite" brushings provided electric insulation for the rods. At the lower end, the Vycor tube terminated at a hollow aluminum ring which had one gas inlet tube and 12 outlet

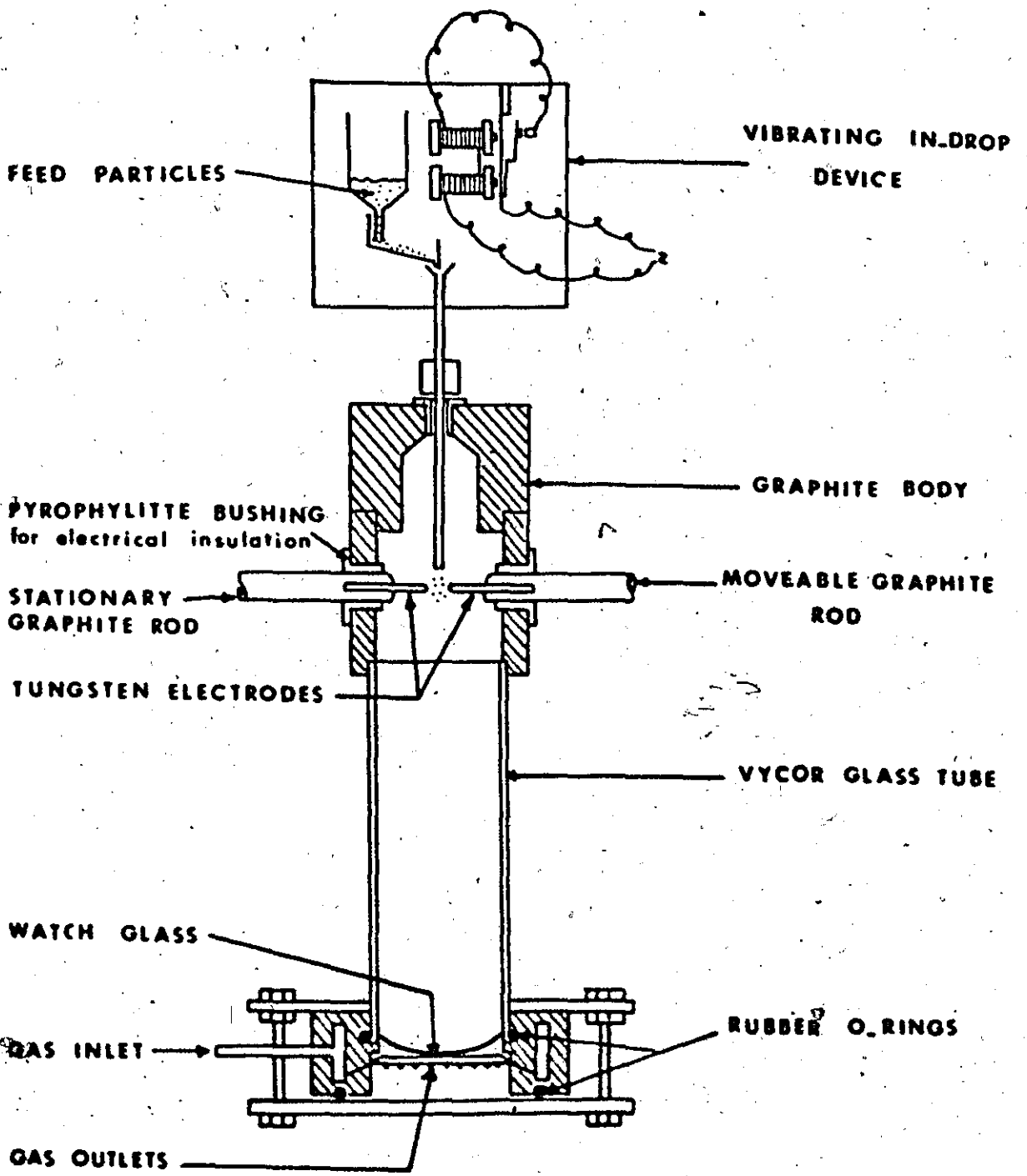

Figure 7 Schematic Cross-Section of the Arc Furnace

orifices providing a uniform distribution of the gas around the internal periphery of the furnace. A flat aluminum disc formed the bottom of the furnace where the spheres and the irregular particles which missed the arc collected in a watch glass after passage through the furnace. The plate could easily be removed to retrieve the watch glass and its content. Two silicone rubber O-rings made the lower part of the furnace gas tight: one between the aluminum ring and the Vycor tube, and the other between the ring and bottom plate. The upper part of the furnace was not gas tight allowing the gas to escape. The powder was introduced by means of a vibrating in-drop device.

3.1.1.2 Arc assembly operation

The operation of the arc furnace was always started by blowing a nitrogen-argon mixture through the bottom of the furnace at a high rate to thoroughly purge the arc region of air. This stage was very important because oxygen, even in small quantities, could react with the nitride during the spheroidization. After a few minutes the flow was reduced to a small rate because an excessive rate of flow interferred with the passage of the powder through the arc or could even blow out the arc. On the other hand, a sufficient flow rate was required to maintain a positive pressure inside the furnace and prevent any introduction of air. Ultra high purity gases (>99.999%) purchased from "Matheson of Canada" were used. As soon as the gas flow rate was reduced the arc was started by simply bringing the electrodes very close together. Then it was drawn to its full operating length of 1.5-2 cm by shifting the moveable electrode. The operating conditions were 100 volts and 10 to 20 amperes. Direct current was used to provide an uninterrupted arc.

A powder charge of approximately 2 grams was put in the reservoir of the vibrating in-drop device and gradually introduced into the arc. Separation of the spheres from irregularly shaped particles which missed the arc was accomplished by dropping the powder on an inverted vibrating watch glass. Particles spread over the glass surface with the spheres rolling free off the edge. The yield, ranging between 5 and 10 w/o, was increased to approximately 25 w/o by recycling the incompletely fused particles through the arc five to six times.

3.1.1.3 Starting material

The starting material was ~99% zirconium nitride powder purchased from "Ventron Corporation - Alfa products". The analytical data given by this company are shown in table III.

3.1.1.4 "Saturation" of spheres

Due to the rather low nitrogen content of the starting material and the possibility of some loss of nitrogen on arc melting[30] the spheres were renitrided for 10 days at 1050°C in the apparatus used for the preparation of slabs and described in the following section.

3.1.2 Preparation of slabs

The slabs were prepared by nitriding zone refined zirconium sheets at high temperature in a nitrogen atmosphere.

3.1.2.1 Description of the nitridation apparatus

Figure 8 shows the schematic arrangement of this apparatus.

The furnace was of the electric resistance type, with a Kanthal A1 element, capable of producing temperatures up to 1350°C. The temperature was controlled at ±1°C by a Honeywell Pyr-O-Vane instrument using a type S (Platinum vs. platinum + 10% rhodium) thermocouple. A thermocouple

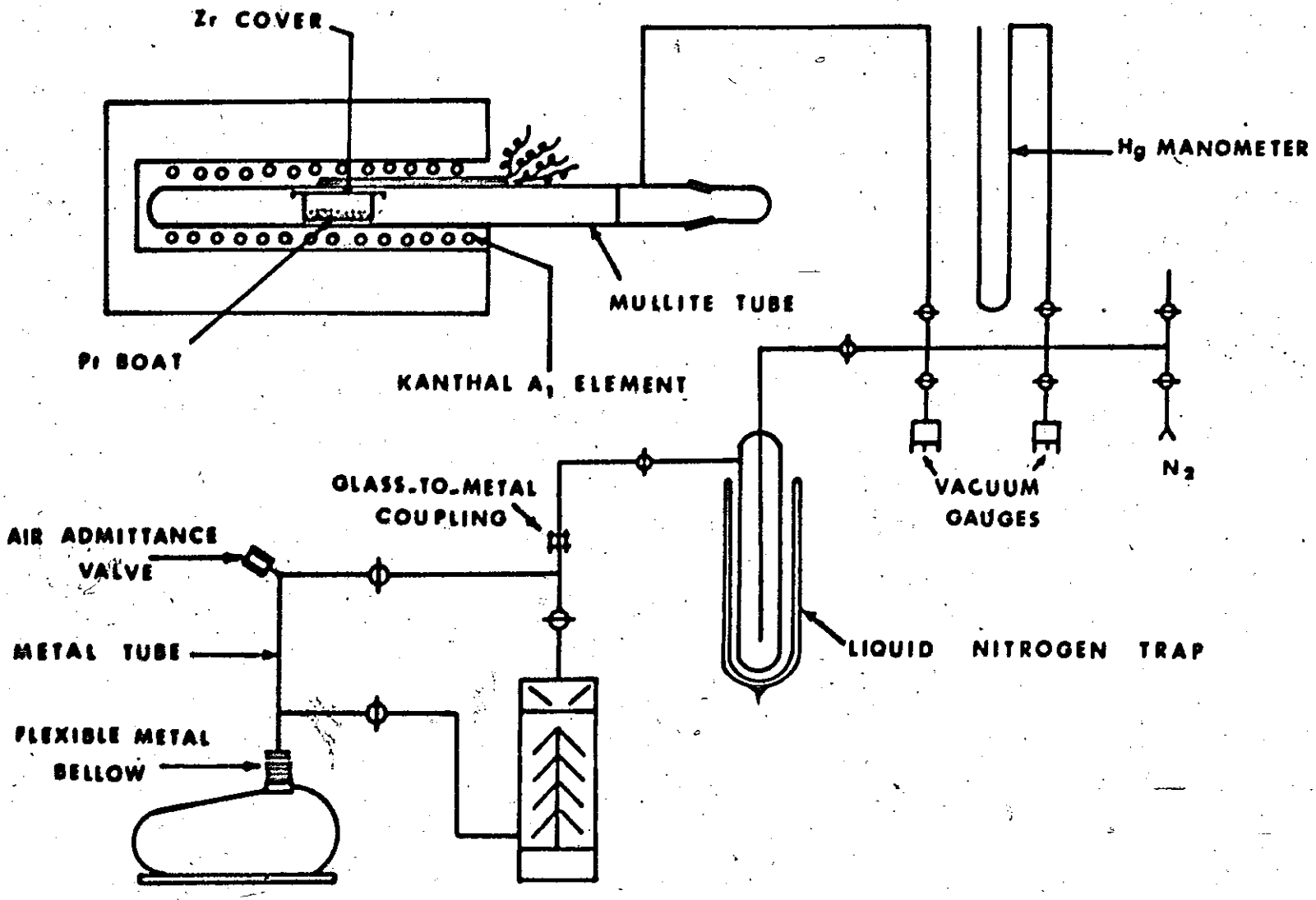

Figure 8 Schematic Diagram of the Nitridation Apparatus

TABLE III

Analysis of the zirconium nitride used for the preparation of spheres

Element	content,* w/o
N	8.76
Fe	0.07
Cu	0.02
Si	0.06
Ca	0.01
Cr	0.06
Ni	0.04
C	(240 ppm)

*After "Ventron Corporation - Alfa Products" (Aldrich Chemical Co. (Canada) Ltd.)

TABLE IV

Analysis of the zone refined zirconium used for the preparation of slabs

Element	content,** ppm
Al	20
Fe	10
Si	5
C	20
O	50
H	5
N	10
Other	10

**After "Atomergic Chemetals Co." (A division of Gallard-Schlesinger Chemical Mfg. Corp.)

potentiometer of P_4 type from "Croydon Precision Instrument", connected to a second Pt-10% Rh thermocouple, was used to measure the temperatures.

The reaction chamber consisted of a mullite tube (MV 30 grade from McDanel Refractory Co.) closed at one end, the other end being directly sealed to a pyrex extension tube connected to the vacuum pumps, a nitrogen supply cylinder, a manometer and two vacuum gauges, a thermocouple gauge NRC 531 and an ionization gauge NRC 518. The cylinder was filled with research purity grade nitrogen (99.9995% min., <1 ppm oxygen) supplied by Matheson of Canada, Ltd. It was equipped with a high purity single stage metal diaphragm regulator from the same company and was connected to the pyrex glass section of the apparatus by means of a "Cajon" ultra high vacuum coupling. "Edwards" vacuum couplings were utilized in the pumping system. In particular a flexible metal bellow removed the vibrations of the rotary pump and a glass-to-metal coupling joined the vacuum system with the rest of the apparatus.

3.1.2.2 Nitridation experiments

The specimens, contained in a platinum boat with a zirconium cover, were introduced at room temperature in the reaction chamber with a metallic rod. The system was purged from air by evacuating it with the mechanical pump and filling it with nitrogen, this operation being repeated several times. Then using the diffusion pump, it was evacuated to about 10^{-4} Torr. Finally the furnace was heated to about 400°C, nitrogen was introduced at a pressure slightly lower than atmospheric and the temperature was brought up close to 1150°C. This temperature was held for four weeks. During all this period a small positive gas pressure was maintained in order to minimize oxygen leakage into the system. The purpose of the zirconium sheet placed

on top of the platinum boat was to getter any oxygen trace diffusing inside the chamber.

3.1.2.3 Starting material

A zirconium sheet 99.995%, 2.54 cm wide x 30.48 cm long x 254μ thick was used. The analysis as supplied by manufacturer is given in table IV. The sheet was cut in pieces 2.54 cm long and approximately 1 to 1.5 cm wide. Before their introduction in the furnace these slabs were chemically polished in a $HF-HNO_3$ bath containing 45 v/o HNO_3 (70%), 5 v/o HF (48%), and 50 v/o H_2O, then they were washed with distilled water and carefully dried.

3.2 Sample characterization

Characterizing nitride samples is a difficult and challenging task not sufficiently appreciated by many investigators. We tried to characterize the most important factors upon which the diffusional properties depend: chemical composition, overall defect structure (including vacancy concentration, grain size and porosity) and sample homogeneity. The techniques used for the characterization of each of these factors are discussed below.

3.2.1 Chemical composition

Our chemical analysis was restricted to the determination of nitrogen and zirconium. Due to a lack of suitable equipment we were not able to determine oxygen. We will note that it was impossible to apply the normal vacuum fusion technique used in the case of metals. To fuse refractory nitrides very high temperatures are necessary, and special techniques are needed, such as fusion in a platinum bath (~ 2000°C) contained in a graphite crucible or fusion in a graphite mold at 2400-3000°C. The evolved oxygen from the sample reacts with carbon to form CO which is collected and analyzed. For the fourth group nitrides, even these techniques are only partially

successful. Stability of oxygen in this group is great, and therefore oxygen is difficult to remove. Neutron activation analysis could be a better technique.[101] We will also note that the detection of impurity phases can be performed using the common Debye Scherrer or diffractometer techniques. However their limit of detection is usually a few percent and can be even larger under certain conditions. For example, impurities such as oxygen form solid solutions with nitrides and therefore failure to observe oxide impurity phase is not complete insurance that contamination has not occurred. Nevertheless, we used systematically these techniques, in particular to check the absence of free zirconium in the samples.

3.2.1.1 Nitrogen analysis

Determination of nitrogen in the refractory nitrides of the metals of groups IIB, VB and VIB has presented difficulties to the analyst. Conventional techniques such as Kjeldahl analysis, vacuum or inert gas fusion, alkali hydroxide fusion were found questionable because incomplete dissolution or decomposition frequently occurred. Sodium peroxide fusions were always complete but partial conversion of the nitrides to nitrogen gas was observed. Dumas method, oxidation or chlorination were found more satisfactory. Due to these difficulties, determination of nitrogen in refractory metal nitrides has been the subject of several investigations.[102-112] Among the different modified methods proposed to improve the validity of results we chose the rapid technique for dissolution of nitrides presented by Bollman.[112] This author showed that a tin(II)-strong phosphoric acid reagent was a remarkable medium for dissolving many transition metal nitrides, zirconium nitride in particular, without loss of nitrogen.

We followed very closely Bollman's procedure. Approximately 100 mg of nitride, 1.5 g of $SnCl_2$, $2H_2O$ and 10 ml of H_3PO_4 are introduced in a 500 ml, long-necked Kjeldahl flask and heated on a hot plate until most of the (free) water has been driven off. Then the flask is heated over a burner until gas evolution nearly stops. During the heating, as well as during the cooling, the flask is swirled to keep suspended the milky phosphates eventually formed. After the solution has cooled, about 100 ml of H_2O, 2 or 3 boiling chips, and 75 ml of NaOH (10N) are added. The flask is immediately joined to a Kjeldahl distillation apparatus and the solution brought to a gentle boil and distilled. One hundred millimeters of distillate were collected in a receiving graduated cylinder containing, originally, 50 ml of 2% boric acid solution with methyl red-methylene blue indicator. The ammonium borate present in the distillates was titrated with a standard

$$NH_3 + HBO_2 \rightleftarrows NH_4^+ + BO_2^- \qquad (3.1)$$

0.1 N HCl solution to the same end point (green to purple). A blank was

$$BO_2^- + H^+ \rightleftarrows HBO_2 \qquad (3.2)$$

carried through the procedure to check for contamination.

3.2.1.2 Zirconium analysis

100 mg samples were calcinated in air or pure oxygen for 24 h at

$$ZrH_x + O_2 \rightarrow ZrO_2 + x/2\ H_2 \qquad (3.3)$$

1000°C. The Zr w/o was deduced from the weight of the white zirconia obtained. The result is only approximate when the samples contain an appreciable amount of metallic or oxygen impurities.

3.2.2 Defect structure

Some types of defects such as porosity and grain size were characterized by metallographic techniques while the vacancy concentration was determined by comparing X-ray density with experimentally determined density.

3.2.2.1 Metallographic observations

Spheres or slabs were mounted in room setting epoxy resin, carefully abraded on 400 and 600 grit silicon carbide papers and polished on 6 and 1μ diamond wheels with kerosene as lubricant. The specimens were then cleaned with petroleum ether and carefully dried. To reveal the grain boundaries, some of them were etched using the HF-HNO_3 solution described in section 3.1.2.3. Specimens were examined with a "Carl Zeiss" optical microscope or with a "stereoscan" scanning electron microscope. The S.E.M. microscope was also used to examine the surface of non-mounted specimens.

3.2.2.2 Lattice parameter measurements

Diffractometer traces were run in the high angle region 1/4° per min on a Norelco diffractometer, using 4° slits and Ni-filtered Cu radiation, and were corrected by means of an external silicon standard. The parameter was calculated on the basis of the (331), (420), (422), (511), and (440) peaks by means of a simple Fortran program run on a CDC 6400 computer and based on the extrapolation method.[113,114] In this program the lattice parameter is computed for each angle and virtually plotted against the chosen extrapolation function $\cos^2\theta/\sin\theta$. The intercept for $\theta = \pi/2$ of the least squares straight line gives the "error-free" value of the lattice constant. The 95 percent confidence limits and the correlation coefficient were also calculated.

In some cases the Debye-Scherrer method was used. The powder photographs were taken with a 114.6 mm diameter Philips camera. The film was mounted according to the asymmetric (or Straumanis) method. In this arrangement the film is split halfway between the points where the direct beam enters and leaves the camera. The complete diffraction record from 0 to 90°θ is recorded on the same film strip and the presence of pairs of arcs about the θ= 0° and θ = 90° positions enables their location on the film with utmost precision. The lattice parameter was calculated as above but in this case the extrapolation function introduced in the program was $1/2(\cos^2\theta/\sin\theta + \cos^2\theta/\theta)$, this function giving linear plots down to small values of θ.[113,115-118]

3.2.2.3 Density measurements

A 2 cm^3 pycnometer (specific gravity flask) was employed. The specimens were weighed at the same temperature in air and in xylene. The sample-xylene mixtures were outgassed under vacuum by vigorous mechanical vibration and the density of xylene was determined with boiled distilled water. Three measurements were done for each specimen.

3.2.2.4 Vacancy concentration calculation

We will explain here, in a more detailed way than in section 2.4, how the vacancy concentration can be evaluated for both sublattice sites from lattice parameter and density measurements.

We will consider the case where the atomic ratio x = N/Zr is less than 1 and assume a 100% occupancy of metal sites. The X-ray density is given by the expression:

$$d_x = \frac{nM}{N a^3} \quad (g/cm^3) \qquad (3.4)$$

where M = Molecular weight = 91.22 + x . 14.0067(g)

N = Avogadro number = $6.0225 \cdot 10^{23}$

a = lattice parameter (cm)

n = Number of metal atoms in the unit cell = 4 for the NaCl-type structure.

Assuming that the difference between d_x and the pycnometric density d_p can be ascribed to defectiveness of the metallic sublattice rather than to the presence of closed micropores or voids, we can write the following equation

$$d_p = \frac{N'M}{N a^3} \tag{3.5}$$

where N' is the real number of metal atoms in the unit cell. The proportion of vacant sites in the Zr and N sublattice defined as

$$V_{Zr} = 1 - \frac{n'}{n} \tag{3.6a}$$

$$V_N = 1 - x\frac{n'}{n} \tag{3.6b}$$

can be directly calculated from the densities. By comparing the equation (3.4) and (3.5) it is easily found that

$$\frac{n'}{n} = \frac{d_p}{d_x} \tag{3.7}$$

Therefore

$$V_{Zr} = 1 - \frac{d_p}{d_x} \tag{3.8a}$$

$$V_N = 1 - x\frac{d_p}{d_x} \tag{3.8b}$$

The measurements of a (or d_x) and d_p must occur at a constant nd known temperature. If their expansion coefficients are not known, the determinations must be made at the same temperature.

3.2.3 Sample homogeneity

Sample homogeneity, particularly in the case of the nonstoichiometric nitrides, can be a problem because of the slow diffusion rate of nitrogen. The sharpness of the splitting of $k_{\alpha 1}$ and $k_{\alpha 2}$ lines of Debye-Scherrer X-ray patterns can be used to indicate the homogeneity. However, we preferred the electronprobe microanalysis technique.

An Acton (Cameca MS-64) microprobe was employed in measuring the concentration profile of zirconium across samples mounted and polished as for microscopic observation. In this method, the weight concentration C_A of an element A in a compound AB is deduced from a comparison between the intensity of a suitable characteristic X-ray line of element A, emitted under given conditions of electron bombardment, and the intensity of the same characteristic radiation when emitted by the pure element A under the same electron bombardment conditions. Indeed, K_A^m, the measured ratio of these intensities corrected for instrumental effects such as the background count rate on either side of the line being used and the loss in count rate due to the dead time of the counter, is equal to a rough approximation to C_A. It is possible to calculate C_A more accurately from K_A^m by using the correction factor concept.[119] This concept assumes that K_A^m is equal to C_A times a series of correction factors for atomic number, Z, absorption, A, and fluorescence, F.

$$K_A^m = C_A Z A F \qquad (3.9)$$

In the present study a computer program was written to obtain a table of C_A and K_A^m corresponding values in the concentration range of interest. The calculations were worked from right to left (i.e. from C_A to K_A^m) because

working in this sense avoids the necessity for iteration. No fluorescence correction was necessary because the Kα characteristic radiation of nitrogen was not able to excite the α characteristic radiation of zirconium used in the analysis. The correction factors Z and A were taken from Birks' book.[119] They are due respectively to Duncumb and Reed[120] for atomic number and Philibert[121] for absorption (modified by Duncumb and Shields[122]).

The intensities of the Zr $L\alpha_1$ (λ = 6.070Å) peak were monitored, at 3μ steps scanning a cross section, using a mica spectrometer and a proportional counter. The electron beam voltage was 15 keV and the take-off angle 18°.

3.3 Diffusion Experiments

3.3.1 Method

The nitrogen diffusion rates were determined by observing the decrement of the ^{15}N isotope concentration in an ambient isotopically enriched nitrogen atmosphere over spheres or slabs of zirconium nitride at constant temperature. The solution of Fick's equation for the diffusion of a solute from a limited and constant volume of well-stirred gas into a solid of known geometry has been given by Carman and Haul[123] and Crank.[124] The following solution is valid for diffusion into a sphere of radius a with the assumption of an instantaneous phase boundary reaction

$$\frac{M_t}{M_\infty} = 1 - \sum_{n=1}^{\infty} \frac{6\lambda(1+\lambda)}{9(1+\lambda)+\lambda^2 q_n^2} \exp - \frac{q_n^2 Dt}{a^2} \qquad (3.10)$$

where:

M_t = amount of solute taken up by the solid at time t

M_∞ = amount of solute the solid would take up in infinite time

t = elapsed time (sec)

D = diffusion coefficient (cm^2/sec)

a = radius of the sphere (cm),

λ = ratio of the number of gram-atoms of nitrogen in the gas phase, ng, to that in the solid, ns,

q_n = one of the non-zero, positive roots of $\tan q_n = 3 q_n/(q_n^2\lambda+3)$.

The corresponding solution for a slab of thickness 2ℓ is

$$\frac{M_t}{M_\infty} = 1 - \sum_{n=1}^{\infty} \frac{2\lambda(1+\lambda)}{1+\lambda+\lambda^2 q_n^2} \exp - \frac{q_n^2 Dt}{\ell^2} \qquad (3.11)$$

where the q_n's are the non-zero, positive roots of $\tan q_n + \lambda q_n = 0$.

Because of the nature of these equations, the diffusion coefficient D as a function of M_t/M_∞ must be obtained by numerical or graphic methods. Carman et Maul[123] developed approximations which are more suited to calculations.

The approximate equation for a sphere is:

$$\frac{C_t-C_s}{C_g-C_s} = \frac{\gamma_1}{\gamma_1+\gamma_2} \operatorname{eerfc} \frac{3\gamma_1}{\lambda} \sqrt{\tau} + \frac{\gamma_2}{\gamma_1+\gamma_2} \operatorname{eerfc} \frac{-3\gamma_2}{\lambda} \sqrt{\tau} \qquad (3.12)$$

where $\gamma_1 = \frac{1}{2}[(1 + \frac{4\lambda}{3})^{\frac{1}{2}} + 1]$, $\gamma_2 = \gamma_1 - 1$

$$\tau = \frac{Dt}{a^2}$$

and C_t, C_s and C_g represent the atom fraction of ^{15}N ($^{15}N/(^{14}N + ^{15}N)$) in

the atmosphere at time t, in the solid at time zero (taken as the natural abundance 0.0037) and in the atmosphere at time zero, respectively.

$$\text{eerfc } x \equiv \exp x^2 \text{ erfc } x = \exp x^2 (1 - \text{erf } x)$$

$$\text{erf } x = \text{error function in } x = \frac{2}{\sqrt{\pi}} \int_0^x e^{-y^2} dy$$

For a slab the approximate expression has a simpler form:

$$\frac{C_t - C_s}{C_g - C_s} = \text{eerfc } \frac{\sqrt{\tau}}{\lambda} \qquad (3.13)$$

where $\tau = \frac{Dt}{\ell^2}$

As noted above, all these equations are valid only when the phase boundary exchange occurs at such a high rate that isotope equilibrium between the gas and the solid

$$^{15}N^{15}N_{gas} + Zr^{14}N_{surf.} \rightleftarrows {}^{14}N^{15}N_{gas} + Zr^{15}N_{surf.} \qquad (3.14a)$$

$$^{14}N^{15}N_{gas} + Zr^{14}N_{surf.} \rightleftarrows {}^{14}N^{14}N_{gas} + Zr^{15}N_{surf.} \qquad (3.14b)$$

surface is immediately established, diffusion in the solid being rate determining. If a phase boundary reaction proceeding at a limited rate is superimposed on the diffusion in the solid, both processes are therefore determining for the progress of isotope exchange and it is necessary to derive new solutions. The usual criterion for a surface exchange limitation is a curvature of a τ vs. time plot or if the curvature is too small, any offset from the origin of an extrapolated line through the experimental points.[125,126] Edwards et al.[125] derived expressions for diffusion from a limited volume into solids of spherical and plane sheet geometry

assuming that the gas-solid surface reaction contributes to the overall rate. For spherical geometry the equation is:

$$\frac{M_t}{M_\infty} = 1 - \frac{2(1+\lambda)}{3\lambda} \sum_{n=1}^{\infty} \frac{q_n^2 \, e^{-q_n^2 \frac{Dt}{a^2}}}{F\left(\frac{q_n^2 Q}{9} + \frac{1}{\lambda}\right) + F^2 + q_n^2 E^2 - \frac{2E}{\lambda}} \qquad (3.15)$$

where the symbols different from those in equation (3.10) are:

q_n = one of the non-zero, positive roots of $\tan q_n = \frac{q_n E}{F}$

$E = \frac{1}{\lambda} - \frac{Q}{9} q_n^2$

$F = \frac{1}{\lambda} + \frac{QN}{9} q_n^2$

$N = \frac{3}{Q} - 1$

$Q = \frac{DS}{K}$

S = surface-to-volume ratio ($=\frac{3}{a}$ for a sphere)

K = rate constant of the surface exchange reaction in cm/sec.

For plane sheet symmetry the corresponding expression is:

$$\frac{M_t}{M_\infty} = 1 - \frac{2(1+\lambda)}{\lambda} \sum_{n=1}^{\infty} \frac{e^{-q_n^2 \frac{Dt}{\ell^2}}}{T^2 + q_n^2 + T + \frac{2}{\lambda}} \qquad (3.16)$$

where the q_n's are the non-zero, positive roots of

$$\tan q_n = \frac{q_n}{T} = \frac{q_n}{Q q_n^2 - \frac{1}{\lambda}}$$

Approximate expressions for (3.15) and (3.16) were stated, without derivation, by Haul et al.[127-129]

3.3.2 Diffusion apparatus

The diffusion apparatus was a slightly modified version of the one used for oxygen diffusion studies in zirconia by Hadeyski, Poulton, and Smeltzer.[130-132] The reaction chamber of the apparatus is shown in Fig. 9 and an overall diagram of the system is given in fig. 10.

The diffusion chamber consisted of a platinum - 10 w/o rhodium alloy tube, 20 mm in diameter, and 380 mm log, closed at the lower end and attached to a glass tube by means of a graded seal at the upper end. The glass tube could be connected to the vacuum manifold, ^{15}N reservoir, ^{14}N cylinder, to a 500 cm^3 calibrated bulk or to the sample collector, as required, by opening corresponding stopcocks. The use of the calibrated bulb was to measure the volume of the chamber (237.5 cm^3). The top of the glass tube carried a ground glass joint whose upper part contained two glass winches for lowering or raising a platinum crucible with zirconium nitride specimens and a quartz crucible with oxygen gettering zirconium nitride powder. The platinum crucible, suspended on a thin platinum wire, was 12 mm in diameter and 15 mm high. The quartz crucible, also held with a platinum wire, was only 8 mm in diameter.

The platinum tube was located inside a ceramic tube made of gas impervious mullite (MV 30 from McDanel Refract. Co.). This outer tube could be connected to the vacuum manifold or argon cylinder as necessary. A glass winch was fixed on the pyrex extension in order to lower or raise an oxygen gettering zirconium foil. The ceramic tube was filled with ultra high purity argon (99.999% min.) at the same pressure as nitrogen inside the platinum tube to prevent the collapse of the thin Pt alloy wall and to

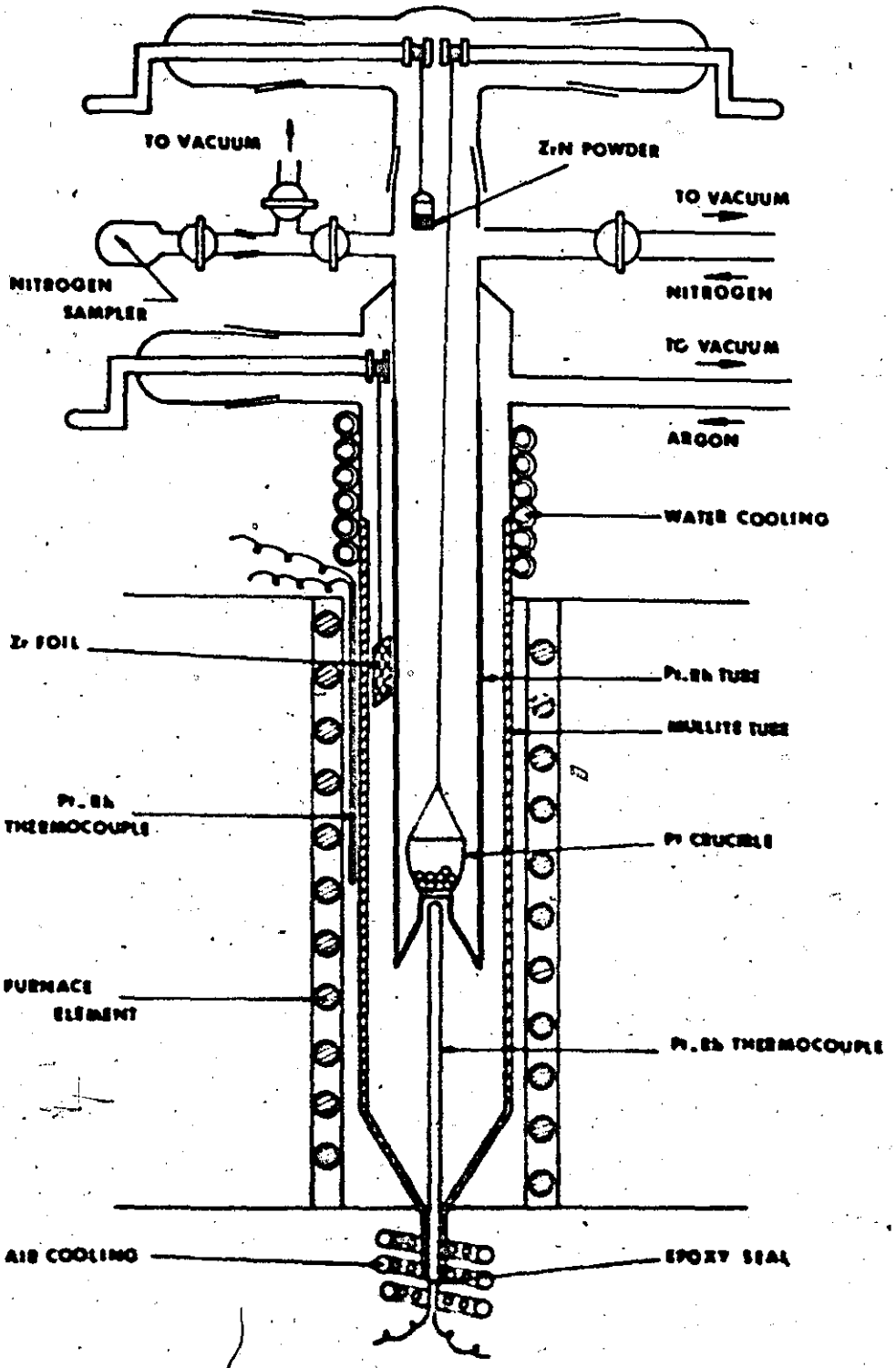

Figure 9 Schematic Diagram of the Reaction Chamber of the Diffusion Apparatus

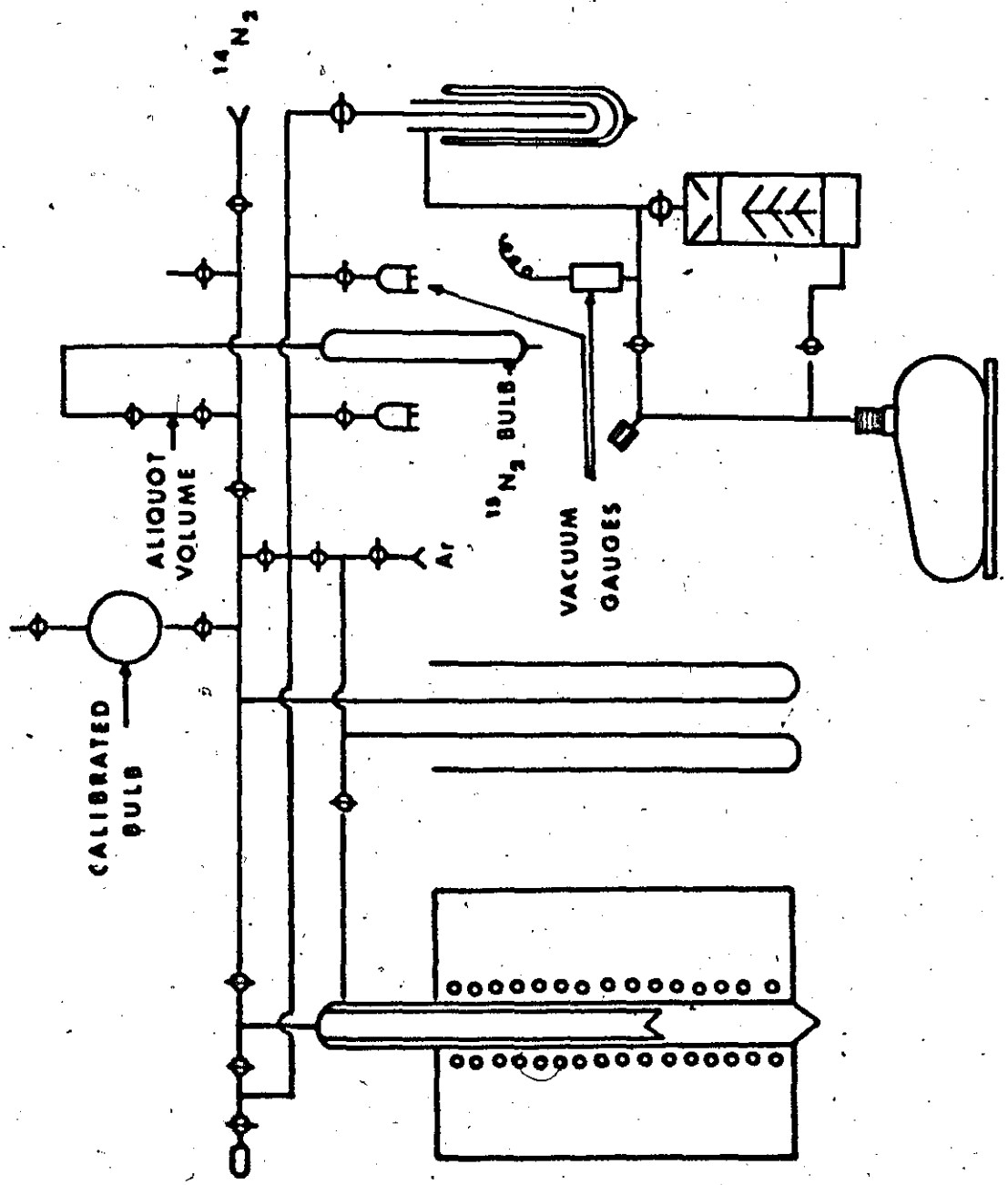

Figure 10 General Schematic Diagram of the Diffusion Apparatus

decrease the possibility for transfer of contaminants such as oxygen or nitrogen, from the atmosphere into the diffusion anneal chamber. The gas pressures inside the two tubes were measured with mercury monometers.

Both tubes were inside a 2500 watt electric resistance furnace with a Kanthal A1 element and vermiculite insulation. The furnace 48 cm diam. x 58 cm high, was supported on a moveable counter-weighted platform for easy lowering and removal for repairs. The temperature inside the furnace was measured and controlled (to within ±1°C) by two "S" type (Pt vs. Pt-10% Rh) thermocouples, one being connected to a Honeywell Pyr-o-Vane temperature controller with a range of 600 to 1300°C and the other to a thermocouple potentiometer.

The actual temperature of the specimens was measured by a third thermocouple whose hot junction was located in a special well almost touching the crucible in its normal position during the diffusion (see Fig. 9). The graded seals between the platinum tube and glass, and between the mullite tube and glass, as well as the glass tube just above the furnace were cooled by means of a cold water-carrying lead tubing wrapped around them.

3.3.3 Nitrogen exchange measurements

The quartz and platinum crucibles, each containing about 500 mg of zirconium nitride, but respectively in the form of powder and spheres or slabs, were introduced in the upper part of the reaction chamber. The diffusion system was evacuated taking the same precautions as in the nitridation experiments (see section 3.1.2.2). Aliquots of 94 atom % ^{15}N enriched nitrogen (Merck, Sharp and Dohme of Canada Ltd.) were introduced into the inner chamber to raise the pressure to 10-15 Torr. Sufficient normal nitrogen

(Research grade, 99.9995 % min.) was admitted at room temperature to give a pressure of about 260 Torr when the system was heated to the diffusion temperature. Argon was introduced in the outer chamber at a slightly smaller pressure. The furnace was then brought up to 880-850°C and the quartz crucible as well as the zirconium foil were lowered into the furnace. This temperature was held overnight allowing the ZrN powder and the Zr foil to getter any residual oxygen traces in the nitrogen or argon atmospheres. The following day the temperature was increased up to the diffusion temperature (1000-1200°C), the quartz crucible raised and the chamber isolated from the rest of the system. The zirconium sheet was also slightly raised to maintain its temperature in the 800-1000°C range. Two one cm^3 gas samples were collected to measure the initial ^{15}N atomic ratio in the gas phase, C_0. Immediately afterwards the Pt crucible was gradually lowered into the hot zone temperature within 15 minutes, the zero time being taken when the crucible reached the bottom of the chamber. Eight to eleven gas samples were collected at suitable time intervals over a period of 24 h. After the end of the exchange run the specimens were cooled in the furnace and the gas samples were analyzed with a mass spectrometer.

3.3.4 Mass spectrometric analyses

The analyses were performed on a Hitachi Perkin Elmer RMU-6A mass spectrometer, at a sample pressure of 2 to 4 x 10^{-7} torr, a low electrode voltage of 15 V, an emission of 70 μA and on the sensitivity scale x 10. A strictly constant room temperature was maintained. The peaks 28 ($^{14}N_2$), 29 ($^{14}N^{15}N$), 30 ($^{15}N^{15}N$), 32 ($^{16}O_2$) and 40 (^{40}Ar) were recorded on a strip chart at a scanning speed of 4 or 5. The ^{15}N concentration was calculated

as $^{15}N/(^{14}N + ^{15}N)$ where ^{15}N is equal to the sum $h_{30} + 1/2\ h_{29}$ and ^{14}N to $h_{28} + 1/2\ h_{29}$, where the h's stand for peak heights measured in cm. To compensate for fluctuations in the instrument six duplicate measurements were made for each sample and the change in ^{15}N concentration was obtained from a probability plot of the average values and the 95% confidence intervals versus time. The peaks 32 and 40 were recorded to check for any oxygen or argon contamination of the gas samples.

3.3.5 Computation of the diffusion coefficient

The equations (3.12) and (3.13) developed by Carman and Haul[123] respectively for spheres and slabs were used to compute the diffusion coefficient from the results of the mass spectrometer analyses. These calculations were performed with a computer, the above error functions being solved for each point by means of successive approximations with the help of their derivative. To reduce the number of iterations approximate values of τ, obtained from an enlarged plot[133,134] of $\frac{C_t - C_s}{C_g - C_s}$ vs. $\sqrt{Dt}/a'\lambda$ ($a' = a/3$ or ℓ), were given to the computer. The calculated values of τ were plotted for each run vs. sampling time in order to determine if the exchange rate was controlled by diffusion or by a slow surface reaction. We will see in the next chapter that it was possible to reject this second eventuality and compute D from the slope D/a^2 or D/ℓ^2 of the best straight line describing the data.

The values of $\log_{10} D$ at various absolute temperatures T were then plotted against $10^3/T$ and the "best" straight line was determined with the least square method using again a computer. The 95% confidence intervals of the frequency factor D_o and the activation energy Q of the Arrhenius equation $D = D_o \exp - \frac{Q}{RT}$ were obtained as well as the correlation coefficient.

CHAPTER IV

RESULTS AND DISCUSSION

In this chapter the results obtained from the various experimental tests for each sample geometry will be first presented in the form of graphs, tables and photomicrographs. Then the diffusion results will be discussed and compared with those available in the literature.

4.1 Results for spheres

4.1.1 Preparation

A batch of 5.827 g was prepared and renitrided for 10 days at 1050°C. After this renitridation, a 1.79% weight increase was measured and a color change from brown yellow to golden yellow was observed. The spheres were passed through Tyler Sieves with openings of 210, 149, 105, 75 and 45μ. The majority of them remained on the two last sieves. Therefore only the spheres in the diameter ranges 45-75μ (average d = 60μ) and 75-105μ (average d = 90μ) were used for diffusion experiments.

4.1.2 Characterization

Powder photographs and diffractometer traces contained only the characteristic lines of zirconium nitride proving the single-phase structure of the material.

4.1.2.1 Composition

The 60μ and 90μ diameter spheres were analyzed separately. The results of the analyses (Table V) indicated that these spheres consisted of substoichiometric zirconium nitride, ZrN_x, with x situated approximately

halfway between the limits of the homogeneity region of this compound.

TABLE V

Chemical composition of the spheres

d(μ)	N(w/o)	Zr(w/o)	N+Zr(w/o)	N/Zr(Atomic ratio)
60	10.12	89.07	99.19	0.74
90	9.76	89.61	99.37	0.71

4.1.2.2 Metallographic examination

Examination of the surface of the spheres showed that in general they were not cracked and had a smooth surface with only a few irregularities (Fig. 11a). However, some were faceted (Fig. 11b and 11c) or wrinkled (Fig. 11d) perhaps because of a beginning of sintering or superficial oxidation.

Non-etched cross-sections (Fig. 12a) presented a rough surface but as we were unable to obtain surface finish by polishing we wonder if this is attributable to some internal porosity or to the brittleness of zirconium nitride. Etching revealed a dense network of grain boundaries delimiting grains of variable size in the 5 to 15μ range (Fig. 12b). The polycrystalline nature of the spheres was confirmed by X-ray diffraction photographs taken of a few spheres with a precession camera using Zr-filtered Mo radiation.

4.1.2.3 Vacancy concentration

The lattice parameter and the experimental density were measured on 60μ spheres at 23°C. Density measurements were carried out on a rather low sample weight (590 mg) which resulted in appreciable fluctuations in the values.

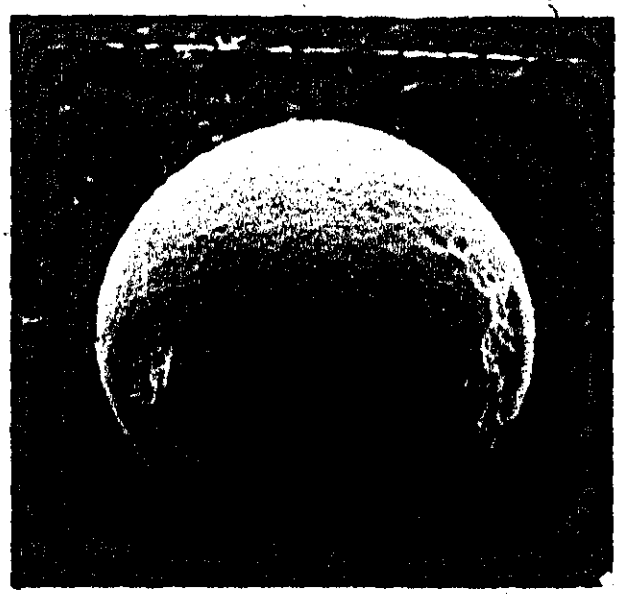

X700
(a)

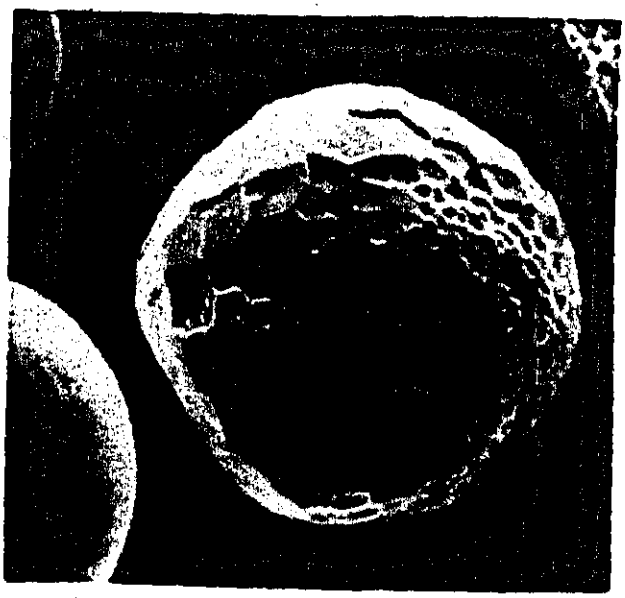

X700
(b)

X700
(c)

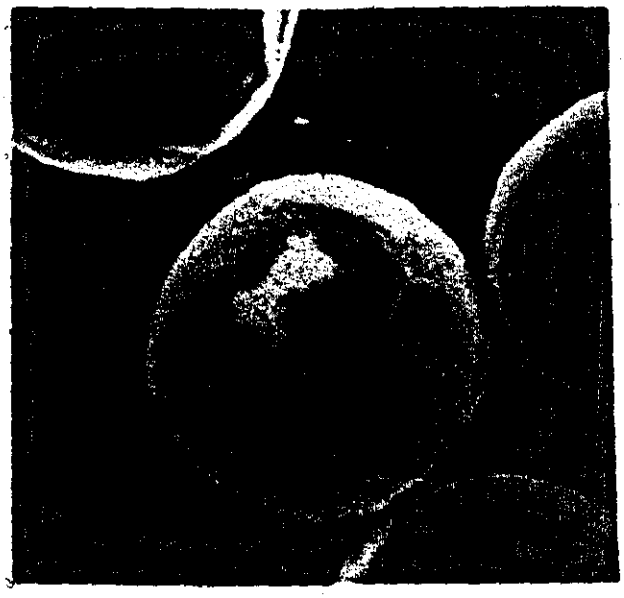

X700
(d)

Figure 11 Scanning electron micrographs of the surface of spheres before diffusion annealing

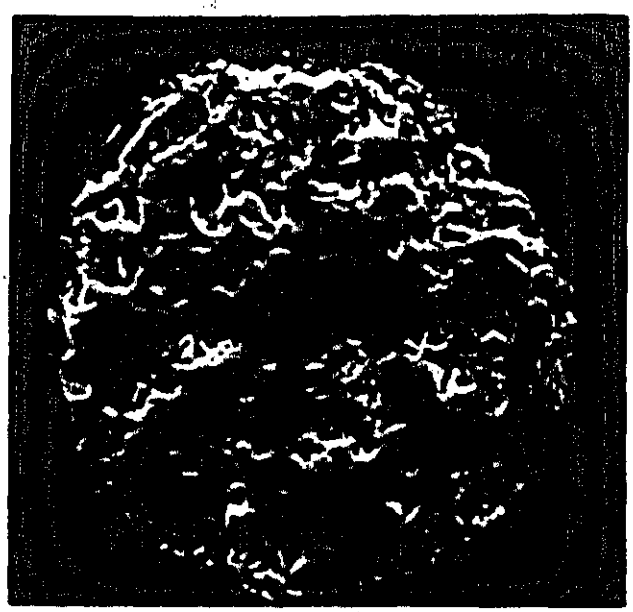

X700

(a)

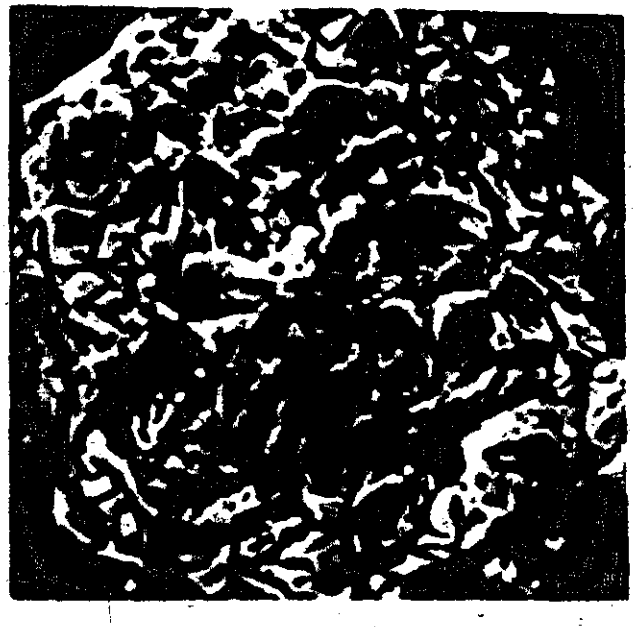

X1400

(b)

Figure 12 Cross-section of spheres before diffusion annealing: (a) unetched; (b) etched.

The average of six measurements (6.71, 6.73, 6.90, 6.81, 6.87 g/cm^3) gave the final result shown in Table VI along with the values of the lattice parameter, the X-ray density, and the corresponding vacancy proportions.

TABLE VI

Vacancy concentration in 60μ spheres at 23°C

d_p(g/cm^3)	a(Å)	d_x(g/cm^3)	V_{Zr}(%)	V_N(%)
6.80±0.08	4.578±0.002	7.03	3.3	28.4

The errors indicated for d_p and a give the 95% confidence interval for these quantities. According to section 2.4 the difference between d_p and d_x (~3%) is too large to be attributed only to the presence of structural defects such as closed micropores and cracks. It is more likely due to the defectiveness of the metallic sublattice linked with dissolution of oxygen in this compound.

4.1.2.4 Homogeneity

Microprobe analysis was made difficult by the bad finish of the surface of the cross-sections. However the results revealed no appreciable change of the zirconium concentration except perhaps near the edges where it decreased slightly, indicating the possible existence of a thin outer layer (a few microns) richer in nitrogen. The concentrations measured with the microprobe were in good agreement with those determined by chemical analysis but they fluctuated from one sphere to another, in the 87.5-91.5 w/o range, showing the existence of some chemical heterogeneity. This was not confirmed by powder photographs which exhibited sharp splitting of the K_{α_1} and K_{α_1} lines for angles greater than 45°.

4.1.3 Diffusion results

All the numerical information concerning each of the five runs performed respectively at 1000, 1053, 1101, 1147.5, and 1203°C are listed in tables A1 to A5 in the appendix. They were reproduced as given by the computer. In these tables, x is equal to $(C_t-C_s)/(C_g-C_s)$, YAP and DAP are approximate values of TAU (τ) and D(cm^2/sec) obtained by graphical means, as explained in section (3.3.5), and used to reduce the number of iterations (ITER). The calculations were made with constant LAMBDA (λ) because this factor was not corrected for the change in n_s caused by the decrease in pressure due to the removal of the gas samples needed for the mass spectrometer analyses. All the ^{15}N concentrations, C_t, C_s and C_g, are multiplied by 100 and are expressed in percent. The quantities n_g and n_s are expressed in milligram-atoms.

For all the runs C_g was maintained in the 4.357-7.604% range and λ was kept approximately equal to 1 (1.0923-1.2061). A smaller value of λ might be preferred in order to increase the change in the isotopic concentration of the gas during a run. However, to decrease λ it would have been necessary to lower the gas pressure or increase the sample weight, these changes both having important disadvantages. Thus gas diffusion through a thick bed of spheres might become rate controlling and low pressures could facilitate the inward diffusion of oxygen through the reaction chamber walls. With the chosen value of λ the overall change in C_t for a run ranged from 2.1 to 4.7%. As the change from one sample to another was small the analyses were very sensitive to any fluctuation of the mass spectrometer and the results showed some scatter. Nevertheless, using probability plots as explained in section (3.3.4) it was possible to evaluate the isotopic depletion in a satisfactory way as the relative errors in the measurements, computed from

the 95% confidence intervals, were small (0.61-0.86%). Two blank runs carried out at 1000 and 1100°C without spheres showed that no appreciable exchange occurred so that it was not necessary to correct the data for background effects.

The diffusion coefficients, computed from the mass spectrometer analyses, were nearly constant during the first half of the run (~12 h) and then decreased. Plots of Dt/a^2 vs. time revealed two regions, one linear portion corresponding to the first period and a curved portion corresponding to the second. In figure 13 the linear parts of these plots are shown. Except perhaps at 1053 and 1101°C they do not exhibit any appreciable offset from the origin. Accordingly, we assumed that nitrogen diffusion was the rate determining process in the isotopic exchange and computed the diffusion coefficients from the slope (D/a^2) of the best straight lines. The average values (AV) obtained in this way are listed in table A6 along with the 95% confidence limits (LCL = lower confidence limit, UCL = upper confidence limit) and error (ERD) and the standard deviation (SDEV). This table gives also the corresponding values of $\log_{10} D$ as a function of the inverse of the absolute temperature. A plot of these values and the best straight line fitted by the method of least squares are shown in figure 14. All the data pertinent to this fit can also be found in table A6 where B1 and B2 are the intercept and the slope of the regression line and D0 and Q are the preexponential factor (cm^2/sec) and the activation energy (cal) of the following Arrhenius equation:

$$D(cm^2/sec) = (2.97^{+18.76}_{-2.56}) \times 10^{-10} \exp(-(23{,}000 \pm 5{,}400)/RT) \qquad (4.1)$$

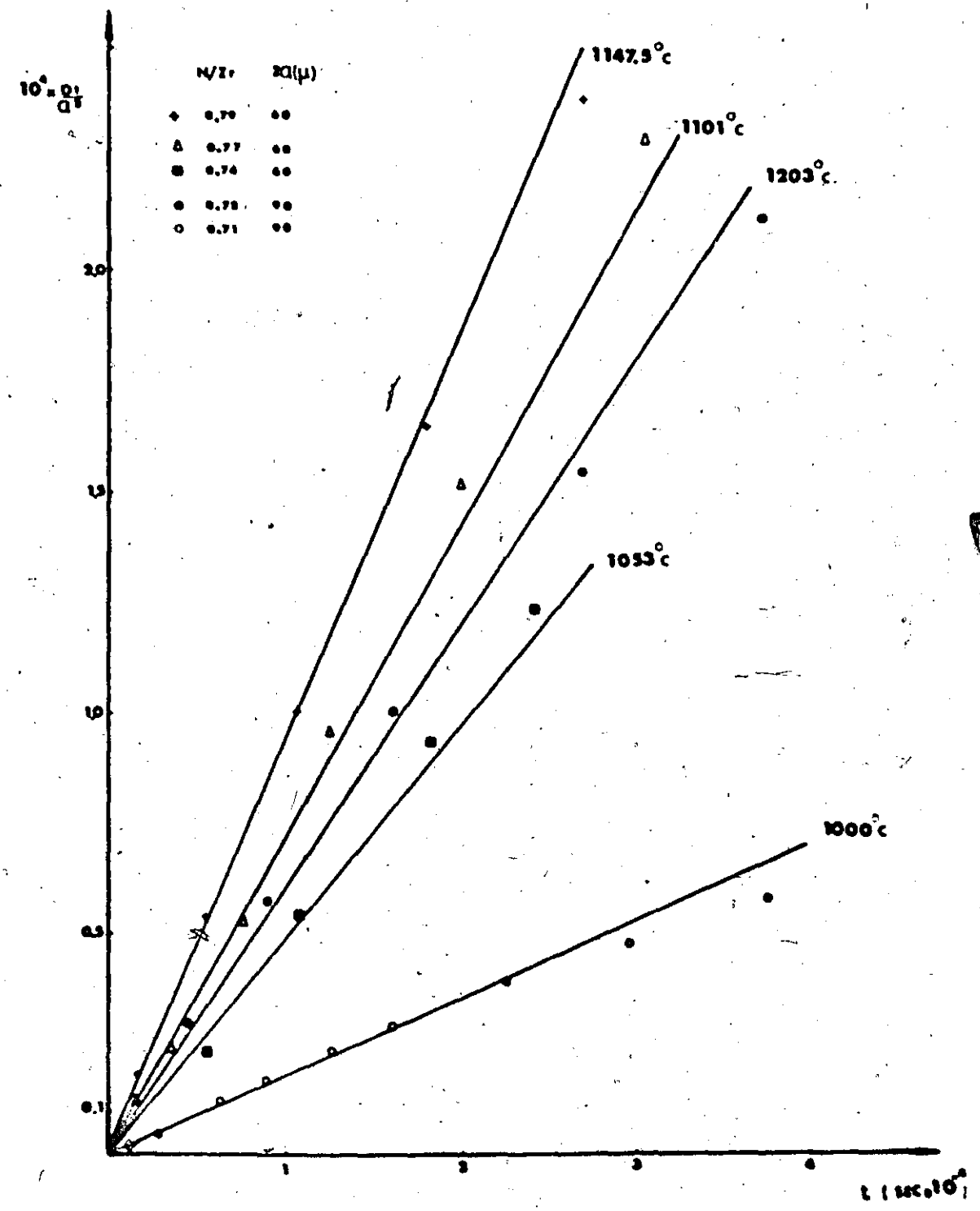

Figure 13 Experimental results for nitrogen diffusion in zirconium nitride spheres

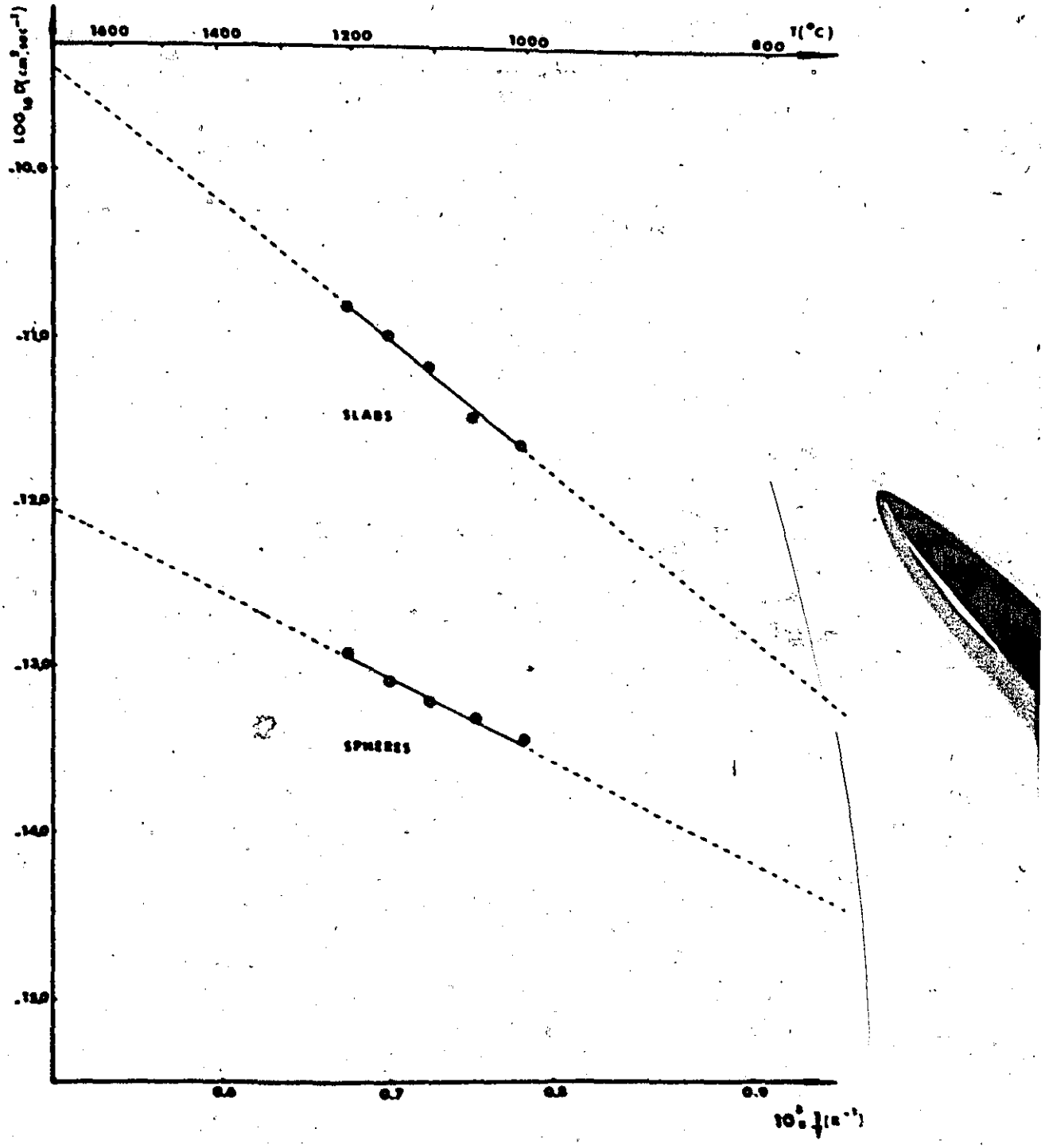

Figure 14. Arrhenius plots of nitrogen diffusivities in zirconium nitride

As shown in figure 13 or in tables A1 to A5, 60μ spheres were used at 1053, 1100 and 1147.5°C and 90μ spheres at the two extreme temperatures. In addition, before the runs at 1101, 1147.5 and 1203°C the samples were annealed in the nitridation apparatus for 2 days at these temperatures and under a 220 Torr nitrogen pressure. This was probably an error because this annealing increased the N/Zr ratio up to 0.79 in the case of 60 spheres and 0.78 for 90μ spheres. During the diffusion annealing itself the samples increased in weight (0.28 to 0.75%). Also, a few superficial layers of spheres took a brown greyish color and became attached to each other, this second effect increasing in intensity with temperature. Examination of the surface of the greyish spheres showed (Fig. 15) the presence of cracks at the limits of polygonal facets. One possible explanation of this phenomenon is the formation of an oxide film causing an increase in volume and subsequent cracking of the surface to relieve the stresses involved.

The sphere (a) on figure 15 could show the initial step of this oxidation process. Surprisingly, despite the agglomeration observed, no evidence of neck formation was found. Powder photographs contained no new lines but diffractometer traces obtained at high sensitivity showed a small extra peak corresponding to the 100 peak of monoclinic zirconia. The spheres located under this layer exhibited unchanged surfaces and gave the initial diffractometer trace. Therefore the observed oxidation was limited to a very thin superficial layer. The more troublesome aspect of this phenomenon is surely the agglomeration of the spheres because it could decrease the volume of the pores between them and, by extension, the gaseous exchange between the internal spheres and the ambient atmosphere.

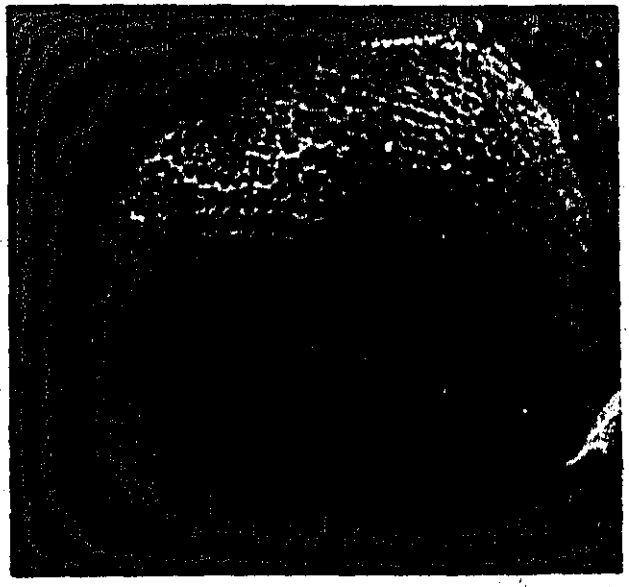

X1400

(a)

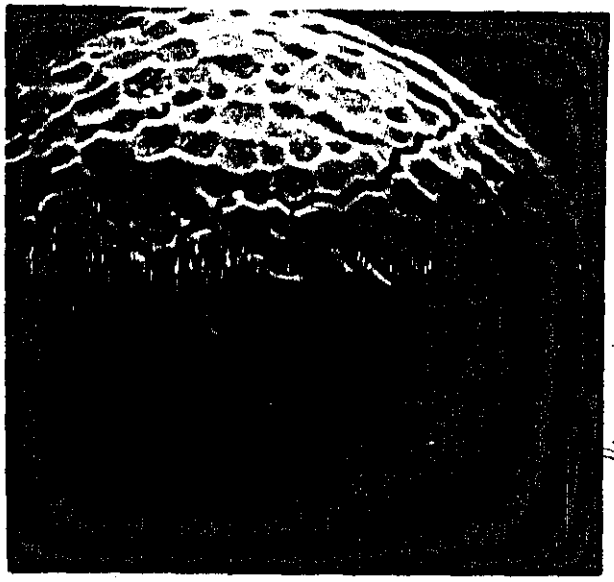

X1400

(b)

X1400

(c)

X1400

(d)

Figure 15 Scanning electron micrographs of the surface of spheres after the diffusion annealing at 1050°C

4.2 Results for slabs

4.2.1 Preparation

In two preliminary runs we obtained samples of overall composition $ZrN_{0.39}$ and $ZrN_{0.71}$. The first (Fig. 16a) was prepared by nitridation at 1000°C for 21 days and the second (Fig. 16b) for 10 days at 1050°C plus 14 days at 1100°C. X-ray diffraction traces of the surface gave in both cases the characteristic pattern of zirconium nitride but after grinding the principal peaks of α-Zr appeared, proving the two-phase structure of these slabs i.e. an outer layer of zirconium nitride appearing badly polished on the micrographs, and an α-Zr core (See Fig. 16). This structure was confirmed by electronprobe microanalysis. The zirconium concentration was found nearly constant in the core and equal to 97.3 ±1.1 w/o in case a and 92.8 ±1.2 w/o in case b. We will note that these concentrations correspond respectively to the α and α + ZrN regions of the Zr-N phase diagram. The zirconium profile in the zirconium nitride scale was very irregular due to the bad surface finish, however the general trend was a decrease (from the inside to the outside) to a composition close to stoichiometric. Nitridation at a temperature of 1150°C for at least 4 weeks yielded single phase samples. We were not able to work at higher temperatures because the Pt crucible was sticking strongly with the mullite tube. All the samples used in the diffusion experiments were prepared at the same time by nitriding 11 g of zirconium.

4.2.2 Characterization

4.2.2.1 Composition

The composition was determined by two means, weight change and chemical analysis. Table VII shows that these two methods gave very similar results. We will note that the N/Zr ratio found here is closer to 1 than the one

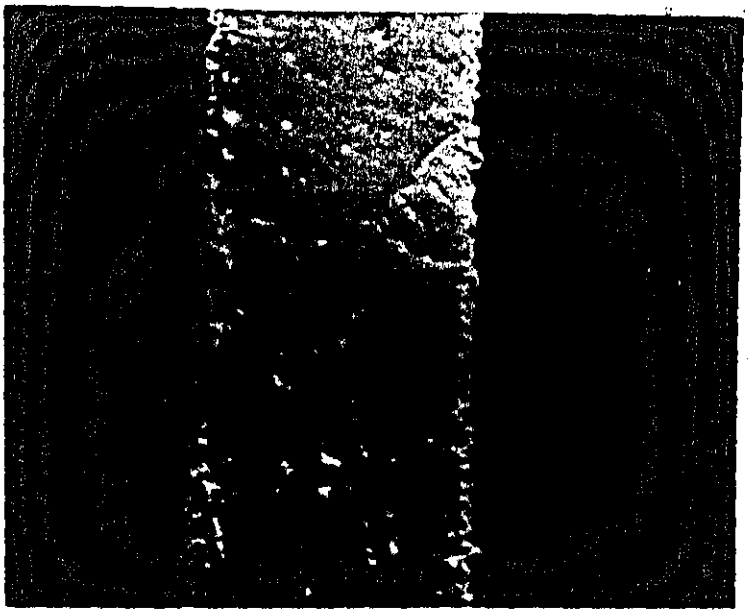

X150

(a)

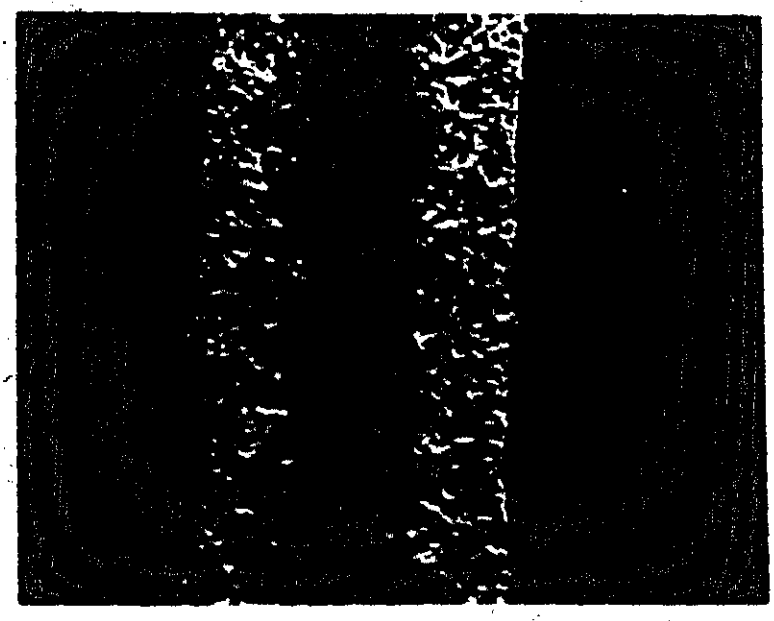

X160

(b)

Figure 16 Cross-section of incompletely nitrided zirconium sheets

obtained in the case of spheres.

TABLE VII

Chemical composition of the slabs

Method	N(w/o)	Zr(w/o)	N+Zr(w/o)	N/Zr
Weight gain	12.51	87.49	100.00	0.93
Chemical analysis	12.59	87.38	99.97	0.94

4.2.2.2 Metallographic examination

By comparison with figure 16, the micrographs shown in figure 17 confirmed the single phase nature of the material. As in the case of the spheres, it was difficult to know if the roughness of the surface obtained after polishing was attributable to the presence of pores or to the brittleness of the nitride. Etching revealed grains of variable size in the 10-30μ range.

Surface examination (Fig. 18) showed the existence of protuberances delimiting polygonal surfaces with a smoother aspect (Fig. 18a). Small holes and cracks were associated with these bulges (fig. 18c). Etching had a very mild effect and mainly produced small pits inside the polygonal area (fig. 18b and 18d). The nature of the protuberances is uncertain. X-ray analysis did not detect any presence of oxide on the surface.

4.2.2.3 Vacancy concentration

The lattice parameter and the pycnometric density were measured at the same temperature (23°C). The lattice parameter calculated from a diffractometer trace of the surface was a little smaller than the one obtained after grinding. For the calculation of the X-ray density we used the second value as it is more representative of the bulk material. To measure the

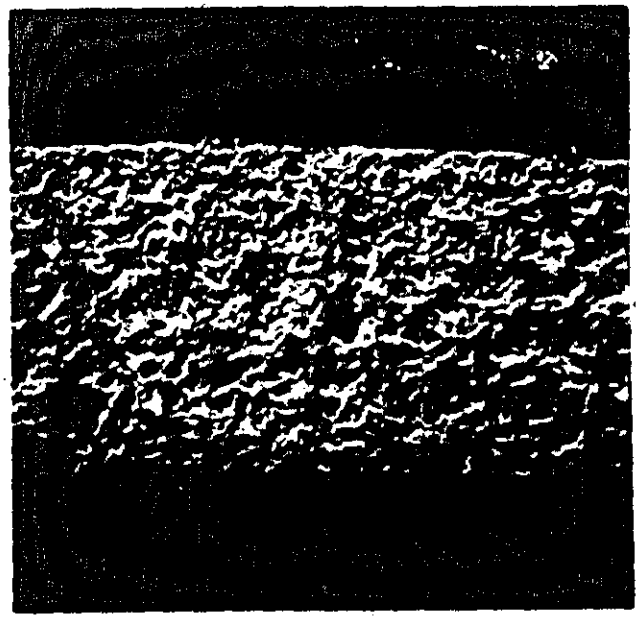

X170
(a)

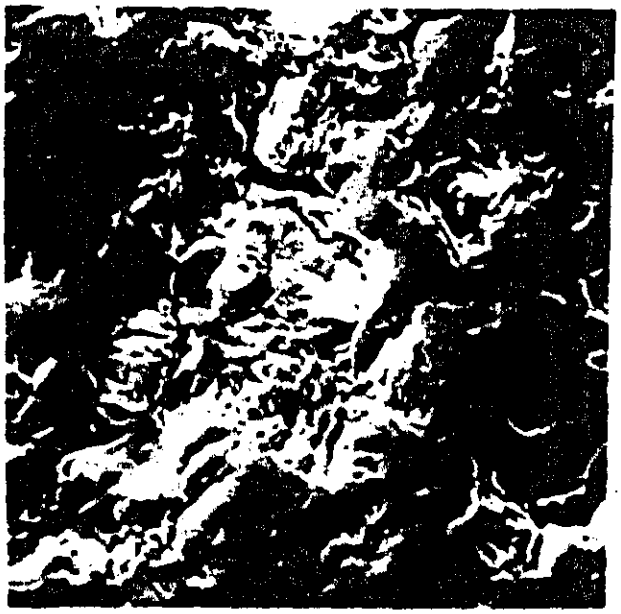

X840
(b)

X150
(c)

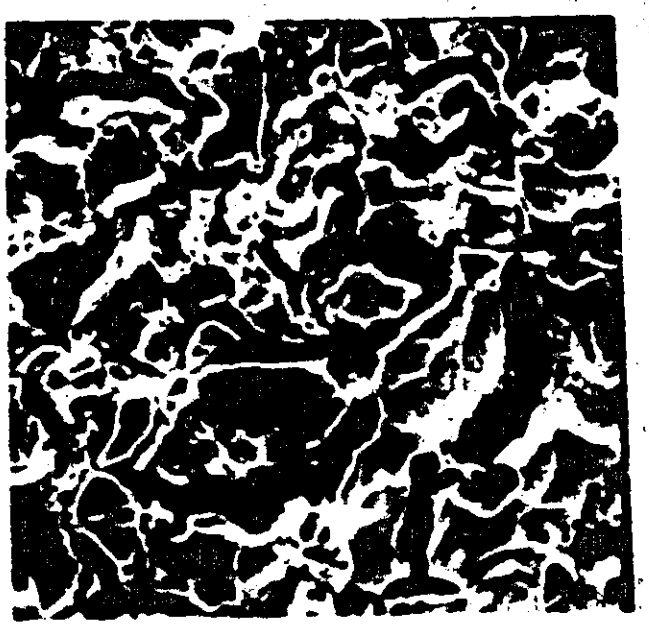

X800
(d)

Figure 17 Cross-section of single phase zirconium nitride slabs.

X140

(a)

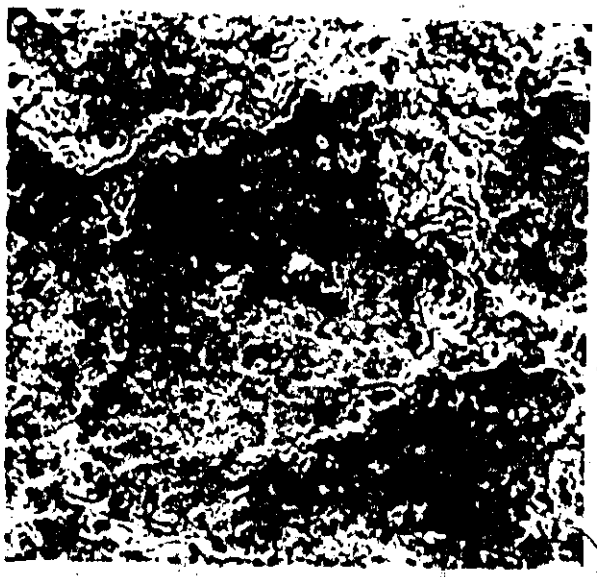

X340

(b)

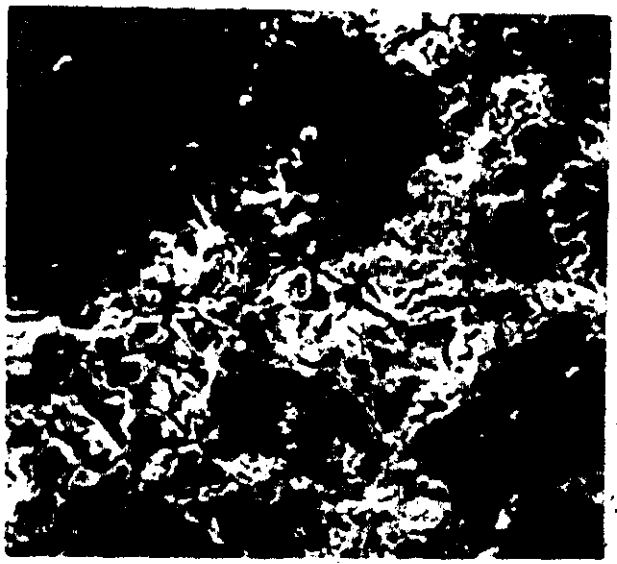

X700

(c)

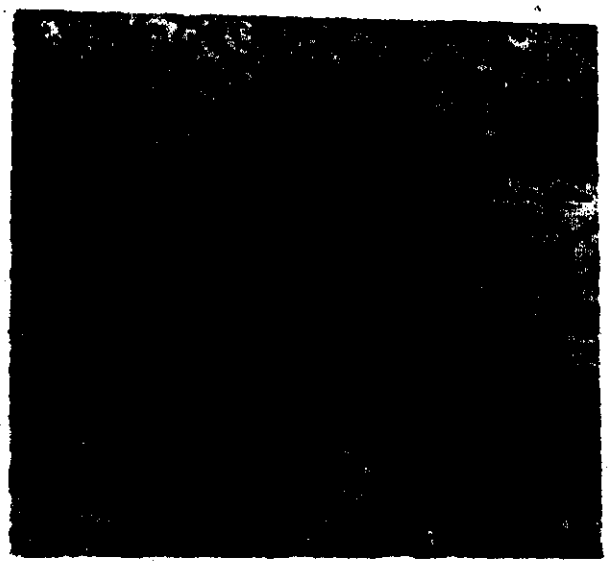

X680

(d)

Figure 18 Scanning electron micrographs of the surface of slabs

pycnometric density a sample weight 3 times greater than in the case of spheres was chosen. The corresponding data can be found in table VIII.

TABLE VIII

Vacancy concentration in slabs at 23°C

$d_p(g/cm^3)$			a(Å)	$d_x(g/cm^3)$	$V_{Zr}(\%)$	$V_N(\%)$
7.174		surface	4.5755±0.0007			
7.188	7.18	bulk	4.578±0.002	7.22	0.55	7.51
7.178						

Unlike the spheres, the small difference d_x-d_p = 0.04 g/cm^3, i.e. 0.56%, can be easily attributable to structural defects. Therefore the value found for the percentage of vacant sites in the zirconium sublattice is questionable. As the above difference is of the same order of magnitude as that recorded by Schevchenko et al.[27] for zirconium nitride containing a low percentage of dissolved oxygen (~0.04 w/o) it is possible to estimate that the O_2 content of our material is less than 0.05%.

4.2.2.4 Homogeneity

Despite the fluctuations in the zirconium profile caused by the irregularities of the surface of the cross-sections, the electron probe microanalyses indicated a small concentration difference between the surface and the interior of the slab. The Zr concentration was close to stoichiometric at the edges and decreased within 20 to 30μ to around the value determined by chemical analysis. Therefore the small difference in lattice parameter noted above could have some significance, the lower value being representative of the stoichiometric compound.

4.2.3 Diffusion results

Three or four slabs having a total mass close to 500 mg were used in each run. They were not stacked but placed in an inclined position with some space between them. Also they were not annealed before the run. All the other experimental conditions were the same as for spheres. The numerical results can be found in tables A7 to A12 and the Dt/a^2 vs. time plots are shown in figure 19 for the first 10 to 12 hours when they are linear. The temperature dependence of the calculated coefficients at 1001, 1050, 1100.5, 1149 and 1200°C can be seen on figure 14. It may be represented by

$$D = (4.08\ ^{+88.23}_{-3.90}) \times 10^{-6} \exp(-(36{,}600 \pm 4{,}500)/RT) \qquad (4.2)$$

After the runs the samples showed a brown-greyish color (fig. 20b). The scanning electron micrographs of the surface (fig. 21) were not very different from those of figure 18. The bulges did not grow but had more rounded shapes (Fig. 21c and 21d). A thin film seemed to have grown inside the polygonal figures (Fig. 21a and e). X-ray diffraction traces of the surface indicated the presence of very small amounts of monoclinic zirconia. The increase in weight of the samples during the diffusion annealing were smaller than for spheres (0.054 to 0.237 w/o).

4.3 Discussion

4.3.1 Error analysis

In the presentation of results the only errors listed were those obtained as deviations from a line determined by a linear least squares treatment. Calculated diffusion coefficients could be affected by errors in determining a, n_g, n_s, t, T, C_g and C_t and in calculating D with the chosen error function.

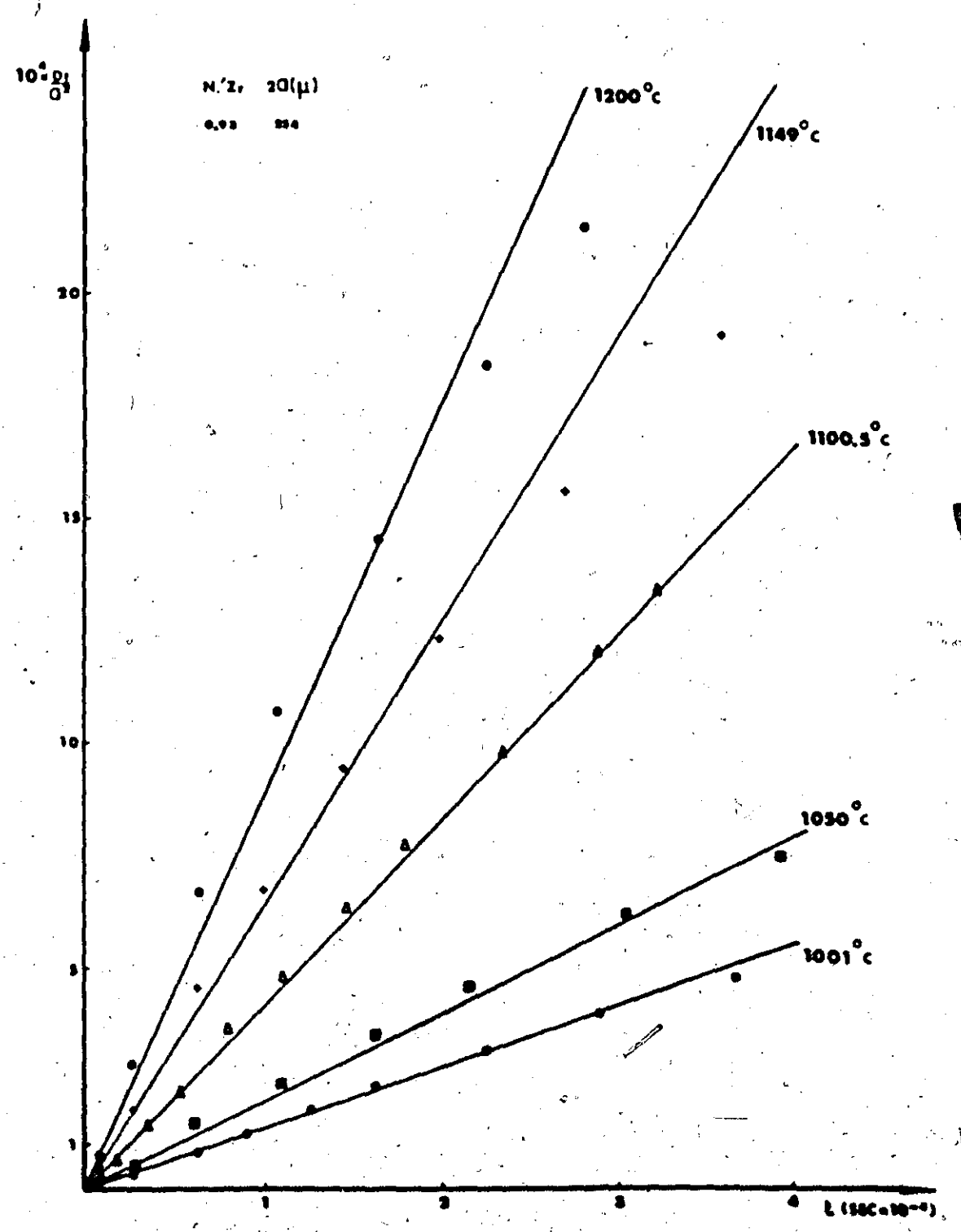

Figure 19 Experimental results for nitrogen diffusion in zirconium nitride slabs

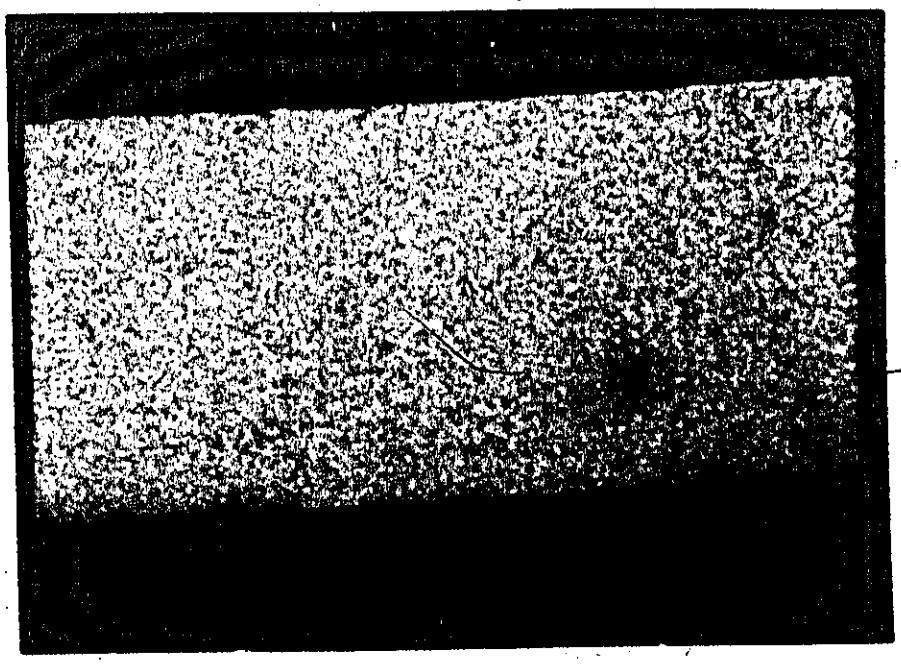

X4

(a)

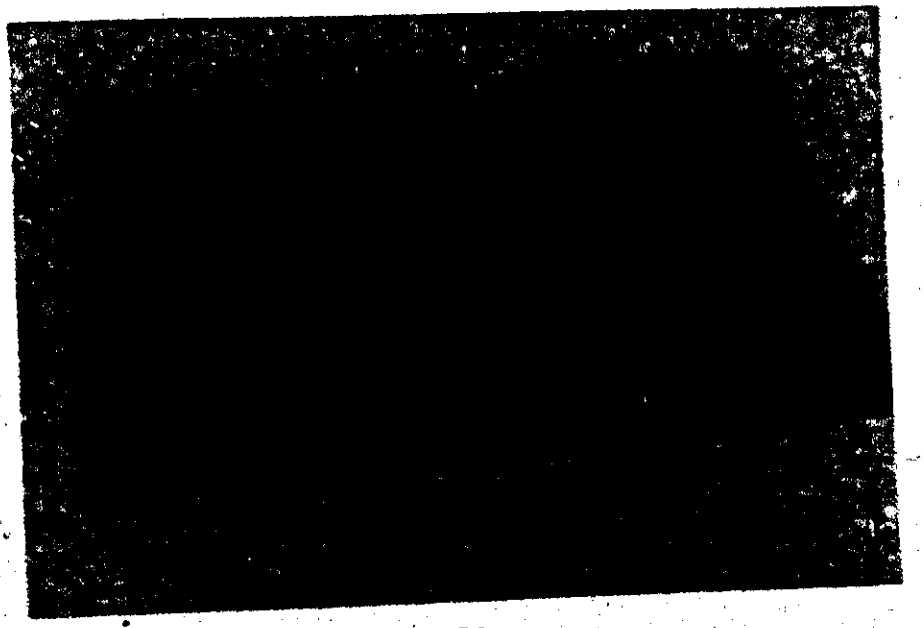

X10

(b)

Figure 20 Color of the slabs before and after diffusion annealing at 1100°C

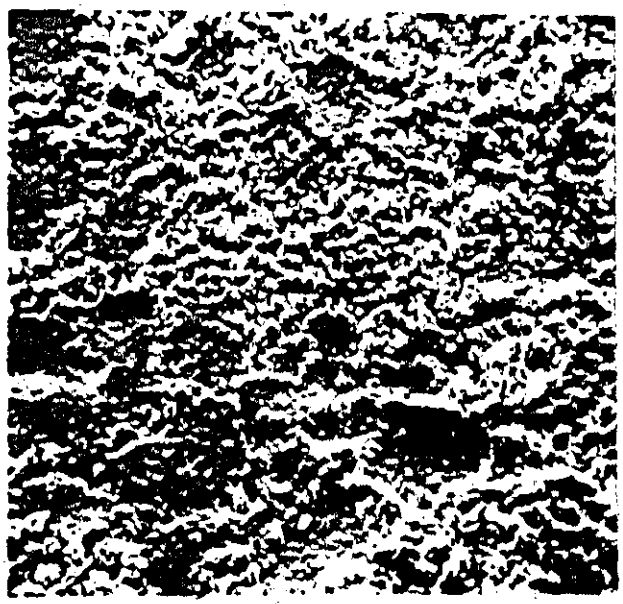

X180

(a)

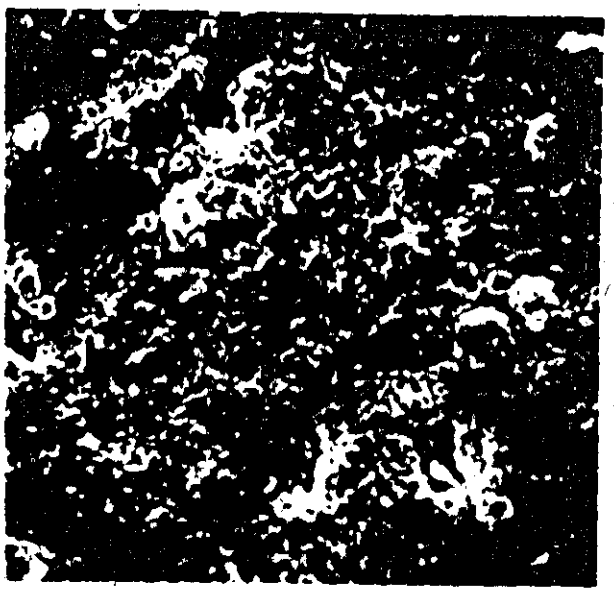

X1400

(b)

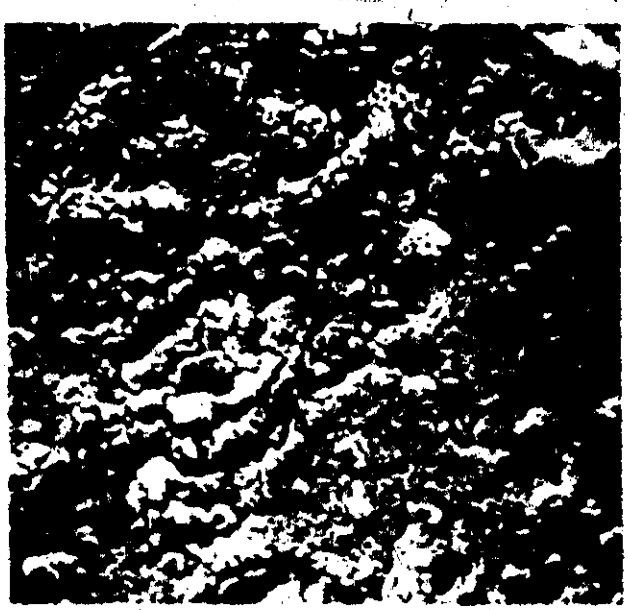

X700

(c)

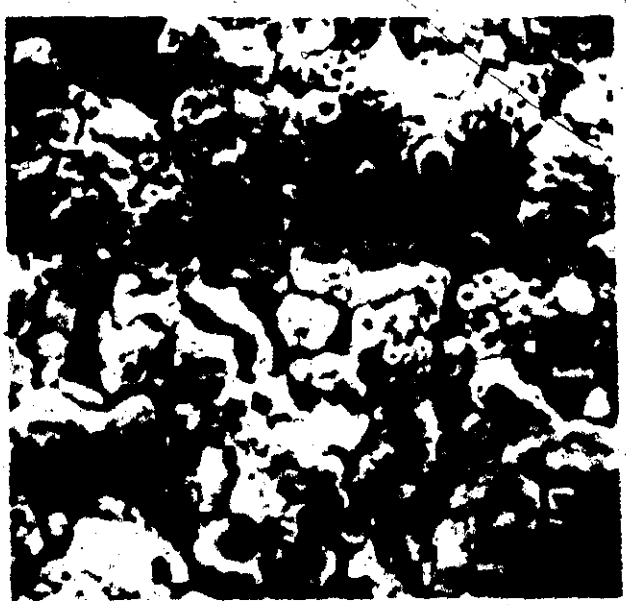

X1800

(d)

Figure 21 Scanning electron micrographs of the slabs after diffusion annealing at 1100°C

The diffusion coefficient is dependent on the square of the radius, a, of the spheres or half the thickness, ℓ, of the slabs employed; therefore, any relative error in the radius or in the thickness will give rise to approximately twice that error in the diffusion coefficient. The spheres were sieved into a 30μ range while the thickness was varying as little as ±5μ. Microscopic examination of the spheres showed that almost all the particles fell within the indicated range, and that within that range the distribution appeared to be nearly uniform.

The n_g term depends on manometric measurements, gas pressure and on the calibration of system volumes; the n_s term depends on the sample weight and chemical nitrogen analysis. The gas pressures were measured within ±2 mm Hg and the volume of the system is known to within ±5 milliliters. The samples were weighed to the nearest one-tenth of a milligram and the corresponding error can be neglected. Due to the lack of standards the accuracy of the nitrogen analysis is not well known but the agreement with weight gain results noted in section (4.2.2.1) indicates that the error is less than 1%.

An error in specifying the elapsed time attributed to a specific gas composition can arise because of the undefined time required for the gas to move from the reaction site to the sampling point, and the diffusion and exchange which occurred prior to the crucible reaching the bottom of the reaction chamber and the samples attaining the desired temperature. The error caused by a lag in the gas mixing was not evaluated but should not be large in the temperature and pressure range employed. The second error is less than expected from the total lowering time of the crucible (15 min). In fact the crucible was held at 800°C for 10 minutes to saturate the surface of the samples with ^{15}N. Since the rate of diffusion is very low at this

preheating temperature the maximum time error should not exceed 5 minutes which is low compared to the reaction time.

An error in the temperature measurement will not affect the calculated value of the diffusion coefficient. It will, however, affect the calculation of the activation energy from the diffusion coefficients. Temperature accuracy is about ±1°C and long-time control fluctuated within ±2°C.

Errors in C_g or C_t can be caused by either leakage of air into the gas sample or by errors made during the mass spectrometric analysis of the samples. Gross air leakage into the sample is readily detected and the analysis of that sample can then be ignored. Undetected amounts of air could produce only inconsequential errors. The precision of the mass spectrometric gas analysis was discussed in section 4.1.3. As a small error of ±0.2 percent in determining the initial ^{15}N concentration could result in a sizable error in the calculated value for the diffusion coefficient when the change in the ^{15}N concentration is small we took the average of two measurements to have a better precision.

It is necessary to note that the removal of gas samples for analysis could cause an error by changing the amount of gas available for exchange. However, the two samples taken before the beginning of the exchange and the last one do not contribute to any possible error.

In view of the appearance of the Dt/a^2 versus time plots and of the fact that in the case of spheres two different particle sizes caused no significant changes in the Arrhenius plots the hypothesis of an instantaneous equilibrium at the surface seems to be correct. Therefore computational errors could arise only from the utilization of the Carman-Haul approximate

equations (3.12) and (3.13) rather than the exact equations (3.10) and (3.11). Edwards et al.[123] compared numerical solutions of the exact equations with numerical solutions of the Carman-Haul approximations and found that the two sets of equations give good agreement to five significant figures for $0.1 \leq F \leq 0.75$ and $0.0004 < Dt/a^2 < 0.09$ where $F = \frac{1}{1+\lambda}$. For values of $Dt/a^2 < 0.0004$, the results of the exact equation are not accurate unless more than 50 roots are used for the computation. In this study the value of F is approximately equal to 0.5 and the values of Dt/a^2 are ranging between 10^{-6} and 10^{-3}. Therefore the computation errors are negligible.

In conclusion to this error analysis we will emphasize that the best way to determine the accuracy of the results would be to calibrate the diffusion apparatus, unfortunately,no standard calibration samples exist. However, it is possible to expect that the absolute errors on the measurements are greater than those obtained from the statistical analysis of the scatter of the experimental points about the regression line.

4.3.2 Comparison of the results for spheres and slabs

In the hypothesis of a vacancy mechanism for nitrogen diffusion in zirconium nitride the tracer diffusion D^*_N is related to the self-diffusion coefficient for vacancies D^*_V through the relation[135]

$$D^*_N = N_V D^*_V \qquad (4.3)$$

where N_V is the vacancy concentration. As we measured that N_V (spheres) was approximately equal to 4 times N_V (slabs) we might expect slightly higher values of D for spheres. In fact figure 14 shows that it is the reverse which is observed, the diffusion coefficients for spheres being nearly

100 times smaller. In addition the activation energy for diffusion in spheres is 1/3 lower than the corresponding energy for slabs. Application of Student's t-test[136] to the slopes of the Arrhenius lines proved that these two activation energies were significantly different.

Several possible explanations can be given for this phenomenon. As the two sets of experiments were carried out under identical conditions we have mainly to consider the differences in geometry, defect structure and impurity content.

The geometrical factor seems to us the more important. Due to the small size of the spheres, diffusion samples made of spherical particles behave like powders. In all kinetical studies involving powders and gas environment it is necessary to be aware of the influence of the sample weight and thickness because as was said in section 4.1.3 a thick powder bed could be a limiting factor in the gas-solid exchange process. For example, Lortholary et al.[137] and Goursat et al.[138] found, in the investigation of the oxidation of 30 to 40μ powdered silicon nitride or silicon oxynitride, that an appreciable mass effect was occurring for sample weights higher than 120 mg. In addition, matters can be made worse in the present case by the small amount of sintering observed at the surface. However, this effect only occurs after 10 to 12 hours and could partially explain the deviation from a straight line of the Dt/a^2 vs. time plots. In one experiment a sample was lowered in the hot zone, kept there for 15 minutes and raised again. No appreciable change in color was seen and the superficial spheres were free to move. Restricted by our choice of a constant value of λ, we were unable to study this mass effect but as we used 500 mg and 3 to 4 mm thick samples we have to consider its possibility.

The structural factor will be considered second in importance. It was used by Madeyski et al.[131] to explain the difference in oxygen diffusivities, measured by the ^{18}O mass spectrometry technique, for zirconia spheres and scales. The diffusivities for the scales were approximately 10^4 larger than those for the spheres. This difference could be easily attributed to the columnar structure of the scale which favoured the migration of oxygen by short-circuit diffusion. In the present work such an explanation has less value because the grain sizes in the two materials are very close. However the microholes and cracks observed on the surface of the slabs could act as high diffusivity paths, this hypothesis being supported by the fact that the diffusion distance of the tracer was small (4 to 11μ). This short diffusion distance can also serve to explain why the difference in vacancy concentration had not the expected effect. Indeed the average penetration of ^{15}N in spheres was as low as 0.6-1μ and corresponds to the outer layer found richer in nitrogen by electron probe microanalysis.

The impurity factor is presumably of non negligible importance. The experiments were conducted in the extrinsic region, the ratio T/T_m, where T_m is the melting point 3273°K, ranged between 0.39 and 0.45, therefore the diffusion process was possibly impurity controlled. We say possibly because due to the high vacancy concentrations found in transition nitrides, even at the stoichiometric composition, it is difficult to know what is the dominant factor in the process. However we must keep in mind that the impurity level was higher in spheres, in particular the oxygen content.

Finally, we will note that during the diffusion annealing, mainly in the case of spheres, the samples increased in weight. Therefore, some nitrogen absorption occurred at the same time as the exchange. We will also

note that, in the case of the Zr-N system, no reliable information is available for the equilibrium nitrogen pressures over zirconium nitride, in its homogeneity range, for temperatures lower than 2000°C. Even for higher temperatures (section 2.6.3) the available data are sparse and not well defined.

4.3.3 Comparison of the present results with those available in the literature

It can be seen in figure 22 that due to the high scatter of the data our results are in good agreement with those reported in the literature. However the results for spheres are at the lower boundary and show the smallest activation energy. In the absence of any other tracer diffusion data it is difficult to decide if this low value is significant or not. Even the activation energy found for slabs is small compared to the value calculated by Iyer,[19] 81.7 kcal/mole, using the following equation for tracer diffusion of nitrogen in B1 structure (fcc) mononitrides

$$D^*_N = a_0^2 \nu N_V \exp\left\{- \frac{2d_{II}[1-(d_{111}/d_{II})^3]}{3a_0\alpha(T)T}\right\} \qquad (4.4)$$

where a_0 = lattice parameter

ν = vibration frequency of the nitrogen atom

d_N = nitrogen atom diameter

d_{111} = maximum diameter of a sphere which fits through a gap in the <111> direction in the crystal = $\frac{\sqrt{6}}{3}\ a_0 - d_M$

d_M = metal atom diameter

$\alpha(T)$ = coefficient of thermal expansion

T = absolute temperature

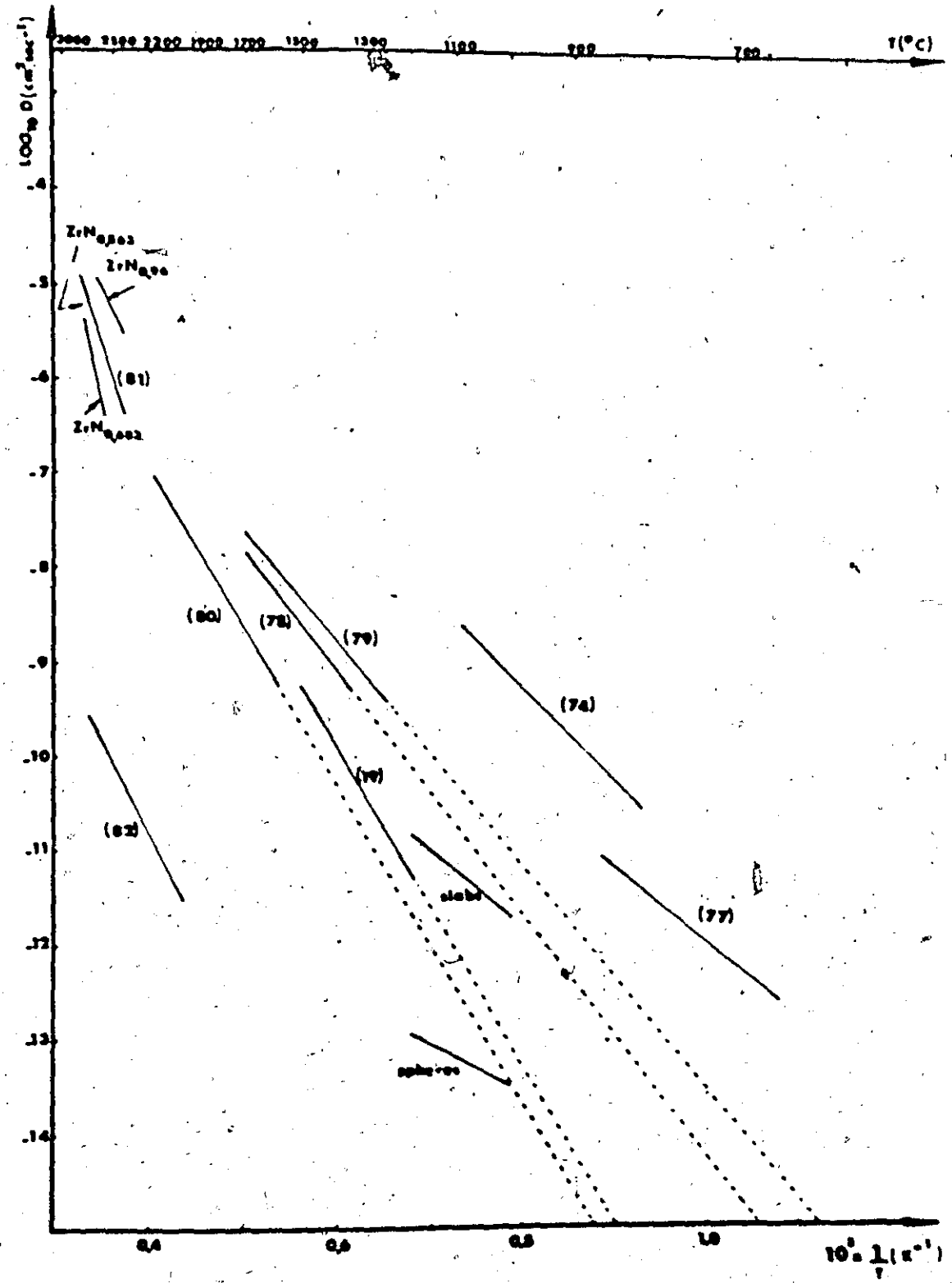

Figure 22 Comparison of the present results with those reported in the literature

This equation was derived by Tobin et al.[139] for B1 structure monocarbides. They postulated a diffusion mechanism for carbon, consisting of a net jump of a carbon atom in the <110> direction into an adjacent carbon vacancy, and applied the volume fluctuation theory of Cohen and Turnbull[140] as extended by Feisel and Armstrong.[141] Calculated values of D_o and Q by DePoorter and Wallace,[5] for the diffusion of carbon in several transition monocarbides proved that the ageeement between theory and experiment was not good. There is no apparent reason why this agreement should be better for nitrides. Therefore our values for the activation energy do not absolutely preclude a vacancy mechanism for nitrogen diffusion in zirconium nitride. After all, the lower activation energy for spheres gives some support to such a mechanism because it can be related to the increase from 0.71 to 0.78-0.79 of the initial N/Zr ratio of the samples in the temperature range investigated. Furthermore this effect was enhanced by the growing nitrogen uptake of the spheres with temperature. If in addition we take into account the possible mass effect to explain the existence of a factor of 10^2 between $D_{spheres}$ and D_{slabs} our results are not necessarily in contradiction with the hypothesis of a vacancy mechanism. However, the apparent wrong overall concentration dependence,which is really troublesome, should be elucidated by further work.

CHAPTER V

CONCLUSIONS AND SUGGESTIONS FOR FURTHER WORK

The self-diffusion coefficients determined in the present study by the ^{15}N isotopic exchange technique are in good agreement with the chemical diffusion coefficients reported in the literature.

The coefficient obtained using spheres obeys the Arrhenius equation

$$D(cm^2/sec) = (2.97^{+18.76}_{-2.56}) \times 10^{-10} \exp(-(23,000 \pm 5,400)/RT) \qquad (5.1)$$

In the case of slabs a coefficient approximately 100 times higher was found under similar experimental conditions

$$D(cm^2/sec) = (4.08^{+88.23}_{-3.90}) \times 10^{-6} \exp(-(36,600 \pm 4,500)/RT) \qquad (5.2)$$

As the vacancy concentration of the spheres was higher than that of the slabs we might have expected from a vacancy mechanism for nitrogen diffusion the reverse situation. Further experiments would be needed to elucidate this point:

a) A systematic study of the influence of a change in weight for spherical samples. This would require a decrease in the volume of the reaction chamber in order to keep reasonable values of λ and of the nitrogen pressure.

b) A second set of experiments with spheres made of the same material as slabs and with the same composition in order to study the influence of the impurity content.

c) Finally the influence of the pressure and of the composition at a fixed temperature should be investigated.

In the case of slabs valuable complementary information could be obtained by using after the runs the nuclear activation technique proposed by Condit et al.[95] and employed by Holt and Almassy[97] to measure nitrogen self-diffusion coefficients in UN. This technique makes use of the nuclear activation, N^{15} (α,n) F^{18}. The location of the original ^{15}N tracer is deduced from the radioactivity of the product ^{18}F by autoradiographic methods. Therefore any enhancement of nitrogen diffusion along grain boundaries, microfractures and dislocations can be directly observed with this technique.

However in the absence of this complementary information we have more confidence in the self-diffusion coefficient obtained from slabs (Eq. 5.2). This preference is mainly based on the fact that for this set of experiments the purity of the material was higher, the difference between the X-ray and the pycnometric densities was very small suggesting the absence of great amounts of oxygen or micropores. Furthermore all the slab experiments were carried out using material of the same composition, the increase in weight due to nitridation during the runs was insignificant and also the results were not affected by any mass effect.

APPENDIX

NITROGEN DIFFUSION RESULTS

This appendix contains all the numerical results for nitrogen self-diffusion in zirconium nitride. They are reproduced as given by the computer. The notations are explained in the text in section (4.1.3). Tables A1 to A6 correspond to the experiments with spheres and tables A7 to A12 to those with slabs.

TABLE A1

DIFF 10 (SPHERES) ***CALCULATION OF D BY ERROR FUNCTION EQUATION***

CALCULATION WITH CONSTANT LAMBDA

SAMPLE = SPHERES
WT PCT N = 0.0
BP(MM) = 498.600 MM
RATIO W/O = 1.00
M1 = 3.410 M, AT.=0.
C1 = .370
C2 = 7.420
ROOM TEMPERATURE = 23.0 C

DIAMETER = .0090 CM
WT PCT O2 = 99.41
AV. PRES. = 21.134 CM HG
AV. DIFF. PRESS. = 14.099 CM HG
AV. M2 = 4.132 M, AT.=0.
VOLUME = 237.494 CM3
DILATATION CORR. FACTOR = 1.331
REACTION TEMPERATURE = 1000.2 C

SAMPLE	PRESSURE	TIME (M)	TIME (S)	CT	X	YAP	LAMUDA	DAP	ITER	TAU	D
1	24.951	.25	.9000E+01	7.046	.9904	.0020	1.2001	.14547E-13	4	.16411E-05	.30425E-13
2	24.157	.75	.2700E+02	7.005	.9838	.0050	1.2001	.30306E-13	3	.69444E-05	.37485E-13
3	23.387	1.25	.4500E+02	7.540	.9804	.0070	1.2001	.42083E-13	3	.12047E-04	.34755E-13
4	22.642	1.75	.6300E+02	7.547	.9804	.0110	1.2001	.44005E-13	1	.17019E-04	.34293E-13
5	21.921	2.25	.8100E+02	7.593	.9806	.0120	1.2001	.37407E-13	2	.23340E-04	.37420E-13
6	21.223	2.75	.9900E+02	7.622	.9851	.0140	1.2001	.39400E-13	3	.29040E-04	.38300E-13
7	20.547	3.25	.1170E+03	7.545	.9828	.0160	1.2001	.37241E-13	2	.39104E-04	.39197E-13
8	19.893	3.75	.1350E+03	7.642	.9810	.0170	1.2001	.31849E-13	2	.47860E-04	.40432E-13
9	19.259	10.50	.3780E+03	7.678	.9791	.0175	1.2001	.26518E-13	3	.49319E-04	.41942E-13
10	18.644	22.50	.8100E+03	7.694	.9752	.0180	1.2001	.13092E-13	1	.82547E-04	.20427E-13
11	18.047	30.75	.1107E+04	7.667	.9744	.0155	1.2001	.88284E-14	4	.84341E-04	.17403E-13

TABLE A2

DIFF % (SPHERES) ***CALCULATION OF D BY ERROR FUNCTION EQUATION***

CALCULATION WITH CONSTANT-LAMBDA

SAMPLE = SPHERES
WT PCT N = 10.12
WEIGHT = 581.113 MG
RATIO W/Wo = .760
N1 = 3.621 M, AT.=0.
CS = .374
CO = 5.828
ROOM TEMPERATURE = 23.0 C

DIAMETER = .0040 CM
WT PCT ZN = 49.07
AV. PRES. = 22.952 CM HG
AV. RTEMP, PRESS. = 14.790 CM HG
AV. NO = 4.318 M, AT.=0.
VOLUME = 237.490 CM3
DILATATION COEF. FURNACE = 1.367
REACTION TEMPERATURE = 1052.7 C

SAMPLE	PRESSURE	TIME (M)	TIME (S)	CT	R	YAP	LAMBDA	DAP	ITER	TAU	D
1	29.314	1.50	.9000E+04	9.795	.9866	.0100	1.1925	.20334F-13	3	.2284AE-04	.38113E-13
2	26.401	3.00	.1800E+05	9.717	.9797	.0150	1.1925	.29629F-13	3	.5370AE-04	.44757E-13
3	23.987	5.00	.3000E+05	9.642	.9733	.0225	1.1925	.39994E-13	3	.9428?E-04	.47143E-13
4	23.233	6.75	.4050E+05	9.641	.9494	.0275	1.1925	.44255F-13	2	.12446E-03	.46095E-13
5	22.477	20.25	.1215E+06	9.619	.9618	.0325	1.1925	.20604F-13	3	.20647E-03	.25490E-13
6	21.941	35.50	.2130E+06	9.610	.9601	.0325	1.1925	.16362E-13	3	.21674E-03	.21949E-13
7	21.322	50.75	.3045E+06	9.608	.9597	.0325	1.1925	.14074F-13	3	.22092E-03	.18465E-13
8	20.721	71.75	.4305E+06	9.605	.9591	.0325	1.1925	.58150F-14	3	.22724E-03	.74193E-14

TABLE A3

DIFF 6 (SPHERES) ***CALCULATION OF D BY ERROR FUNCTION EQUATION***

CALCULATION WITH CONSTANT LAMBDA

SAMPLE = SPHERES
WT PCT N = 10.52
WEIGHT = 568.8448 MG
RATIO N/20 = .173
N1 = 3.156 M. AT.-G.
C1 = .370
C2 = 4.308
ROOM TEMPERATURE = 23.0 C

DIAMETER = .0040 CM
WT PCT ZN = 88.67
AV. PRES. = 22.497 CM HG
AV. DTEMP. PRESS. = 14.348 CM HG
AV. N0 = 4.215 M. AT.-G.
VOLUME = 237.490 CM3
DILATATION COEF. FURNACE = 1.348
REACTION TEMPERATURE = 1101.2 C

SAMPLE	PRESSURE	TIME (M)	TIME (S)	CT	X	YAP	LAMBDA	DAP	ITER	TAU	
1	25.250	.50	.1800E+04	4.347	.9898	.0050	1.1222	.17401E-13	4	.11641E-04	.54245E-13
2	24.478	1.00	.3600E+04	4.344	.9894	.0130	1.1222	.59118E-13	2	.27513E-04	.58783E-13
3	23.724	2.17	.7740E+04	4.310	.9782	.0225	1.1222	.81740E-13	3	.55010E-04	.63541E-13
4	22.995	3.50	.1260E+05	4.293	.9714	.0265	1.1222	.70197E-13	2	.85695E-04	.59164E-13
5	22.280	5.50	.1980E+05	4.246	.9643	.0350	1.1222	.77012E-13	3	.15208E-03	.69112E-13
6	21.605	8.50	.3060E+05	4.222	.9563	.0400	1.1222	.65867E-13	2	.23117E-03	.68019E-13
7	20.942	21.50	.7740E+05	4.172	.9439	.0550	1.1222	.69218E-13	3	.39284E-03	.69569E-13
8	20.299	26.75	.9630E+05	4.141	.9412	.0570	1.1222	.62687E-13	2	.47644E-03	.64421E-13

TABLE A4

DIFF P [illegible] ***CALCULATION OF D BY PROBE FUNCTION EQUATION***

CALCULATION WITH CONSTANT LAMBDA

SAMPLE = SAMPLES
WT PCT H = 10.77
WEIGHT = 444.774 MG
RATIO H/Z = .741
MS = 7.887 M, 27.0 G.
CC = .174
CG = 5.656
ROOM TEMPERATURE = 23.0 C

DIAMETER = .0868 CM
WT PCT Z = 89.23
AV. PRES. = 22.154 CM HG
AV. STAND. PRESS. = 16.317 CM HG
AV. MC = 6.194 M, 27.0 G.
VOLUME = 237.609 CM3
OXIDATION COEF. FURNACE = 1.374
REACTION TEMPERATURE = 1147.8 C

SAMPLE	PRESSURE	TIME (MI)	TIME (S)	CC	X	VAP	LAMBDA	DAP	ITER	TAU	D
1	25.767	.99	.[illegible]E+04	5.790	.9474	.0154	1.0927	.14914E-12	4	.16955E-04	.84777E-17
2	24.589	1.49	.5490E+02	5.767	.9748	.0724	1.0927	.14975E-12	4	.53016E-04	.88360E-17
3	22.814	3.00	.1798E+03	5.708	.9697	.0359	1.0923	.17533E-12	4	.10210E-03	.85042E-17
4	21.102	5.01	.[illegible]E+03	5.268	.9614	.1640	1.0927	.13495E-12	3	.16499E-03	.82467E-17
5	22.701	7.50	.2700E+03	5.222	.9946	.9459	1.0927	.89645E-13	3	.27999E-03	.79989E-13
6	21.795	10.26	.4770E+03	5.188	.9661	.3590	1.0927	.42512E-17	2	.34117E-03	.64771E-13
7	21.019	13.80	.4643E+03	5.166	.9790	.3590	1.0923	.42662E-17	3	.44403E-03	.67218E-17
8	24.193	17.00	.[illegible]E+03	5.134	.9778	.3460	1.0923	.38494E-17	3	.54899E-03	.63425E-17
9	19.747	27.00	.[illegible]E+03	5.176	.9771	.3569	1.0923	.[illegible]E-17	3	.87217E-03	.62926E-17

TABLE A5

DIFF & ISOTHERM ***CALCULATION OF D/R² FROM FOURIER FUNCTION EQUATION***

CALCULATION WITH CONSTANT LAMBDA

SAMPLE = SOMEBODY
WT PCT H = 1.65
WEIGHT = 407.368 MG
RATIO WATER = .745
MS = 2.2703 M. AT.-GR.
CS = .779
CC = 6.991
BOMB TEMPERATURE = 25.0 C.

DIAMETER = .0000 CM
WT PCT Z0 = 88.79
AV. PRES. = 27.119 CM HG
AV. REFND. PRESS. = 16.119 CM HG
AV. NG = 6.143 M. AT.-GR.
VOLUME = 237.69 CM3
DILATATION CORR. FURNACE = 1.000
REACTION TEMPERATURE = 1203.1 C

SAMPLE	PRESSURE	TIME (MI)	TIME (S)	PT	X	YAP	LAMBDA	DAP	TYPE	TAU	D
1	25.189	.59	.1800E+04	6.824	.9990	.0050	1.0952	.3748[illegible]E-13	4	.1[illegible]627E-04	.11956E-12
2	24.109	1.25	.4548E+04	6.784	.9946	.3125	1.0952	.9[illegible]715E-13	3	.[illegible]992J7E-04	.13143E-12
3	23.522	2.50	.9018E+04	6.747	.9773	.1210	1.0952	.11906E-12	2	.5664[illegible]E-04	.12748E-12
4	22.769	4.50	.1623E+05	6.697	.9787	.1250	1.0952	.1041[illegible]E-12	1	.9[illegible]910E-04	.1236[illegible]E-12
5	22.341	7.50	.2710E+05	6.668	.9658	.0338	1.0952	.1[illegible]8[illegible]6E-12	1	.1[illegible]51[illegible]E-03	.11[illegible]5E-12
6	21.[illegible]5	10.25	.3689E+05	6.619	.9569	.0759	1.0952	.[illegible]9631E-13	3	.[illegible]13[illegible]E-[illegible]	.11[illegible]7E-12
7	20.651	13.25	.4870E+05	6.557	.9448	.0678	1.0952	.[illegible]7873E-13	2	.[illegible]1775E-[illegible]	.[illegible]285[illegible]F-1[illegible]
8	19.[illegible]92	22.75	.8189E+05	6.575	.9656	.1590	1.0952	.[illegible]2787E-1[illegible]	2	.[illegible]5256E-[illegible]	.[illegible]7172E-1[illegible]
9	19.[illegible]52	28.[illegible]	.9[illegible]91E+05	6.52[illegible]	.9[illegible]71	.[illegible]822	1.0952	.[illegible]02[illegible]7E-13	3	.3[illegible]4697E-[illegible]	.[illegible]57[illegible]1E-13

TABLE A6

[illegible] OF THE ARRHENIUS EQUATION FROM A LEAST SQUARES FIT OF DATA

[illegible] DIFFUSION IN ZIRCONIUM NITRIDE [illegible] WITH [illegible]

[illegible]	LCL	AVG	UCL	ERR	SDEV
[illegible]	.[illegible]E-13	.[illegible]E-13	.[illegible]E-13	.[illegible]E-14	.[illegible]E-14
[illegible]	.[illegible]E-13	.[illegible]E-13	.[illegible]E-13	.[illegible]E-14	.[illegible]E-14
[illegible]	.[illegible]E-13	.[illegible]E-13	.[illegible]E-13	.[illegible]E-14	.[illegible]E-14
[illegible]	.[illegible]E-13	.[illegible]E-13	.[illegible]E-13	.[illegible]E-14	.[illegible]E-14
[illegible]	.[illegible]E-12	.[illegible]E-13	.[illegible]E-13	.[illegible]E-14	.[illegible]E-14

ALPHA AT THV. ERS. T

-.[illegible]E+[illegible]	.[illegible]E-[illegible]
-.[illegible]E+[illegible]	.[illegible]E-[illegible]
-.[illegible]E+[illegible]	.[illegible]E-[illegible]
-.[illegible]E+[illegible]	.[illegible]E-[illegible]
-.[illegible]E+[illegible]	.[illegible]E-[illegible]

COEFFICIENTS A = -.[illegible]E+[illegible] -.[illegible]E+[illegible]

CORRELATION COEFFICIENT = -.[illegible]

LCL A	B	UCL A	ERR1	LCL A2	A2	UCL A2	ERR2
-.[illegible]E+[illegible]	-.[illegible]E+[illegible]	-.[illegible]E+[illegible]	.[illegible]E+[illegible]	-.[illegible]E+[illegible]	-.[illegible]E+[illegible]	-.[illegible]E+[illegible]	.[illegible]E+[illegible]

LCL N	N	UCL N	ERLOD	ERUOD	LCL Q	Q	UCL Q	ERR
.[illegible]E-[illegible]	.[illegible]E-[illegible]	.[illegible]E-[illegible]	.[illegible]E-[illegible]	.[illegible]E-[illegible]	.[illegible]E+[illegible]	.[illegible]E+[illegible]	.[illegible]E+[illegible]	.[illegible]E+[illegible]

ALPHA AT THV. ERS. T

-.[illegible]E+[illegible]	.[illegible]E-[illegible]
-.[illegible]E+[illegible]	.[illegible]E-[illegible]
-.[illegible]E+[illegible]	.[illegible]E-[illegible]
-.[illegible]E+[illegible]	.[illegible]E-[illegible]
-.[illegible]E+[illegible]	.[illegible]E-[illegible]

TABLE A7

DIFF II (CLARKE) CALCULATION OF D BY ERROR FUNCTION EQUATIONS

CALCULATION WITH CONSTANT LAMBDA

SAMPLE = SL8RC
WT PCT N = 19.51
WEIGHT = 618.348 MG
DENSITY = 3.091
WT = 6.742 M, AT.PC.
P1 = .778
P2 = 7.110
ROOM TEMPERATURE = 29.0 C

THICKNESS = .0254 CM
WT PCT P = 47.69
AV. PRES. = 21.731 CM HG
AV. DIFF. PRESS. = 15.917 CM HG
AV. NO = 6.171 M, AT.PC.
VOLUME = 237.608 CM3
DILATATION COEF. FURNACE = 1.368
REACTION TEMPERATURE = 1006.1 C

SAMPLE	PRESSURE	TIME (H)	TIME (S)	PT	X	FAP	LAMBDA	DAP	ITER	TAU	D
1	25.775	.25	.900E+03	7.073	.9761	.1025	.9603	.10729E-11	4	.11732E-04	.21924E-11
2	24.137	.75	.270E+04	7.052	.9329	.1068	.9607	.19932E-11	3	.37261E-04	.22259E-11
3	23.629	1.25	.450E+04	7.027	.9199	.1118	.9607	.24864E-11	3	.46531E-04	.22194E-11
4	22.924	2.50	.900E+04	7.012	.8869	.1125	.9607	.25423E-11	3	.47563E-04	.22657E-11
5	22.249	3.50	.126E+05	6.995	.8566	.1158	.9607	.30221E-11	4	.56077E-04	.23173E-11
6	21.594	4.50	.162E+05	6.980	.8292	.1175	.9607	.29119E-11	3	.54048E-04	.23544E-11
7	20.999	5.75	.207E+05	6.969	.8045	.1199	.9607	.31619E-11	2	.58625E-04	.23587E-11
8	20.461	6.83	.246E+05	6.965	.7823	.1220	.9607	.33659E-11	3	.62422E-04	.22719E-11
9	19.963	10.25	.369E+05	6.959	.7619	.1220	.9607	.33618E-11	3	.62111E-04	.21029E-11
10	19.494	22.25	.801E+05	6.977	.7429	.1240	.9603	.12563E-11	3	.83864E-03	.16848E-11
11	19.504	24.10	.868E+05	6.978	.7454	.1240	.9607	.11879E-11	3	.99345E-03	.16679E-11

TABLE A8

DIFF 12 (SLABS) ***CALCULATION OF D AV ERROR FUNCTION EQUATION***

CALCULATION WITH CONSTANT LAMBDA

SAMPLE = SLABS
WT PCT N = 12.51
WEIGHT = 498.138 MG
RATIO N/ZR = .931
NS = 4.431 M, AT.-G.
CS = .370
XO = 6.021
ROOM TEMPERATURE = 23.0 C

THICKNESS = .0754 CM
WT PCT ZR = 87.49
AV. PRES. = 22.372 CM HG
AV. ATEMP. PRESS. = 16.733 CM HG
AV. NO = 4.303 M, AT.-G.
VOLUME = 237.498 CM3
DILATATION COEF. FURNACE = 1.337
REACTION TEMPERATURE = 1050.4 C

SAMPLE	PRESSURE	TIME (M)	TIME (S)	CT	X	YAP	LAMBDA	DAP	ITER	TAU	D
1	25.589	.25	.9000E+03	6.805	.9960	.0025	.9712	.10564E-11	4	.11741E-04	.21042E-11
2	24.815	.75	.2700E+04	6.847	.9918	.0075	.9712	.31692E-11	2	.50991E-04	.30460E-11
3	24.064	2.00	.7200E+04	6.826	.9855	.0150	.9712	.47538E-11	3	.15939E-03	.35706E-11
4	23.336	3.00	.1080E+05	6.805	.9823	.0180	.9712	.45636E-11	3	.23887E-03	.35474E-11
5	22.630	4.50	.1620E+05	6.780	.9785	.0210	.9712	.41411E-11	3	.35509E-03	.35154E-11
6	21.946	6.00	.2160E+05	6.740	.9754	.0225	.9712	.35643E-11	2	.46525E-03	.34741E-11
7	21.282	8.50	.3060E+05	6.735	.9716	.0260	.9712	.33606E-11	2	.62480E-03	.32933E-11
8	20.638	11.00	.3960E+05	6.717	.9689	.0300	.9712	.34573E-11	3	.75493E-03	.30748E-11
9	20.014	22.50	.8100E+05	6.680	.9632	.0330	.9712	.20452E-11	2	.10633E-02	.21174E-11
10	19.408	29.00	.1044E+06	6.677	.9628	.0330	.9712	.15868E-11	2	.10908E-02	.16852E-11

TABLE A9

DIFF @ (SLABS) ***CALCULATION OF D BY ERROR FUNCTION EQUATION***

CALCULATION WITH CONSTANT LAMBDA

SAMPLE = SLABS
WT PCT N = 12.51
WEIGHT = 48[illegible].24[illegible] MG
RATIO N/TA = .931
NS = 4.352 M. AT. G.
CS = .370
CO = 7.269
ROOM TEMPERATURE = 23.0 C

THICKNESS = .0954 CM
WT PCT TA = 87.49
AV. PRES. = 22.823 CM HG
AV. RTEMP. PRESS. = 16.757 CM HG
AV. NO = 4.309 M. AT.-G.
VOLUME = 235.690 CM3
DILATATION COEF. FURNACE = 1.362
REACTION TEMPERATURE = 1100.5 C

SAMPLE	PRESSURE	TIME (M)	TIME (S)	CT	X	YAP	LAMBDA	DAP	ITER	TAU	D
1	24.602	.25	.9000E+03	7.520	.9937	.0050	.9902	.43931E-11	3	.30423E-04	.54922E-11
2	23.773	.50	.1800E+04	7.506	.9910	.0010	.9902	.87863E-13	5	.63755E-04	.57128E-11
3	24.970	1.00	.3600E+04	7.445	.9851	.0150	.9902	.98845E-11	3	.15207E-03	.68132E-11
4	24.193	1.50	.5400E+04	7.442	.9829	.0200	.9902	.11775E-10	4	.23125E-03	.69470E-11
5	23.439	2.25	.8100E+04	7.410	.9785	.0230	.9902	.10329E-10	3	.34985E-03	.73445E-11
6	22.709	3.00	.1080E+05	7.387	.9753	.0250	.9902	.91524E-11	3	.49027E-03	.73218E-11
7	22.001	4.00	.1440E+05	7.362	.9718	.0270	.9902	.80065E-11	3	.64124E-03	.71423E-11
8	21.316	5.00	.1800E+05	7.341	.9689	.0275	.9902	.66446E-11	2	.78447E-03	.70293E-11
9	20.652	6.50	.2340E+05	7.313	.9650	.0280	.9902	.52988E-11	3	.99915E-03	.68869E-11
10	20.009	8.00	.2880E+05	7.288	.9615	.0285	.9902	.44604E-11	3	.12141E-02	.67993E-11
11	19.386	9.00	.3240E+05	7.273	.9594	.0287	.9902	.40206E-11	3	.13538E-02	.67791E-11

TABLE A10.

DIFF IS (SLAB?) RECALCULATION RE-D BY ERROR FUNCTION EQUATIONS

CALCULATION WITH CONSTANT LAMBDA

SAMPLE = SLAB
WEIGHT = 644.914 MG
RATIO WIDTH = .941
CC = .375
ROOM TEMPERATURE = 23.0 C

THICKNESS = .0256 CM
AV. PRESS. = 23.472 CM HG
AV. DIFUS. PRESS. = 17.500 CM HG
AV. NO = 4.804 M AT STP
VOLUME = 237.409 CM3
OXIDATION CUP, FURNACE = 1.787
REACTION TEMPERATURE = 1149.9 C

SAMPLE	PRESSURE	TIME (MI)	TIME (SE)	CF	Y	YAP	LAMBDA	DAD	ITER	TAU	D
1	24.755	.25	.9999E+03	6.829	.9315	.3870	1.0102	.896[illegible]E-11	7	.540645E-04	.10406E-10
2	24.909	.75	.2700E+04	6.779	.9051	.0150	1.0102	.177145E-10	4	.192475E-03	.10900E-10
3	24.110	1.75	.6911E+04	6.773	.8764	.0260	1.0102	.150491E-10	3	.454165E-03	.11627E-10
4	24.143	2.75	.9999E+04	6.699	.8718	.1270	1.0102	.191200E-10	4	.678[illegible]E-03	.11051E-10
5	23.594	4.00	.1440E+05	6.657	.8555	.0320	1.0102	.117945E-10	3	.969655E-03	.10637E-10
6	22.971	5.67	.1999E+05	6.607	.8419	.0760	1.0102	.137717E-10	3	.123[illegible]E-02	.10[illegible]07E-10
7	22.164	7.50	.2700E+05	6.597	.8273	.0410	1.0102	.1[illegible]2477E-10	3	.156[illegible]E-02	.93654E-11
8	21.499	10.00	.3600E+05	6.564	.8129	.1460	1.0102	.967422E-11	3	.197[illegible]E-02	.96292E-11
9	20.899	22.75	.8190E+05	6.499	.8023	.1590	1.0102	.877911E-11	2	.295[illegible]E-02	.98231E-11

TABLE A11

[illegible] CALCULATION OF D AT FOUND DIFFUSION POSITIONS

CALCULATION WITH CONSTANT LENGTH

[illegible]

SAMPLE	[illegible]	[illegible]	[illegible]	[illegible]	[illegible]	[illegible]	[illegible]	[illegible]	[illegible]	[illegible]	[illegible]
1	[illegible]	.75	[illegible]	[illegible]	[illegible]	[illegible]	[illegible]	[illegible]	[illegible]	[illegible]	[illegible]
2	[illegible]	.75	[illegible]	[illegible]	[illegible]	[illegible]	[illegible]	[illegible]	[illegible]	[illegible]	[illegible]
3	[illegible]	1.75	[illegible]	[illegible]	[illegible]	[illegible]	[illegible]	[illegible]	[illegible]	[illegible]	[illegible]
4	[illegible]	2.99	[illegible]	[illegible]	[illegible]	[illegible]	[illegible]	[illegible]	[illegible]	[illegible]	[illegible]
5	[illegible]	4.99	[illegible]	[illegible]	[illegible]	[illegible]	[illegible]	[illegible]	[illegible]	[illegible]	[illegible]
6	[illegible]	6.25	[illegible]	[illegible]	[illegible]	[illegible]	[illegible]	[illegible]	[illegible]	[illegible]	[illegible]
7	[illegible]	7.75	[illegible]	[illegible]	[illegible]	[illegible]	[illegible]	[illegible]	[illegible]	[illegible]	[illegible]
8	[illegible]	10.99	[illegible]	[illegible]	[illegible]	[illegible]	[illegible]	[illegible]	[illegible]	[illegible]	[illegible]
9	[illegible]	[illegible]	[illegible]	[illegible]	[illegible]	[illegible]	[illegible]	[illegible]	[illegible]	[illegible]	[illegible]
10	[illegible]	22.99	[illegible]	[illegible]	[illegible]	[illegible]	[illegible]	[illegible]	[illegible]	[illegible]	[illegible]
11	[illegible]	28.01	[illegible]	[illegible]	[illegible]	[illegible]	[illegible]	[illegible]	[illegible]	[illegible]	[illegible]

TABLE A12

DETERMINATION OF THE ARRHENIUS EQUATION FROM A LEAST SQUARES FIT OF DATA–

NITROGEN DIFFUSION IN ZIRCONIUM NITIDE EXPERIMENTS WITH SLABS

TEMP (C)	LCL	AVG	UCL	POU	SDEV
[illegible]	[illegible]	[illegible]	[illegible]	[illegible]	[illegible]
[illegible]	[illegible]	[illegible]	[illegible]	[illegible]	[illegible]
[illegible]	[illegible]	[illegible]	[illegible]	[illegible]	[illegible]
[illegible]	[illegible]	[illegible]	[illegible]	[illegible]	[illegible]
[illegible]	[illegible]	[illegible]	[illegible]	[illegible]	[illegible]

[illegible]	INV. ABS. T.
[illegible]	[illegible]
[illegible]	[illegible]
[illegible]	[illegible]
[illegible]	[illegible]
[illegible]	[illegible]

COEFFICIENTS [illegible] [illegible] [illegible]

CORRELATION COEFFICIENT [illegible] [illegible]

LCL A1	A1	UCL A1	[illegible]		LCL B	B	UCL B	[illegible]
[illegible]	[illegible]	[illegible]	[illegible]		[illegible]	[illegible]	[illegible]	[illegible]

LCL [illegible]	[illegible]	UCL [illegible]	[illegible]	[illegible]	LCL [illegible]	[illegible]	UCL [illegible]	[illegible]
[illegible]	[illegible]	[illegible]	[illegible]	[illegible]	[illegible]	[illegible]	[illegible]	[illegible]

[illegible]	INV. ABS. T
[illegible]	[illegible]
[illegible]	[illegible]
[illegible]	[illegible]
[illegible]	[illegible]
[illegible]	[illegible]

REFERENCES

1. Blocher, J.M., in "High-temperature materials and technology", edited by I.E. Campbell and E.M. Sherwood, Wiley, New York, 1967, p. 379.
2. Kieffer, R., Ettmayer, P., and Freudhofmeier, M., in "Modern developments in powder metallurgy", edited by H.H. Hausner, Vol. 5, Plenum Press, New York, 1971, p. 201.
3. Toth, L.E., Transition metal carbides and nitrides, Academic Press, New York, 1971.
4. Storms, E., in "Fundamentals of refractory compounds", edited by H.H. Hausner and M.G. Bowman, Plenum Press, New York, 1968, p. 67.
5. De Poorter, G.L. and Wallace, T.C., in "Advances in High Temperature Chemistry", edited by Leroy Eyring, Vol. 4, Academic Press, New York, 1971, p. 107.
6. Williams, W.S., Transition-metal carbides, in "Progress in Solid State Chemistry", edited by H. Reiss and J.O. McCaldin, Vol. 6, Pergamon Press, Oxford, 1971, p. 57.
7. Streiff, R. and Smeltzer, W.W., J. Nucl. Mat., 41, (1971), 109.
8. Schwarzkopf, P. and Kieffer, R., Refractory hard metals, MacMillan, New York, 1953.
9. Langeron, J.-P., in "Nouveau traite de chimie minerale", edited by P. Pascal, Vol. 9, Masson, Paris, 1963, p. 628.
10. Storms, E.K., A critical review of refractories, LA-2942, Pt. II, 1963, p. 106.
11. Shaffer, P.T.B., High-temperature materials, materials index, Plenum Press, New York, 1964.

12. Samsonov, G.V., High temperature materials, Properties index, Plenum Press, New York, 1964.

13. Lynch, J.F., Ruderer, C.G., and Duckworth, W.H., Engineering properties of selected ceramic materials, Am. Ceram. Soc., Columbus, Ohio, 1966.

14. Schick, H.L., ed., Thermodynamics of certain refractory compounds, Vols. 1 and 2, Academic Press, New York, 1966.

15. Glasson, D.R., and Jayaweera, S.A.A., J. Appl. Chem. Lond., 18 (1968), 65.

16. Hausner, H.H. and Bowman, M.G., ed., Fundamentals of refractory compounds, Plenum Press, New York, 1968.

17. Nowotny, H. and Neckel, A., J. Inst. Metals, 97 (1969), p. 161.

18. Goldschmidt, H.J. , J. Inst. Metals, 97 (1969), p. 173.

19. Iyer, S.K., Ph.D. Thesis, University of Pennsylvania, Philadelphia, 1971.

20. Storms, E.K., M.T.P. Int. Rev. Sci.: Inorg. Chem., Ser. One, 1972, 37.

21. Hansen, M. and Anderko, K., Constitution of binary alloys, MacGraw Hill, New York, 1958, p. 995.

22. Elliot, R.P., Constitution of binary alloys, First supplement, MacGraw Hill, New York, 1965, p. 647.

23. Shunk, A.F., Constitution of binary alloys, Second supplement, MacGraw Hill, New York, 1969, p. 537.

24. Rudy, E. and Benesovsky, F., Monatsh. Chem., 92 (1961), 415.

25. Smagina, E.I., Kutsev, V.S. and Ormont, B.F., Dokl. Akad. Nauk S.S.S.R., 115 (1957), 354 [487]*.

26. Smagina, E.I. and Kutsev, V.S., Zh. Fiz. Khim., 37 (1963), 1813 [977].

27. Shevchenko, A.S., Andrievskii, R.A., Kalinin, V.P., and Lyutikov, R.A., Porosh. Met., 10 (1970), No. 1 , 89 [71].

*The number between brackets indicates the first page in the English translation of a Russian journal.

28. Gal'Braikh, E.I., Kulik, O.P., Kuznetzov, A.A., Lyutaya, M.D., and Morozova, M.P., Porosh. Met., 10 (1970), No. 9, 62 [748].

29. Chiotti, P., J. Am. Ceram. Soc., 35 (1952), 123.

30. Domalga, R.F., McPherson, D.J., and Hansen, M., J. Metals, 8 (1956), 98.

31. Samsonov, G.V. and Verkhoglyadova, T.S., Dopovidi Akad. Nauk. Ukr. R.S.R., No. 1 (1962), 48.

32. Samsonov, G.V., Kuchma, A.Ya., and Timofeeva, I.I., Porosh. Met. 10 (1970), No. 9, 69 [754].

33. Juza, R., Gabel, A., Rabenau, H., and Klose, W., Z. Anorg. Allgem. Chem., 329 (1964), 136.

34. Juza, R., Rabenau, A., and Nitschke, I., Z. Anorg. Allgem. Chem., 332 (1964), 1.

35. Orlovskii, V.P., Rudenko, N.V., and Ivanov-Emin, B.N., Zh. Neorg. Khim., 12 (1967), 2305 [1217].

36. Collongues, R., Gilles, J.-C., and Lejus, A.M., Bull. Soc. Chim. Fr., 1962, 2113.

37. Gilles, J.-C., Bull. Soc. Chim. Fr., 1962, 2118.

38. Friederich, E. and Sittig, L., Z. Anorg. Allg. Chem., 143 (1925), 293.

39. Agte, C. and Moers, K., Z. Anorg. Allg. Chem., 198 (1931), 233.

40. Yanchur, V.P., Andrievskii, R.A., Spivak, I.I., and Fedotov, M.A., Izv. Akad. Nauk SSSR, Neorg. Mater., 5 (1962), 1012 [861].

41. Eron'Yan, M.A., Avarbe, R.G., and Nikol'skaya, T.A., Zh. Prikl. Khim. (Leningrad), 46 (1973), 428.

42. Samsonov, G.V., Zh. Strukt. Khim., 1 (1960), 447 [415].

43. Straumanis, M.E., Faunce, C.A., and James, W.J., Inorg. Chem., 5 (1966), 2027.

44. Straumanis, M.E., in "Anisotropy in single-crystal refractory compounds," edited by W. Vahldiek and S.A. Mersol, Vol. 1, Plenum Press, New York, 1968, p. 121.

45. Gilles, J.-C., Rev. Hautes Temper. et Refract., 2 (1965), 237.

46. Collongues, R., Gilles, J.-C., Lejus, A.M., Perez y Jorba, M., and Michel, D., Mat. Res. Bull., 2 (1967), 837.

47. Schonberg, N., Acta Chem. Scand., 8 (1954), 627.

48. Zainulin, Yu.G., Alyamovskii, S.I., Shveikin, G.P., and Gel'd, P.V., Zh. Neorg. Khim., 16 (1971), 315 [164].

49. Smagina, E.I., Kutsev, V.S., and Ormont , B.F., Zh. Fiz. Khim., 34 (1960), 2328 [1105].

50. Baker, T.W., Acta Cryst., 11 (1958), 300.

51. Neshpor, V.S., Davydov, V.S., Ermakov, B.G., and Mogilevich, B.V., Porosh. Met., 7 (1967), No. 2, 65 [135].

52. Shvedova, L.K., Izv. Akad. Nauk SSSR, Neorg. Mater., 7 (1971), 517 [455].

53. Bittner, H. and Goretzky, H., Monatsh. Chem., 93 (1962), 1000.

54. Fridlender, B.A. and Neshpor, V.S., Izv. Akad. Nauk SSSR, Neorg. Mater., 6 (1970), 1004 [880].

55. Petrova, I.I., Petrov, V.A., Ermakov, B.G., and Sokolov, V.V., Teplofiz. Vys. Temp., 10 (1972), 1007.

56. Samsonov, G.V. and Verkhoglyadova, T.S., Dokl. Akad. Nauk SSSR, 142 (1962), 608 [74].

57. Neshpor, V.S., Novikov, V.I., and Sokolov, V.V., Izv. Akad. Nauk SSSR., Neorg. Mater., 6 (1970), 425 [373].

58. Giorgi, A.L., Szklarz, E.G., and Wallace, T.C., Proc. Brit. Ceram. Soc., 10 (1968), 183.

59. Kibler, G.M., Lyon, T.F., Linevsky, M.J., and De Santis, V.J., WADD-TR-60-646, Part III, Vol. II, 1964.

60. Krieger,F.J., U.S. Clearinghouse Fed. Sci. Techn. Inform. AD 1970, No. 706886.

61. Lyutaya, M.D., and Kulik, O.P., Izv. Akad. Nauk SSSR, Neorg. Mater., 5, (1969), 885 [753].

62. Lyutaya, M.D. and Kulik, O.P., Porosh. Met., 10 (1970), No. 10, 48 [821].

63. Kyo, B., Uchida, K., and Imoto, S., Nippon Kinzoku Gakkaishi, 37 (1973), 411.

64. Glasson, D.R. and Jayaweera, S.A.A., J. Appl. Chem. Lond., 19 (1969), 182.

65. Lyutaya, M.D., Kulik, O.P., and Kachkovskaya, E.T., Porosh. Met. 10 (1970), No. 3, 72 [233].

66. Billy, M. and Teyssedre, B., C.R. Acad. Sc. Paris, Ser. C, 276 (1973), 421.

67. Gulbransen, E.A. and Andrew, K.F., J. Metals, 1 (1949), 515.

68. Dravnieks, A., J. Am. Chem. Soc., 72 (1950), 3568.

69. Mallet, M.W., Baroody, E.M., Belson, H.R., and Papp, C.A., J. Electrochem. Soc. 100 (1953), 103.

70. Mallet, M.W., Belle, J., and Cleland, B.B., J. Electrochem. Soc. 101 (1954), 1.

71. Salibekov, S.Ye., Levinskii, Yu.V., Khvostikov, V.C., and Levinskaya, M.Kh., Fiz. Metal. Metalloved. 18 (1964), 858 [57].

72. Rosa, C.J. and Smeltzer, W.W., Electrochem. Technol., 4 (1966) 149.

73. Samsonov, G.V. and Kaplina, G.S., Izv. Akad. Nauk SSSR, Metal. 1970, No. 6, 222 [144].

74. Paidassi, J. and Le Delliou, R., C.R. Acad. Sc. Paris, Ser. C, 272 (1971), 249.

75. Sallach, R.A., J. Phys. Chem., 76 (1972), 2156.

76. Debuigne, J., Metaux Corrosion Ind., 1967, No. 501, 186.

77. Rosa, C.J. and Hagel, W.C., J. Electrochem. Soc., 115 (1968), 467.

78. Eremeyev, V.S., Ivanov, Yu.M., and Panov, A.S., Izv. Akad. Nauk SSSR, Metal., 1969, No. 4, 262 [169].

79. Levinskii, Yu.V., Kiparisov, S.S., and Strogonov, Yu.D., Izv. Vyssh, Ucheb. Zaved., Tsvet. Met., 13 (1970), 91.

80. Spivak, I.I., Izv. Akad. Nauk SSSR, Neorg. Mater., 5 (1969), 1138 [967].

81. Andrievskii, R.A., Spivak, I.I., and Chevasheva, K.L., Porosh. Met., 8 (1968), No. 7, 65 [559].

82. Khromov, Yu.F., Yanchur, V.P., and Eremeev, V.S., Fiz. Metal. Metalloved. 33 (1972), 642.

83. Kuczynski, G.C., in "Modern developments in Powder Metallurgy", edited by H.H. Hausner, Vol. 1, Plenum Press, New York, 1966, p. 332.

84. White, J., in "Sintering and related phenomena", edited by Kuczynski, G.C., Hooton, N.A., and Gibbon, C.F., Gordon and Breach, New York, 1967, p. 245.

85. Wasilewski, R.J. and Kehl, G.L., J. Inst. Metals, 83 (1954-55), 94.

86. Levinskii, Yu.V., Strogonov, Yu.D., Salibekov, S.E., Levinskaya, M.Kh., and Prokof'ev, S.A., Izv. Akad. Nauk SSSR, Neorg. Mater., 4 (1968), 2068 [1799].

87. Repkin, V.D., Kurtukov, G.V., Kornilov, A.A., and Bespalov, V.V., Metallotherm. Protsessy Khim. Met., 1971, 320 (from Chem. Abstr., 78 (1973), 7982 R).

88. Iyer, S.K. and Worrel, W.L., in "7th Inter. Symp. on the reactivity of solids", Bristol, 1972, p. 294.

89. Levinskii, Yu.V., Kiparisov, S.S., and Strogonov, Y.D., Izv. Akad. Nauk SSSR, Metal, 1973, No. 1, 70.

90. Schwerdtfeger, K., Trans. AIME, 239 (1967), 1432.

91. Schwerdtfeger, K., Grieveson, P., and Turkdogan, E.T., Trans. AIME, 245 (1969), 2461.

92. Prenosil, B., Kovove Mater., 3 (1965), 69.

93. Benz, R., J. Electrochem. Soc., 119 (1972), 1596.

94. Sturiale, T.J. and Decrescente, M.A., PWAC-477, 1965.

95. Condit, R.H., Holt, J.B., and Himmel, L., J. Electrochem. Soc. 114 (1967), 1100.

96. Reimann, D.K. and Lundy, T.S., J. Met., 20 (1968), No. 8. 54A.

97. Holt, J.B. and Almassy, M.Y., J. Am. Ceram. Soc., 52 (1969), 631.

98. Benz, R. and Hutchinson, W.B., J. Nucl. Mat., 36 (1970) 135.

99. Reimann, D.K., Kroeger, D.M. and Lundy, T.S., J. Nucl. Mat., 38 (1971), 191.

100. Madeyski, A. and Smeltzer, W.W., Mat. Res. Bull., 2 (1967), 467.

101. Cosgrove, J.F., Waltham research center of the general telephone and electronics laboratories, Inc., Waltham, Massachussetts, Private communication.

102. Kriege, O.H., LA-2306 (1959).

103. Passer, R.G., Hart, A. and Julietti, R.J., Analyst, 87 (1962), 501.

104. Hynek, R.J. and Nelen, J.A., Anal. chem., 35 (1963), 1655.

105. Morgenthaler, L.P. and Menichelli, R.P., Anal. Chem., 37 (1965), 570.

106. Dutton, R.E., McKinley, G.J., McLean, D., and Wendt, H.F., AEC Rept. No. NP-14952, (1965).

107. Fischer, W. and Steinruecken, D., AEC Rept. No. IS-TRANS-37, (1965).

108. Meyer, R.A., Parry, E.P., and Davis, J.H., Anal. Chem., 39 (1967), 1321.

109. Selezna, N.A. and Plotnikova, O.M., Izv. Akad. Nauk Kaz. SSR, Ser. Khim., 18 (1968), 80 [Chem. Abstr., 70 (1969), 73936 q].

110. Schneider, H. and Hein, W., High Temp. Mater., Pap. Plansee Semin., 6th, 1968, edited by Benesovsky, E., Springer-Verlag, Vienna, Austria, 1969, p. 2028.

111. Healy, C. and Parker, A., U.K. Energy Auth., Res. Group Rep., AERE-R6491, (1970).

112. Bollman, D.H., Anal. Chem., 44 (1972), 887.

113. Parrish, W. and Wilson, A.J.C., in "International Tables for X-ray Crystallography", Vol. II, Kynoch Press, Birmingham, 1959, p. 216.

114. Wilson, A.J.C., Mathematical Theory of X-ray powder diffractometry, Philips Technical Library, Eindhoven, 1963, p. 74.

115. Azaroff, L.V., Elements of X-ray Crystallography, McGraw-Hill Book Co., New York, 1968, p. 480.

116. Nuffield, E.W., X-ray diffraction methods, Wiley, New York, 1966, p. 157.

117. Edmunds, I.G., Lipson, H. and Steeple, H., in "X-ray diffraction by polycrystalline materials", edited by H.S. Peiser, H.P. Rooksby and A.J.C. Wilson, Chapman and Hall, London, 1960, p. 366.

118. Azaroff, L.V. and Buerger, M.J., The powder method in X-ray crystallography, McGraw-Hill, New York, 1958, p. 238.

119. Birks, L.S., Electron Probe Microanalysis, Second edition, Wiley-Interscience, New York, 1971, p. 112.

120. Duncumb, P. and Reed, S.J.B., in "Quantitative electron probe microanalysis", K.F.J. Heinrich, Ed., Nat. Bur. Std. Spec. Publ. 298, 1968.

121. Philibert, J., in "X-ray Optics and X-ray Microanalysis", H.H. Pattee, V.E. Cosslett and A. Engstrom, Eds., Academic Press, New York, 1963, p. 379.

122. Duncumb, P. and Shields, P.K., Brit. J. Appl. Phys., 14 (1963), 617.

123. Carman, P.C. and Haul, R.A.W., Proc. Roy. Soc., London, A, 222 (1954), 109.

124. Crank, J., Mathematics of diffusion, Clarendon Press, Oxford, 1956.

125. Edwards, H.S., Rosenberg, A.F. and Bittel, J.T., Tech. Documentary Rept. ASD-TDR-63-635, (1963).

126. Simpson, L.A. and Carter, R.E., J. Am. Ceram. Soc., 49 (1966), 139.

127. Haul, R., Dumbgen, G. and Just, D., J. Phys. Chem. Solids, 23 (1962), 153.

128. Haul, R., Dumbgen, G. and Just, D., Z. Phys. Chem. N.F., 31 (1962), 309.

129. Haul, R. and Just, D., J. Appl. Phys., 33 (1962), 487.

130. Madeyski, A. and Smeltzer, W.W., Mat. Res. Bull., 3 (1968), 369.

131. Madeyski, A., Poulton, D.J., and Smeltzer, W.W., Acta Met., 17 (1969), 579.

132. Poulton, D.J. and Smeltzer, W.W., J. Electrochem. Soc., 117 (1970), 378.

133. Hagel, W.C., J. Am. Ceram. Soc., 48 (1965), 70.

134. Madeyski, A., Ph.D. Thesis, McMaster University, Hamilton, Ontario, Canada, August 1967, p. 104.

135. Kofstad, P., Nonstoichiometry, diffusion, and electrical conductivity in binary metal oxides, Wiley-Interscience, New York, 1972.

136. Walpole, R.E. and Myers, R.H., Probability and statistics for engineers and scientists, MacMillan, New York, 1972.

137. Lortholary, P., Goursat, P., Tetard, D. and Billy, M., Rev. Int. Hautes Temper. et Refract., 9 (1972), 325.

138. Goursat, P., Lortholary, P., Tetard, D. and Billy, M., 7th Int. Symposium on reactivity of solids, Bristol, 1972, 315.

139. Tobin, J.M., Adelsberg, L.M., Cadoff, L.H., and Brizes, W.F., in "Nuclear applications of non-fissionable ceramics", A. Boltax and J. H. Handwerk, eds., Interstate Printers, Danville, Illinois, 1966, pp. 257-277.

140. Cohen, M.H. and Turnbull, D., J. Chem. Phys. 31 (1959) 1164.

141. Feisel, D.H. and Armstrong, R.W., Trans. AIME 230 (1964), 867.